

รายงานวิจัยฉบับสมบูรณ์

โครงการ การศึกษาและออกแบบสารประกอบที่มีโครงสร้าง

ในระดับนาโนเมตร

ศ.ดร. จำรัส ลิ้มตระกูล



รายงานวิจัยฉบับสมบูรณ์

โครงการ การศึกษาและออกแบบสารประกอบที่มีโครงสร้างใน ระดับนาโนเมตร

คณะผู้วิจัย

สังกัด

ศ.ดร. จำรัส ถิ้มตระกูล ภาควิชาเคมี คณะวิทยาศาสตร์

มหาวิทยาลัยเกษตรศาสตร์

สนับสนุนโดยสำนักงานกองทุนสนับสนุนการวิจัย

(ความเห็นในรายงานนี้เป็นของผู้วิจัย สกว. ไม่จำเป็นต้องเห็นค้วยเสมอไป)

สารบัญ

บทศัลย่อ/Abstract	1
Executive summary	3
เนื้อหางานวิจัย	6
ผลลัพธ์ที่ใค้จากโครงการ	7
ภาคผนวก	11

บทคัดย่อ

การศึกษาวิจัยกระบวนการเร่งปฏิกิริยาเคมี ส่งผลต่อการพัฒนาอุตสากรรมเคมือย่างมาก ประกอบกับการวิจัยค้านนาโนเทคโนโลยี ทำให้ค้นพบสารประกอบที่มีโครงสร้างในระดับนาโน เมตร ที่มีคุณสมบัติพีเสษหลายประการ และสามารถประยุกต์ใช้เป็นตัวเร่งปฏิกิริยาเคมีที่มีคุณสมบัติคื ได้ เช่น ซีโอไลต์ ซึ่งเป็นผลิกที่มีรูพรุนที่มีขนาดใกล้เคียงกับขนาดของโมเลกุลของสารเคมี (~0.5 nm) และมีคุณสมบัติในการเลือกเกิดปฏิกิริยาที่จำเพาะกับขนาดและรูปร่างของโมเลกุล และอนุภาคโลหะ ทรานซิชั่น ขนาดนาโนเมตร มีสมบัติเป็นตัวเร่งปฏิกิริยาออกซิเดชันที่ดีและมีความจำเพาะสูงกว่า โลหะทั่วไปมาก การศึกษาวิจัยเกมีของสสารในระดับนาโนเมตรหรือระดับโมเลกุลและความก้าว หน้าค้านนาโนเทคโนโลยีมีความสำคัญและจะช่วยให้เกิดความก้าวหน้าทางวิทยาศาสตร์และ เทคโนโลยีเกมีและอุตสาหกรรมที่เกี่ยวข้อง และการพัฒนาการคำนวณทางเคมีคอมพิวเตอร์และการ จำลองแบบโมเลกุลจะช่วยสนับสนุนการพัฒนาดังกล่าวได้อย่างดียิ่ง

กลุ่มวิจัยเมธิวิจัยอาวุโสนี้จัดตั้งขึ้นเพื่อส่งเสริมการศึกษาวิจัยและรวบรวมความรู้ความ เชี่ยวชาญจากนักวิจัยและนักวิจัยรุ่นใหม่ในสาขาเคมีและวิศวกรรมเคมีจากมหาวิทยาลัยเกษตรศาสตร์ และนักวิจัยรุ่นใหม่จากมหาวิทยาลัย สถาบันเทคโนโลยีพระจอมเกล้า - ลาดกระบัง มหาวิทยาลัย เชียงใหม่ และมหาวิทยาลัยมหิดล เพื่อร่วมกันสร้างสรรค์งานวิจัยและความเป็นเลิศด้านเคมีการเร่ง ปฏิกิริยาในระคับโมเลกุลและวัสดุที่มีโครงสร้างระคับนาโนเมตร กลุ่มวิจัยที่สร้างขึ้นมีผลงานวิจัย จำนวน 25 เรื่องในวารสารวิชาการนานชาติชั้นนำ และเสริมสร้างนักวิจัยวิจัยรุ่นใหม่ จำนวน 12 คน และนักวิจัยรุ่นใหม่ที่เป็นผลผลิตจากกลุ่มวิจัยเมธิวิจัยอาวุโสนี้จะมีส่วนช่วยในการพัฒนาทาง วิทยาศาสตร์และเทคโนโลยีของประเทศต่อไปในอนาคต

Abstract

Catalytic and nanostructured materials are perhaps of the utmost importance to areas of research that have direct impact on the chemical industries. Nanochemistry creates a new dimension of chemistry as many materials in small nanometer sizes have significantly different properties from the bulk phases. Zeolites, which are nanostructured crystalline materials, are much better catalysts than normal silica-alumina oxides. Highly dispersed metal clusters show different chemical and electronic properties from large particles of the same metal. Knowledges of nanochemistry or molecular chemistry and nanotechnology are increasingly important and predicted to lead to dramatic impacts to the way we practice and study chemistry and other fields of science and technology. With the advance in computing technology, the computational chemistry and molecular modeling can be an effective route to advancing in chemistry and nanotechnology and related industries.

The proposed "TRF Senior Research Scholar" Unit is designed to provide a unique research environment for the integration of knowledge and expertise from different divisions within the KU faculty of science and engineering. The "Unit" combines the expertise of science and engineering faculties with the talents of new and young members in various universities (Chiang Mai University, and Kasetsart University, and King Mongkut Institute of Technology Lardkrabung, and Mahidol University) to pursue the excellence and integration of research in the areas of Molecular Catalytic and Nanostructured materials. The forming research team has published 25 articles in prestige international journals and fostered 12 young scientists. These outputs of this research unit will contribute to the development and science and technology in Thailand.

หน้าสรุปโครงการ (Executive Summary) ทุนเมธีวิจัยอาวุโส สกว. (ทุนส่งเสริมกลุ่มวิจัย)

1. ชื่อโครงการ (ภาษาไทย) การศึกษาและออกแบบสารประกอบที่มีโครงสร้างในระดับนาโน เมตร

(ภาษาอังกฤษ) Molecular Design, Structures, and Reaction Mechanisms of Nanostructured Materials Systems

2. ชื่อหัวหน้าโครงการ

ศ.คร. จำรัส ลิ้มตระกูล ภาควิชาเคมี คณะวิทยาศาสตร์ มหาวิทยาลัยเกษตรศาสตร์ จตุจักร กรุงเทพฯ 10900

โทรศัพท์: 02-942-8900 ต่อ 304

โทรสาร: 02-942-8900 ต่อ 324

e-mail: fscijrl@ku.ac.th

3. สาขาที่ทำการวิจัย เคมีเชิงฟิสิกส์

4. ปัญหาที่ทำการวิจัย และความสำคัญของปัญหา

การศึกษาวิจัยกระบวนการเร่งปฏิกิริยาเคมีส่งผลต่อการพัฒนาอุตสากรรมเคมือย่างมาก ประกอบกับการวิจัยค้านนาโนเทคโนโลยี ทำให้ค้นพบสารประกอบที่มีโครงสร้างในระคับนาโน เมตร (Nanomaterials) ซึ่งมีคุณสมบัติพิเศษหลายประการ และสามารถประยุกต์ใช้เป็นตัวเร่งปฏิกิริยา เคมีที่มีคุณสมบัติดีได้ ตัวอย่างเช่น ซีโอไลต์ ZSM-5 ซึ่งเป็นผลึกที่มีรูพรุนที่มีขนาดใกล้เคียงกับขนาด ของโมเลกุลของสารเคมี (~0.5 nm) และมีคุณสมบัติในการเลือกเกิดปฏิกิริยาที่จำเพาะกับขนาดและ รูปร่างของโมเลกุล (Shape Selectivity) และเมื่อเติมอนุภาคโลหะทรานซิชั่น ขนาดเล็กกว่า 1 nm ไป ในซีโอโลต์จะทำให้มีสมบัติเป็นตัวเร่งปฏิกิริยาออกซิเคชัน (selective oxidation) ที่ดีและมี ความจำเพาะสูงกว่าโลหะทรานซิชั่นทั่วไปมาก ตัวอย่างเหล่านี้ แสดงให้เห็นถึงความสำคัญในการ ศึกษาวิจัยสารในระดับนาโนเมตร ซึ่งจะช่วยให้เกิดความก้าวหน้าทางวิทยาศาสตร์และเทคโนโลยีเคมี ได้อย่างดียิ่ง

งานวิจัยนี้ทำการศึกษากลไกปฏิกิริยาเคมีโดยละเอียด อาศัยเทคโนโลยีที่ทันสมัยในค้าน ต่างๆ ได้แก่ ด้าน Spectroscopy โดยได้นำเอาเทกนิกของ IR Raman และ NMR มาใช้ในการวิเคราะห์ และศึกษาสมบัติของตัวเร่งปฏิกิริยาตลอดจนกระบวนการการเร่งปฏิกิริยาที่เกิดขึ้นจริงที่สภาวะต่างๆ ด้าน Reaction Techniques ใค้มีการใช้เทคนิค Temporal Analysis of Products (TAP) และ IR เพื่อ ทำนายที่สทาง และกลไกของการเกิดปฏิกิริยา และได้อาสัยการศึกษาทางทฤษฎีในการจำลองแบบ โมเลกุล (Modeling and Molecular Simulations) โดยใช้ความรู้ทาง Quantum Chemistry, Statistical Mechanics, Reaction Dynamics และ Reaction Engineering ในการจำลองแบบระบบที่สนใจ เพื่อ ศึกษาถึงสมบัติของตัวเร่ง และทำนายกลไกการเกิดปฏิกิริยาที่สภาวะต่างๆ ทำให้เกิดความเข้าใจใน กระบวนการเคมีที่เกิดขึ้นบนพื้นผิวของปฏิกิริยา โครงการวิจัยนี้ได้ทำการศึกษาทั้งโดยการศึกษา ทคลองกับระบบจริงและการศึกษาทางทฤษฎี ด้วยการจำลองแบบโมเลกุลเพื่อให้บรรลุตาม วัตถุประสงค์ คือเกิดความรู้ความเข้าใจปฏิกิริยาเลมีถึงระดับโมเลกุล และเข้าใจผลของโครงสร้างใน ระดับนาโนเมตรของตัวเร่งปฏิกิริยาต่อปฏิกิริยาเคมีที่สนใจศึกษา ซึ่งความรู้ที่ได้ สามารถนำมาใช้ให้ เกิดประโยชน์สูงสุดในการพัฒนาและออกแบบตัวเร่งปฏิกิริยาที่มีประสิทธิภาพ นอกจากนั้นยังได้ทำ การพัฒนาวิธีการสังเคราะห์ซีโอไลต์โดยอาศัยเทคนิคการสังเคราะห์แบบใหม่ และพัฒนาระเบียบ วิธีการคำนวณทางคอมพิวเตอร์เพื่อช่วยในการศึกษาและการออกแบบตัวเร่งปฏิกิริยา เพื่อให้ได้ตัวเร่ง ปฏิกิริยาที่มีประสิทธิภาพสูง สำหรับอุตสาหกรรมเคมีและปีโตรเคมี

5. วัตถุประสงค์

- สร้างองค์ความรู้ใหม่ค้านกลไกการเร่งปฏิกิริยาเคมีระคับ โมเลกุล (molecular catalysis) และ nanostructed materials และ computational methodologies
- 2. สร้างกลุ่มวิจัยที่ประกอบด้วยนักวิจัยรุ่นใหม่และนักวิจัยอาวุโส ให้มีศักยภาพสูง ทัดเทียม ระดับสากล และสร้างความร่วมมือในด้านงานวิจัยระหว่างสถาบันการศึกษาทั้งในประเทศ และต่างประเทศ
- สนับสนุนให้มีการวิจัยในระดับสากลเพื่อยกระดับมาตรฐานการศึกษาและวิจัยทาง
 วิทยาศาสตร์ และเทคโนโลยีของประเทศไทย
- 4. ตีพิมพ์ผลงานในวารสารนานาชาติ เพื่อเผยแพร่และประชาสัมพันธ์งานวิจัย

6. สรุปผลการดำเนินการของโครงการ

จากการดำเนินการในระยะ 3 ปี ด้วยทุนเมชีวิจัยอาวุโส สกว. (ทุนส่งเสริมกลุ่มวิจัย) ทำให้ เกิดความร่วมมือกันอย่างใกล้ชีดระหว่างนักวิจัย และเสริมสร้างนักวิจัยวิจัยรุ่นใหม่ จำนวน 12 คน จากหลายสถาบันได้แก่ มหาวิทยาลัยเกษตรศาสตร์ มหาวิทยาลัยมหิดล สถาบันเทคโนโลยีพระจอม เกล้าฯ ลาดกระบัง มหาวิทยาลัยเชียงใหม่ โดยร่วมมือกันทำงานวิจัยมุ่งเน้นศึกษาการเร่งปฏิกิริยาใน ระดับโมเลกุล (Molecular Catalysis) บนสารประกอบที่มีโครงสร้างในระดับนาโนเมตร อันได้แก่ สารซีโอไลต์ สารประกอบ TS1 อนุภาคโลหะขนาดเล็ก (Metal Cluster) โดยเน้นศึกษาปฏิกิริยาใน ห้องปฏิบัติการจริง และค้นคว้าวิธีการสังเคราะห์สารประกอบที่โครงสร้างระดับนาโนเมตรแบบใหม่ เพื่อการประยุกด์ใช้ในกระบวนการเคมี ควบคู่ไปกับการใช้วิธีเคมีคอมพิวเตอร์ เพื่อให้เกิดความเข้าใจ ในโครงสร้างและกลไกปฏิกิริยาอย่างลึกซึ้ง และเพื่อเป็นแนวทางในการนำไปใช้ประโยชน์ต่อไป นอกจากนั้นแล้ว ในโครงการวิจัยนี้ ยังมีเป้าหมายเพื่อ ทำการพัฒนาระเบียบวิธีทาง Computational Chemistry ให้ได้วิธีใหม่ ที่มีความถูกต้องและมีประสิทธิภาพสูงยิ่งขึ้น

ผลลัพธ์ของโครงการทำให้เกิดงานวิจัยที่ตีพิมพ์ในวารสารวิชาการนานาชาติ จำนวน 25เรื่อง

เนื้อหางานวิจัย

จากการศึกษาโดยใช้วิธีทางเคมีทฤษฎีควบคู่กับข้อมูลที่ได้จากการทดลองในห้องปฏิบัติการ จริง ทำให้เข้าใจถึงสมบัติตัวเร่งปฏิกิริยาและกลไกการเร่งปฏิกิริยาเกมีระคับ โมเลกุลของสารประกอบ ที่มีโครงสร้างระคับนาโนเมตรที่มีความสำคัญในอุคสาหกรรม โดยอาศัยหลักการของระเบียบวิธี Hybrid methods ซึ่งเป็นการรวม Density Functional Theory กับ Embedded Structure Theory ศึกษา การคูคซับของสารคูคซับประเภทต่างๆ บนซีโอไลค์ซึ่งถือว่าเป็นขั้นแรกและขั้นสำคัญของ กระบวนการเร่งปฏิกิริยาโดยซีโอไลต์ พบว่าค่าพลังงานคูดซับของสารคูดซับมีความสัมพันธ์โดยตรง กับโครงสร้างและสมบัติเฉพาะทางเคมีของซีโอไลค์ ในกรณีที่สารดูดซับที่มีขนาดของโมเลกูล ใกล้เคียงกับรูพรุนของซี โอ ไลต์และเป็นโมเลกุลไม่มีขั้วจะมีพลังงานการคูคซับที่เกิดจากแรงคึ่งคูค ระหว่างโมเลกุลดูคซับกับผนังรูพรุนของซีโอไลต์ซึ่งส่วนใหญ่เป็นแรง van der Waals อย่างไรก็ตาม เมื่อสารคูคซับเป็นโมเลกุลมีขั้วแรง van der Waals จะมีผลต่อพลังงานการคูคซับน้อยลงแต่ผลของ electrostatic interactions จากโครงผลึกของซีโอไลต์ต่อพลังงานการดูคซับจะเพิ่มขึ้น คังนั้น การเลือก Hybrid methods ให้เหมาะสมกับระบบที่ศึกษาจึงเป็นอีกปัจจัยหนึ่งที่มีผลต่อความน่าเชื่อถือของ ข้อมูลที่ได้ เช่น เมื่อศึกษาการคูดซับของสารประกอบแอ โรมาติกส์บนตัวเร่งซี โอไลต์ ควรเลือกใช้ Hybrid method ที่รวมอิทธิพลของแรง van der Waals ด้วย ซึ่งวิธีหนึ่งที่ประหยัดเวลาและให้ผลที่ เชื้อถือได้คือ DFT:UFF Hybrid method ในขณะที่ระบบมีสารดูคชับเป็นโมเลกุลมีขั้ว เช่น น้ำหรือเม ทานอล ควรเลือกใช้ Hybrid methods ที่รวมผลของ electrostatic interactions ด้วย เช่น SCREEP method ถึงแม้ DFT:UFF และ SCREEP Hybrid methods สามารถใช้ศึกษาการดูคซับของสารดูคซับ บนตัวเร่งซีโอไลต์ได้คื แต่ทั้งสองวิธีนี้ยังมีข้อจำกัด โดยเฉพาะอย่างยิ่งเมื่อต้องการศึกษากลไกการเร่ง ปฏิกิริยาของซีโอไลต์ที่เกี่ยวข้องกับ transition states หรือ intermediates ที่มีโครงสร้างเกะกะและมี ประจุ การใช้แบบจำลองที่มีเพียงแรง van der Waals หรือ electrostatic interactions อย่างใคอย่างหนึ่ง ไม่เพียงพอที่จะอธิบายโครงสร้างที่ไม่เสถียรเหล่านี้ได้ กลุ่มวิจัยจึงได้พัฒนาระเบียบวิธีใหม่บน พื้นฐานของ Hybrid methods เดิม โดยการรวมอิทธิพลของแรง van der Waals และ electrostatic interactions ไว้ในแบบจำลองเคียวกันเพื่อเปรียบเทียบการคูคซับและการเร่งปฏิกิริยาของซีโอไลต์ที่มี โครงผลึกต่างกัน และเรียกแบบจำลองนี้ว่า Embedded ONIOM method

ผลลัพธ์ที่ได้จากโครงการ

- 1. สรุปผลงานที่ได้รับการตีพิมพ์ในวารสารวิชาการนานาชาติในตลอดระยะเวลา 3 ปี ของการ ดำเนิน โครงการ จำนวน 25 ผลงาน อันได้แก่
 - Pantu, P., Pabchanda, S., and Limtrakul, J. (2004) "Theoretical Investigation of Selective Oxidation of Methane to methanol on Nanostructured Fe-ZSM-5 by ONIOM method", ChemPhysChem, 5, 1901-1906.
 - Namuangruk, S., Pantu, P., Limtrakul, J. (2004) "Alkylation of benzene with ethylene over faujasite zeolite investigated by the ONIOM method", Journal of Catalysis, 2004, 225(2), 523-530.
 - Limtrakul, J., Inntam, C., Truong, T.N. (2004) "Density functional theory study of the ethylene epoxidation over Ti-substituted silicalite (TS-1)", Journal of Molecular Catalysis A: Chemical, 207(2), 139-148.
 - Nokbin, S., Limtrakul, J., Hermansson, K. (2004) "DFT plane-wave calculations of the Rh/MgO(001) interface", Surface Science, 566-568, 977-982.
 - Rungsirisakun, R., Jansang, B., Pantu, P. and Limtrakul, J. (2004) "The adsorption of Benzene on industrially important nanostructured catalysts (H-BEA, H-ZSM-5, and H-FAU): confinement effects", J. Mol. Struct., 733, 239-246.
 - Sirijaraensre, J., Limtrakul, J. (2004) "The influence of the framework to structures
 and energetic profiles of the vapor phase of the Beckmann rearrangement on different
 types of zeolite", Petroleum Chemistry, Preprints, 49(2), 222-226.
 - Chareonpanich, M., Namto, T., Kongkachuichay, P., Limtrakul, J. (2004)
 "Synthesis of ZSM-5 zeolite from lignite fly ash and rice husk ash", Fuel
 Processing Technology, 85(15), 1623-1634.
 - Feil, S., Gluch, K., Matt-Leubner, S., Scheier, P., Limtrakul, J., Probst, M., Deutsch, H., Becker, K., Stamatovic, A., Märk, T.D. (2004) "Partial cross sections for positive and negative ion formation following electron impact on uracil", Journal of Physics B, 37, 3013-3020.
 - Ketrat, S., Limtrakul, J. (2003) "Theoretical study of the ethylene on alkaliexchanged zeolites", International Journal of Quantum Chemistry, 94(6), 333-340.

- Kasuriya, S., Namuangruk, S., Trecsukol, P., Tirtowidjojo, M., Limtrakul, J.,
 (2003) "Adsorption of ethylene, benzene and ethylbenzene over faujasit zeolite investigated by the ONIOM method", Journal of Catalysis, 219, 320-328.
- Bobuatong, K., Limtrakul, J. (2003) "Effects of the zeolite framework on the adsorption of ethylene and benzene on alkali-exchanged zeolite: an ONIOM study", Applied Catalysis A: General, 253, 49-64.
- Sailer, W., Pelc, A., Probst, M., Limtrakul, J., (2003) "Dissociative electron attachment to acetic acid (CH3COOH)", Chemical Physics Letters, 378 (3-4), 250-256.
- 13. Tonmunphean, S., Wijitkosoom, A., Tantirungrotechai, Y., Nuttavut, N., Limtrakul, J. (2003) "Magnetizabilities of Ring-structured Molecules, [8]-cyclacene, [8]-BN-cyclacene and [8]-Collarene, and their Effect on 3He Nuclear Shielding Tensor", Bulletin of the Chemical Society of Japan, 76, 1537-1541.
- Dungsrikaew, V., Limtrakul, J., et. al. (2003) "Comparison of methods for point charge representation of electrostatic fields", International Journal of Quantum Chemistry, 96, 17-22.
- Sailer, W., Pelc, A., Limao-Vieira, P., Mason, N.J., Limtrakul, J, and Probst, M.,
 (2003) "Low energy electron attachment to CH3CN", Chemical Physics Letters,
 381(1,2), 216-222.
- Panjan, W., Limtrakul, J. (2003) "The influence of the framework on adsorption properties of ethylene/H-ZSM-5 system: an ONIOM study", Journal of Molecular Structure, 654(1-3), 35-45.
- Raksakoon, C., Limtrakul, J. (2003) "Adsorption of aromatic hydrocarbon onto H-ZSM-5 zeolite investigated by ONIOM study" THEOCHEM 631, 147-156.
- Boekfa, B., Sirijareansre, J., Pantu, P. and Limtrakul, J., (2004) "A quantum chemical study of the interaction of carbonyls with H-ZSM-5 zeolite", Stud Surf Sci Catal. 154, 1582-1588.
- Wongthong, P., Soonthornpalin, C., Pantu, P. and Limtrakul, J., (2004) "Adsorption of Toluene over Faujasite zeolite investigated by the combined quantum mechanics/molecular mechanics method", Stud Surf Sci Catal., 154, 1817-1822.

- Pabchanda, S., Pantu, P., Tantanak, D. and Limtrakul, J., (2004) "Structure and energetics of nitrous oxide and methane adsorption on the Fe-ZSM-5 zeolite: ONIOM and density functional studies", Stud Surf Sci Catal., 154, 1844-1848.
- Jungsuttiwong, S., Limtrakul, J. and Truong, T.N., (2005) "Theoretical Study of Modes of Adsorption of Water Dimer on H-ZSM-5 and H-Faujasite Zeolites" Journal of Physical Chemistry B, 109, 13342-13351.
- Sirijaraensre, J., Truong, T.N. and Limtrakul J., (2005) "Density Functional Study of the Mechanism of the Beckmann Rearrangement Catalyzed by H-ZSM-5: A Cluster and Embedded Cluster Study" Journal of Physical Chemistry B 109 (24), 12099-12106.
- Treesukol, P., Srisuk, K., Limtrakul J. and Truong T.N, (2005) "Nature of the Metal-Support Interaction in Bifunctional Catalytic Pt/H-ZSM-5 Zeolite" Journal of Physical Chemistry B, 109, 11940-11945.
- Sangthong, W., Probst, M. and Limtrakul J., (2005) "Computational study of the carbonyl-ene reaction of encapsulated formaldehyde in Na-FAU zeolite" Journal of Molecular Structure, 748, 119-127.
- Rujiwatra, A. and Limtrakul, J., (2005) "Ethane-1,2-diaminium hexaaquazinc(II) sulfate" Acta Crystalloraphica, E61, M1403-M1404.

2. สรุปผลงานในการประชุมนานาชาติตลอคระยะเวลา 3 ปี ของการคำเนินโครงการ อันได้แก่

- แสดงผลงานในการประชุมนานาชาติในงาน ACS National Meeting ครั้งที่ 225
 ระหว่างวันที่ 23 ถึง 27 มีนาคม 2546 ณ เมือง New Orleans, LA. ประเทศ สหรัฐอเมริกา จำนวน 4 เรื่อง
- 2. แสดงผลงานในการประชุมนานาชาติในงาน Advances in Petrochemicals and Polymers in the New Millennium ครั้งที่ 1 ระหว่างวันที่ 22 ถึง 25 กรกฎาคม 2546 ณ กรุงเทพมหานคร ประเทศไทย จำนวน 4 เรื่อง
- 3. แสดงผลงานในการประชุมนานาชาติในงาน American Chemical Society National Meeting ครั้งที่ 227 ระหว่างวันที่ 28 มีนาคม ถึง 1 เมษายน 2547 ณ เมือง Anaheim, CA. ประเทศสหรัฐอเมริกา จำนวน 5 เรื่อง
- 4. แสดงผลงานในการประชุมนานาชาติในงาน International Zeolite Conference ครั้งที่ 14 ระหว่างวันที่ 25 ถึง 30 เมษายน 2547 ณ เมือง Cape Town, ประเทศแอฟริกาใด้ จำนวน 3 เรื่อง

- 5. แสคงผลงานในการประชุมนานาชาติในงาน American Chemical Society National Meeting ครั้งที่ 229 ระหว่างวันที่ 13 มีนาคม ถึง 17 มีนาคม 2548 ณ เมือง San Diego ประเทศสหรัฐอเมริกา จำนวน 12 เรื่อง
- 3. สรุปกิจกรรมที่เกี่ยวข้อง ตลอคระยะเวลา 3 ปี ของการคำเนิน โครงการ อันได้แก่
 - จัดการประชุมเมธีวิจัยอาวุโส ในหัวข้อเรื่อง การออกแบบโครงสร้างและกลไกการ เกิดปฏิกิริยาของซีโอไลต์และสารประกอบที่มีโครงสร้างในระดับนาโนเมตร เมื่อวันที่ 9-11 พฤศจิกายน 2546 ณ โรงแรมรามาการ์เดน
 - 2. จัดการประชุมเมรีวิจัยอาวุโส ในหัวข้อเรื่อง "Molecular Design, Structure and Reaction Mechanisms of Nanostructured Materials Systems" เมื่อวันที่ 22 มกราคม 2548 ณ โรงแรมซิดี้ปีช รีสอร์ท หัวหิน

ภาคผนวก

ภาคผนวก ก.

สรุปผลงานที่ได้รับการตีพิมพ์ ในวารสารวิชาการนานาชาติ จำนวน 25 เรื่อง

Theoretical Investigation of the Selective Oxidation of Methane to Methanol on Nanostructured Fe-ZSM-5 by the ONIOM Method**

Piboon Pantu, Suwat Pabchanda, and Jumras Limtrakul*^(a)

The Intracrystalline nanostructured pore network of zeolites has an astonishing ability to stabilize small metal complexes, leading to extraordinary catalytic activities. Small iron complexes in ZSM-5 (Fe-ZSM-5), for example, have a remarkable redox behavior and received great attention. The Fe-ZSM-5 shows a unique activity in the selective oxidation of methane to methanol at room temperature using nitrous oxide as an oxidant. Due to this catalytic property, the Fe-ZSM-5 has been widely compared with the enzyme methane mono-oxygenase (MMO), whose active site contains a binuclear iron cluster. The Fe-ZSM-5 zeolite also exhibits high activity for the direct partial oxidation of benzene to phenol using nitrous oxide as an oxidant. In and also for selective catalytic reduction of nitrogen oxides. In an also for selective catalytic reduction of nitrogen oxides.

The highly selective and active catalytic site in the Fe-ZSM-5 is generally denoted as a site, of which the exact structure is still not understood, though it has been extensively studied. Generally, the active iron atoms in Fe-ZSM-5 are highly dispersed from complexes, which can form isolated ions, binuclear complexes, or small aggregates of iron atoms, in a zeolite matrix. [6-10] After activation at high temperatures under vacuum or in a flow of steam, the active form of Iron is formed. (6) This active site has a strong affinity for nitrous oxide decomposition. At low temperatures (below 300°C), the decomposition of nitrous oxide leads to deposition of active surface oxygen denoted as α oxygen.^[4] According to in situ X-ray absorption near edge structure (XANES) and Mössbauer studies, iron atoms at the a site are in a bivalent state (Fest). After decomposition of nitrous oxide, the iron atoms are oxidized to a trivalent state (Fe^{ti}). Earlier, proposed structures for the active site mostly were the oxo- or hydroxo-bridged binuclear iron complexes in ZSM-5 pores resembling the structure of the active site of the MMO enzyme. Extended X-ray absorption fine structure (EXAFS) studies have supported the presence of binuclear iron complexes in over-exchanged Fe-ZSM-5 catalysts.⁽⁷⁾ Recently, it has been reported that the isolated iron cations can be found at the ion exchange site in Fe-ZSM-5 samples, especially at low iron loadings (Fe/Al < 1).[6-10] Based on the infrared spectroscopic results of nitric oxide (NO) adsorption on Fe-ZSM-5, Berlier et al. [8] suggested that the active site is the highly coordinately unsaturated isolated Fe^h site that is located at the Brønsted acid site. Choi et al. [10] reported EXAFS studies of Fe-ZSM-5 samples with a Fe/Al ratio < 1, which are prepared by solid-state ion exchange with iron species uniformly present in a form of mononuclear iron complexes as either [FeO₃]⁺ or [Fe(OH)₃]⁺.

Quantum-chemical studies have been utilized to characterize the active site in the Fe-ZSM-5 and to study its activity in various selective oxidation reactions. The first quantum model of active iron species inside zeolites proposed binuclear iron clusters. [11] Yoshizawa et al. [12] proposed a model of mononuclear iron oxide cation in a 3T zeolite cluster and demonstrated that these cations can catalyze the direct oxidation of methane to methanol and of benzene to phenol, although their model involves an unrealistic conversion of Fe^N to Fe^I species which has not been experimentally proven. Recently, Ryder et al. [13, 14] and Kachurovskaya et al. [15] proposed a ferryl-type mononuclear iron species in a ZSM-5 zeolite cluster. These two slightly different models demonstrated catalytic decomposition of nitrous oxide^[13] and direct oxidation of benzene to phenol. [14-15]

However, in earlier reported quantum-chemical studies, electronic properties of zeolites are usually modeled with size-limited cluster fragments of a particular zeolite. With such limited models, the effect of the framework, which can significantly change the structure and energetics of the system, is not taken into account. It has been shown that neglecting the microporous framework effect leads to discrepancies between cluster results and the actual zeolite behavior. [16]

Recent developments in hybrid methods, such as embedded cluster or combined quantum mechanics/molecular mechanics (QM/MM) methods, as well as the more general ONIOM (our own n-layer integrated molecular orbital and molecular mechanics)⁽¹⁷⁾ method, have brought large systems within reach of accurate calculation results.

Herein, we report the quantum-chemical study of structure and activity of Fe-ZSM-5 for decomposition of nitrous oxide and oxidation of methane to methanol using an ONIOM method. The active site is modeled as a highly coordinately unsaturated Isolated Fe cation located at the Brønsted acid site of ZSM-5, and the effects of the extended zeolitic framework are explicitly included by utilizing a two-layered ONIOM model. This is one of the first theoretical studies[18-19] adopting the ONIOM scheme for characterizing the reactivity of active sites inside zeolites. The extended structure of the zeolite is found to have profound effects on the structure, the electronic properties and the catalytic activity of the Iron species. These findings are in agreement with a recent FTIR study by Berlier et al., [85] which shows that the Fe^{II} species hosted inside the MFI channels exhibits significantly more pronounced coordinative unsaturation than the Fe[®] species anchored on MCM-41 and amorphous silica surfaces and, thus, their higher reactivity towards NO molecules.

⁽a) Or. P. Pantu, S. Pabchanda, Prof. Dr. J. Limtrakul Laboratory for Computational and Applied Chemistry Physical Chemistry Division, Department of Chemistry Kasetsart University, Bangkok 10900 (Thailand) Fax: (4-662)942-8900-324 E-mail: fscijrl@ku.ac.th

^[**] ONIOM = our own n-layer integrated molecular orbital and molecular mechanics

Results and Discussion

Model of the a Site [FeO+/ZSM-5-]

The active site in Fe-ZSM-5 is modeled as an isolated mononuclear iron oxide ion at the ion-exchange sites of the ZSM-5. The existence of such an active site has been found by Fourier Transform (FT) IR spectroscopy⁸⁹ and was recently confirmed by EXAFS experiments¹⁰⁸ on Fe-ZSM-5 with low iron loadings of Fe/Al = 0.17-0.80. In this model, the active oxygen atom, which is bound to the iron cation, is considered to be an O- radical anion since EPR experiments reported the formation of OT radical anions by decomposition of nitrous oxide on a surface of reduced metal oxides.[20] The effects of nanostructured zeolite pores are included by using the 46T ONIOM2 model in which the active region, consisting of the iron oxide, reactive species and the 5T structure of the ZSM-5 acid site, is modeled by densitiy funtional theory (DFT) calculations, whereas the surrounding ZSM-5 crystal lattice is modeled by the universal force field (UFF) force field with up to 46T atoms in order to cover the cavity at the intersection of the straight and the zigzag pore channels, where reactions normally take place. Since the main interactions between adsorbed molecules and zeolite pore walls are van der Waals Interactions, pil the UFF force field has been found to be adequate in representing the confinement effects of zeolite pore walls. The active model used in this study is similar to that proposed by Ryder et al. in their studies on nitrous oxide decomposition and oxidation of benzene to phenol, 113-141 except that in this study the effects of the extend-

ed zeolite framework is explicitly taken into account by using the ONIOM scheme. Therefore, we will make comparisons wherever possible and point out the effects of the zeolite framework on the reaction inside the zeolite pores.

The optimized structure of the Fe-ZSM-5 model is shown in Figure 1 a. At the active site, the iron cation [FeO]⁺ is coordinated with the two bridging oxygen atoms of the zeolite framework which act as Lewis bases exerting bidentate interactions. These interactions are found to be approximately sym-

metric, with almost equal Fe-O bond lengths of 2.02 and 2.03 Å (see Table 1). The distance between the Fe and Al atoms is 2.83 Å. An O" radical anion (O1) is covalently bonded to the Iron atom with a bond distance of 1.66 Å.

Oxidation of the α Site by Nitrous Oxide Decomposition

At temperatures below 300 °C, nitrous oxide decomposition can take place on the α site in Fe-ZSM-5 and leave an active

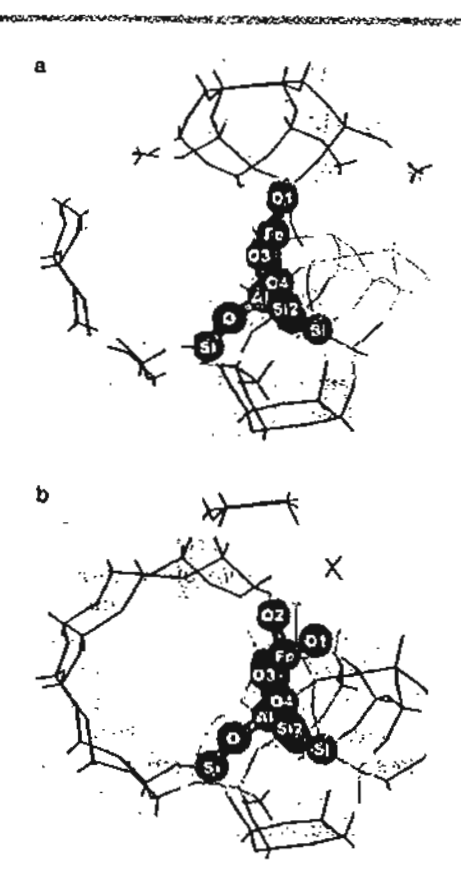


Figure 1. 46T ONIOM model of the Fe-ZSM-5 zeolite, AlSi_aO₄H₄, Atoms belonging to the active region are drawn as sphere: a) FeO-ZSM-5 and b) FeO₂ZSM-5.

Table 1 The pola	Park market spirit	Legine	des della difficial	Cresiologica	Meral Signer
mediates by a tran		ious est permit	e conflorionses	is Marger 112 (G+10	
Parameters	$N_2O + (FeO)$	N ₂ O/(FeO)	TSa	N,/[FeO ₂]	N ₂ +(FeO ₂
distances					
Fe-Al	2.83	2.83	2.79	2.80	2.80
Fe-01	1.66	1.67	1.71	1.68	1.67
Fe02	_	2.29	1.90	1.67	1.67
Fe-03	2.03	2.04	2.01	1.99	1.98
Fe-04	2.02	2.03	2.01	2.00	1,98
Fe-N1	~	3.10	2.71	2.47	-
N1O2	1.19	1.20	1.56	3.00	(0.65)
N1-N2	1.13	1.12	1.12	1.09	3,10
angles					
 \$01 - Fe-02	-	96.9	101.7	85.4	86.4
₹2103-AI	129.2	129_5	129.9	129.7	129.4
≰Si2O4AJ	130.3	130.4	129.8	128.6	128.9

surface oxygen species (α oxygen) deposited on the active iron center. The reaction pathway is depicted in Figure 2 and selected structural parameters are tabulated in Table 1. First, a nitrous oxide molecule adsorbs on the [FeO]⁺ site. It is found that structure and energetics of the adsorbed nitrous oxide molecule are significantly affected by the extended zeolite crystal structure. The steric confinement of the zeolite pore walls included in the 46T ONIOM model causes the adsorbed nitrous oxide molecule to point with its nitrogen end towards the empty space in the intersection cavity of the ZSM-5 zeolite,

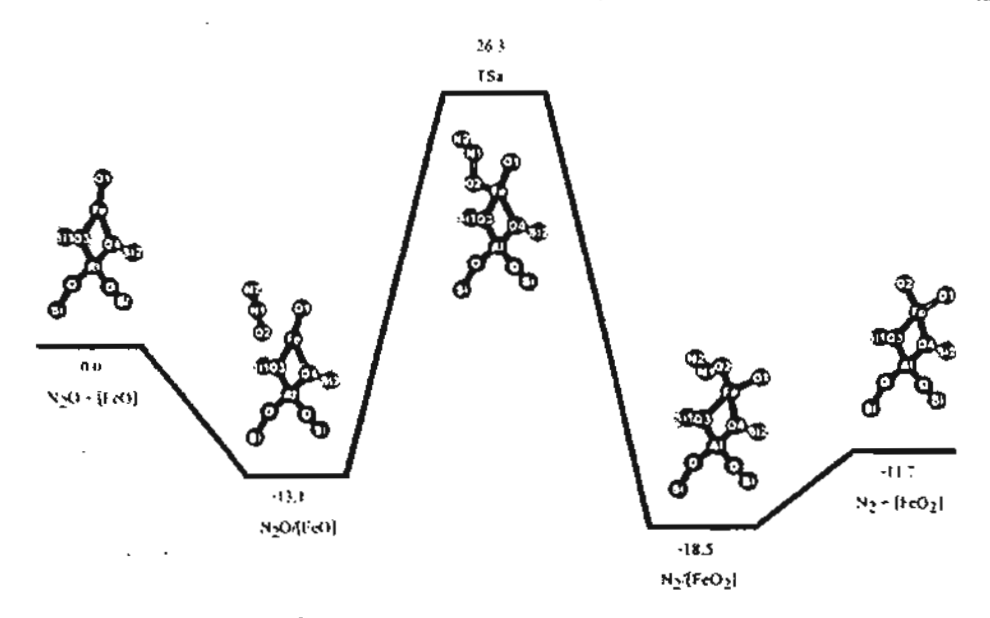


Figure 2. Energy profile [kcalmol $^{-1}$] for nitrous axide decomposition over Fe-ZSM-5 by the 46T ONIOM method (B3LYP/6-311 + G(3df,2p):UFF).

whereas in a bare 5T model the nitrogen end of the nitrous oxide leans towards the 5T cluster fragment due to stabilizing electronic interactions. The energetics of the adsorbed molecule is also markedly affected by the extended framework of the zeolite. In the 46T ONIOM model, the adsorption energy is calculated to be -13.1 kcal mol⁻¹, which is reasonably close to the averagemental estimate of 15 kcal mol⁻¹, which is reasonably close to (CO). The second of the adsorption energy is the average of the adsorption and the α-oxygen atom (CO). The second of the adsorption energy is (CO).

the experimental estimate of -16 kcalmol-1221 whereas, in the case of 5T bare cluster, the computed adsorption energy is only -6.6 kcal mol-1,[13] Subsequently, the adsorbed nitrous oxide can undergo the decomposition reaction by breaking the N-O bond, releasing a nitrogen molecule, and leaving an active surface a oxygen deposited on the active iron site. The activation energy for the nitrous oxide decomposition is evaluated to be 39.4 kcalmol-1, which agrees reasonably with the energy barrier for the same step computed by Ryder et al. of 37.6 kcal mol⁻¹ [13] However, the apparent activation energy for this step is calculated to be 26.3 kcalmol-1, which is considerably lower than the value of 31.0 kcalmol⁻¹ reported by Ryder et al.[13] for the same reaction step mainly due to the effects of the extended zeolite framework included ONIOM scheme that stabilizes the reactive complexes inside the zeolite pores.

After decomposition of nitrous oxide, an active α -oxygen atom is deposited on the active iron center and the optimized structure of the α -oxygen-loaded site is presented in Figure 1 b. The Fe-Al distance is computed to be 2.80 Å (see Table 1), which agrees well with the Fe-Al distance of \approx 2.9 Å experimentally measured by EXAFS for the mononuclear iron dioxide $\{\text{FeO}_2\}^+$ or rather the dihydroxide $\{\text{Fe}(\text{OH})_2\}^+$ at the ion exchanged site of the ZSM-5 zeolite by Choi et al. The Fe-O distances are 1.98 Å between the iron atom and the two bridging atoms of the zeolite framework and 1.67 Å between the iron atom and the α -oxygen atoms, it is noted that the Fe-O bond distance of 1.67 Å is close to the bond distance of 1.65 Å

between an active oxygen atom bound to the heme iron in the enzyme cytochrome P450cam, D31 but significantly shorter than the normal Fe-O single bond distance of 1.8 Å. The distance between the two oxygen atoms is 2.29 Å, which Indicates that these two OToxides do not form a chemical bond. The configurations of the two oxygen atoms around the iron atom are slightly different. The Fe-O1 bond is close to the zigzag pore wall while the Fe-O2 bond is pointing towards the free space in the intersection cavity. Therefore, the O2 is slightly more accessible to incoming adsorbates.

Methane Selective Oxidation on the $\alpha\textsc{-Oxygen-Loaded}$ Site [FeO2+/ZSM-5-]

the a-oxygen-loaded site is proposed in Figure 3 and selected structural parameters are presented in Table 2. Initially, methane weakly adsorbs on the active site with one hydrogen atom (H1) pointing towards the iron atom and the α-oxygen atom (O2). The computed adsorption energy is -6.1 kcal mol-1. The weak Interactions between the adsorbed methane and the active site do not significantly disturb the structure of the active site. Nevertheless, the adsorbed methane molecule is apparently activated to some extent as the C-H1 bond distance is slightly elongated from 1.090 Å to 1.095 Å. Then, the adsorbed methane is activated by hydrogen abstraction forming a hydroxyl group on the iron center and a methyl radical. The transition state structure shows the characteristic feature of the direct H-abstraction process with an almost linear angle for the C-H1-Oα angle (172.7 degree). At the transition state, the C-H1 bond of the methane molecule is elongated from 1.095 Å to 1.21 Å and, at the same time, the H1-Oa bond is forming as the H1-Ox distance decreased from 3.30 Å to 1.33 Å. The energy barrier for this step is calculated to be 15.3 kcalmol⁻¹, which is close to the energy barrier of 14-18 kcalmol⁻¹ for Habstraction from methane by the MMO enzymeted and also close to the energy barrier of 16 kcal mol-1 for C-H bond dissociation of methane on the surface O- radical anion of MoO, [25]

The methyl free radical intermediate can rapidly recombine with the surface O⁻ radical anion forming a highly stable methoxide species. The bond distances between the iron atom and methoxide as well as between the iron atom and hydroxide are 1.79 and 1.81 Å, respectively reflecting the typical Fe—O single bond distance. The O1—Fe—O2 bond angle Increases from 86.4 to 119.2 degrees to reduce the repulsive interactions between the methoxide and the hydroxide which are situated

CHEMPHYSCHEM

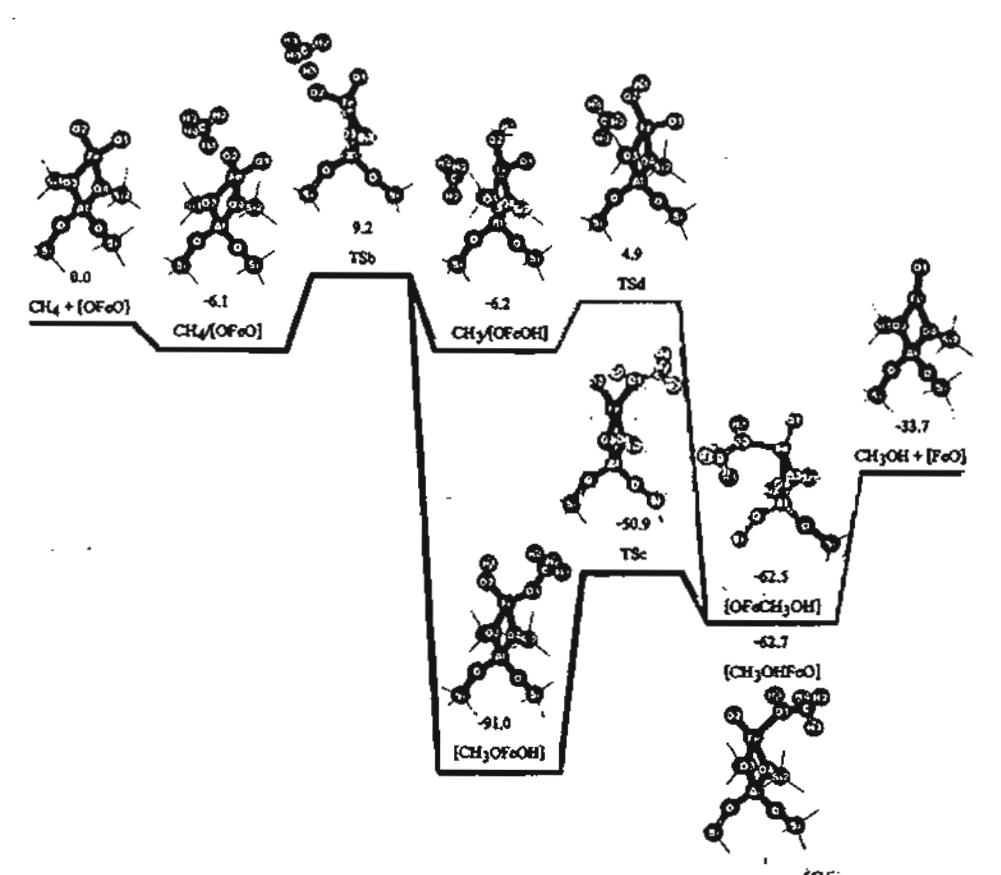


Figure 3. Energy profile [kcal mol⁻¹] for selective axidation of methane over Fe-ZSM-5 by the 46T ONIOM method (83LYP/6-311+G(3df,2p):UFF).

on the same iron atom. The methoxide product is more stable than the starting reactants and, therefore, this process is highly exothermic with a reaction energy of -91.0 kcal mol⁻¹. This fast radical recombination step is assumed to be a barrierless process, since a transition state for this step cannot be found.

This stable methoxide can be converted to methanol via a hydrogen shift reaction. The transition structure shows that the hydrogen atom of the hydroxyl group is moving to the oxygen atom of the methoxide to form the methanol product. However, the conversion of methoxide to methanol is quite difficult, as this reactions requires a high activation energy of 40.1 kcal mol-1 and is endothermic by 28.5 kcal mol-1. However, the exothermic conversion of methanol back to methoxide is relatively easy achievable and requires a small activation energy of 11.8 kcal mol-1 as the methoxide species is more stable than the adsorbed methanol.

Alternatively, the methyl radical is stabilized by the ZSM-5 framework by forming a loosely bound complex with the iron atom at a Fe--CH₃ distance of 2.78 Å. The formation of strongly bound methyl species on the iron active site with a much shorter bond distance (1.97 Å) as proposed by Yoshizawa et al.^[12] has not been found in this model, the

space around the active iron atom is more crowded than in the model of Yoshizawa et al. as the iron atom is covalently bound to two oxygen atoms and surrounded by zeolite pore walls. Therefore, the space around the iron atom appears to be too crowded to accommodate a strong bonding of a methyl group. The relative energy of this loosely bound methyl radical complex is evaluated to be -6.2 kcal mol⁻¹. The methyl radical

Parameters	$CH' + \{OEGO\}$	CH_AOFeO)	tsp.	ICH _t OFeOH[TS¢	(CH ₁ OHFeO)	CH_XOFeOH	TSd	(OF _F CH ₃ Ot
distances									
Fe Al	2.80	2.79	2.77	2.64	2.82	2.85	2:64	2.85	2.84
e-01	1.67	1,67	1,61	1.79	2.03	2.13	1.61	1.65	1,67
Fe -02	1.67	\ <i>i</i> Śፖ	1.75	1.81	1.74	1.67	1.78	1.87	2.12
c-03	1.98	1.98	1.99	2.04	2.03	2:07	2.03	2.07	207
e ∙04	1.96	1.99	2.03	202	2.03	2.06	2.05	2,04	2.07
e-C	_	3.46	3.66	3.09	3.23	3,40	2.78	2.48	3,31
C H1	1.09	1.09\$	1.21	-	~		3.87	-	_
O1O2	2.29	2.27	2,58	3.10	231	2.76	2.59	2,77	2.98
11-02	-	3.30	1,33	0.96	1,29	2.53	0.97	0.97	0,96
(1 - O)	-	3.33	2.74	3.39	1.20	0.97	2.55	-	-
ingles									
₹01 Fe-02	86.4	85.8	100,1	119.2	75.2	.92.2	99,3	103.5	102.9
%Si1O3 ;Ai	129.4	129.9	129.9	129.1	129.4	129.4	129.3	129.0	129.5
≰\$£2+04+A1	128.9	128,4	129.1	130.6	129.6	130.4	130.5	130.7	131,0
¢C-R102		84.5	172.7	-	- A-	-	_	_	•

COMMUNICATIONS

can then be transformed to methanol by reacting with the hydroxyl group on the active iron center. This reaction is also highly exothermic with a reaction energy of -56.3 kcal mol⁻¹ and a calculated activation energy of 11.1 kcal mol⁻¹. The resulting adsorbed methanol is strongly attached to the catalyst. Desorption of the adsorbed methanol would require a high activation energy to overcome the strong adsorption energy of 28.8 kcal mol⁻¹.

The methoxide and methanol products are both strongly attached to the active site and, thus, are not easy to be desorbed, which is in agreement with experimental observation, which show that the product from the direct oxidation of methane to methanol on Fe-ZSM-5 is so strongly attached to the catalyst surface that it cannot be directly desorbed. A solvent extraction by water or a mixture of water and acetonitrile^[1] is needed to hydrolyze and remove the adsorbed products from the surface of Fe-ZSM-5.

When we examine the energy profile of the selective oxidation of methane, the activation of methane via hydrogen abstraction is found to be the rate-limiting step in agreement with the kinetic isotope effects, which indicate that a step involving C—H dissociation is the rate-limiting step. The predicted activation energy of 15.3 kcal mol⁻¹ is comparable to the energy barrier for H abstraction by the MMO enzyme.^[24] This is also in agreement with the experimental observation that this reaction can occur at room temperature similar to the enzymatic system.^[1-2] The reaction then preferably proceeds via a rapid recombination of the methyl radical and the surface oxygen radical anion forms the highly stable methoxide which is strongly adsorbed to the active site.

Conclusions

Using the ONIOM method to investigate the reactivity of Fe-ZSM-5, we observe that the confinement of the zeolite pore structure can stabilize the adsorbed reactive species and affect structures, electronic properties and catalytic activity of the active Iron species. On the active iron center, the oxidation of methane proceeds through the direct hydrogen abstraction of adsorbed methane forming a methyl radical with an energy barrier of 15.3 kcalmol⁻¹ which is comparable to the energy barrier found in the MMO enzyme system. The methyl radical can undergo the barrier-less recombination with the surface Or radical anion and produces the strongly adsorbed methoxide. Alternatively, the methyl radical can be stabilized by the zeolite framework and, then, react rapidly with the hydroxyl group on the iron center forming the adsorbed methanol. Due to the relative stability, the adsorbed methanol can be easily converted to the more stable methoxide species which should become the dominant product and is strongly adsorbed on the catalyst surface.

Computational Methods

The structure of the duster model was taken from the crystal structure of the ZSM-5 lattice.^[26] In this study, the Fe-ZSM-5 structure was represented by a 46T ONIOM2 model. The

46T cluster that coveres the three different channel structures (channel intersection, the straight channel and the zigzag channel), where reactions normally take place, was selected with one aluminum atom that substituted a silicon atom at the T12 position. The negative charge of the cluster was balanced by either the [FeO]⁺ or the [FeO₂]⁺ ion to form the active center (Figure 1).

The accuracy of the ONIOM method depends significantly on the choice of the level of calculations for high- and lowlevel regions, in the ONIOM2 model the 5T active center was treated quantum chemically at the 83 LYP level of theory using the 6-311+G(3df,2p) basis set for all types of atoms, except for the Iron atom, for which the energy-consistent pseudo-potential (ECP) of Stuttgart and Born in the small-core approximation[27] was used as it has been shown by Ryder et al.[13-14] that this basis set gives reasonable results for catalytic decomposition of nitrous oxide and oxidation of benzene to phenol in the Fe-ZSM-5 catalyst. Using the experimental adsorption energy as a benchmark, we have demonstrated that the UFF method provides reasonable values corresponding to experimental measurements.[10] This is due to the explicit consideration of van der Waals interactions, which are the dominant contribution for adsorption-desorption mechanisms in zeolites. [21] This suggests that the UFF method is a practical choice for the low-level methodology whereas the high-level region is treated by the B3LYP method. Therefore, the rest of the extended framework, up to 46T, was treated at molecular mechanics force field.

Geometry optimizations were done at the B3LYP/6-311 + G(3df,2p) level of theory. The total spin of the system was kept constant at the sextet state throughout all calculations. During the structure optimization, only the 5T portion of the active site region and the adsorbates were allowed to relax while the rest was fixed at the crystallographic coordinates. Normal mode analyses were carried out to verify the transition states to have one imaginary frequency whose mode corresponds to the designated reaction. All calculations have been performed by using the Gaussian 98 code.^[28]

Acknowledgements

This work was supported by grants from the Thailand Research Fund (TRF Senior Research Scholar to JL) and the Kasetsart University Research and Development Institute (KURDI) as well as by the Ministry of University Affairs under the Science and Technology Higher Education Development Project (MUA-ADB funds).



a) K. A. Dubkov, V. I. Sobolev, G. I. Panov, Kinet. Catal. 1998, 39, 72-79;
 b) G. I. Panov, V. I. Sobolev, K. A. Dubkov, V. N. Parmon, N. S. Ovanesyan, A. E. Shilov, A. A. Shteinman. React. Kinet. Catal. Lett. 1997, 61, 251-258;
 c) V. I. Sobolev, K. A. Dubkov, O. V. Panna, G. I. Panov, Catal. Today 1995, 24, 251-252.

CHEMPHYSCHEM

- [2] G. L. Panov, V. L. Sobolev, K. A. Dubkov, A. S. Kharitonov, Stud. Surf. Sci. Catal. 1996, 101, 493 – S02.
- [3] a) G. L. Panov, G. A. Sheveleva, A. S. Kharitonov, V. N. Romannikov, L. A. Vostrikova, Appl. Catal. A 1992, 82, 31–36; b) R. Burch, C. Howitt, Appl. Catal. A 1993, 103, 135–162.
- [4] G. I. Panov, V. I. Sobolev, A. S. Kharitonov, J. Mol. Catal. 1990, 61, 85-97.
- [5] a) R. Joyner, M. Stockenhuber, J. Phys. Chem. B 1999, 103, 5963-5976;
 b) V. I. Sobolev, G. I. Panov, A. S. Kharitonov, V. N. Romannikov, A. M. Volodin, K. G. Ione, J. Catal. 1993, 139, 435-443;
 c) X. Feng, W. K. Hall, Catal. Lett. 1996, 41, 45-46;
 d) J. Perez-Ramirez, F. Kapteijn, G. Mul, J. A. Moulijn, Chem. Commun. 2001, 693-694.
- [6] a) G. Berlier, G. Spoto, S. Bordiga, G. Ricchlardi, P. Fiskaro, A. Zecchina, L. Rossetti, E. Seili, L. Forni, E. Giarnello, C. Lamberti, J. Catal. 2002, 208, 64–82; b) J. Jia, Q. Sun, B. Wen, L. X. Chen, W. M. H. Sachtler, Catal. Lett. 2002, 82, 7–11; c) K. A. Dubkov, N. S. Ovanesyan, A. A. Shteinman, E. V. Starokon, G. I. Panov, J. Catal. 2002, 207, 341–352.
- [7] a) A. Battiston, J. H. Bitter, F. M. F. de Groot, A. R. Overweg, O. Stephan, J. A. van Bokhoven, P. J. Kooyman, C. van der Spek, G. Vanko, D. C. Koningsberger, J. Catal. 2003, 213, 251–271; b) K. A. Dubkov, N. S. Ovanesyan, A. A. Shteinman, E. V. Starokon, G. L. Panov, J. Catal. 2002, 207, 341–352; c) T. V. Voskoboinikov, H.-Y. Chen, W. M. H. Sachtler, Appl. Catal. 8 1998, 19, 279–287; d) P. Marturano, L. Drozdova, A. Kogelbauer, R. Prins, J. Catal. 2000, 192, 236–247.
- [8] a) G. Berlier, A. Zecchina, G. Spoto, G. Ricchiardi, S. Bordiga, C. Lamberti, J. Catal. 2003, 215, 264-270; b) G. Berlier, F. Bonino, A. Zecchina, S. Bordiga, C. Lamberti, ChemPhysChem 2003, 4, 1073-1078.
- (9) L. J. Lobree, L.-C. Hwang, J. A. Reimer, A. T. Bell, J. Catal. 1999, 186, 242–253.
- [10] S. H. Chol, B. R. Wood, J. A. Ryder, A. T. Bell, J. Phys. Chem. B 2003, 107, 11843-11851.
- [11] M. J. Filatov, A. G. Peimenschikov, G. M. Zhidomirov, J. Mol. Catal. 1993, 80, 243-251.
- [12] K. Yoshizawa, Y. Shiota, T. Yumura, T. Yamabe, J. Phys. Chem. 8 2000, 104, 734-740.
- [13] J. A. Ryder, A. K. Chakraborty, A. Y. Bell, J. Phys. Chem. 8 2002, 106, 7059-7064.
- [14] J. A. Ryder, A. K. Chakraborty, A. T. Bell, J. Catal. 2003, 220, 84-91.
- [15] N. A. Kachurovskaya, G. M. Zhildomirov, E. J. M. Hensen, R. A. van Santen, Catal. Lett. 2003, 86, 25–31.
- [16] a) P. E. Sinclair, A. H. de Vries, P. Sherwood, C. R. A. Catlow, R. A. van Santen, J. Chem. Soc. Faraday Trans. 1998, 94, 3401-3408; b) M. Brandle, J. Brandle, J. Am. Chem. Soc. 1998, 120, 1556-1570.
- [17] a) M. Svensson, S. Humbel, R. D. J. Froese, T. Matsubara, S. Sieber, K. Morokuma, J. Phys. Chem. 1996, 100, 19357-19363; b) S. Dapprich, I. Komaromi, K. S. Byun, K. Morokuma, M. J. Frisch, J. Mol. Struct. 1999, 461, 1-21.
- [18] a) C. Raksakoon, J. Umtrakul, J. Mol. Struct. 2003, 631, 147-156; b) W. Panjan, J. Limtrakul, J. Mol. Struct. 2003, 654, 35-45; c) S. Kasuriya, S. Namuangruk, P. Treesukol, M. Tirtowidjojo, J. Limtrakul, J. Catal. 2003, 219, 320-328; d) K. Bobuatong, J. Limtrakul, Appl. Catal., A 2003, 253, 49-64.
- [19] a) M. Boronat, P. M. Viruela, A. Corma, J. Am. Chem. Soc. 2004, 126, 3300-3309; b) A. Damín, S. Bordiga, A. Zecchina, C. Lamberti, J. Chem. Phys. 2002, 117, 226-237; c) F. Bonino, A. Damin, G. Ricchiardi, M. Ricci, G. Spano, R. D'Aloisio, A. Zecchina, C. Lamberti, C. Prestipino, S. Bordiga, J. Phys. Chem. B 2004, 108, 3573-3583; d) F. Bonino, A. Damin, S. Bordiga, C. Lamberti, A. Zecchina, Langmulr 2003, 19, 2155-2161; e) S. Bordiga, A. Damin, F. Bonino, A. Zecchina, G. Spano, F. Rivetti, V. Bolís, C. Prestipino, C. Lamberti, J. Phys. Chem. B 2002, 106, 9892-9905.
- [20] a) V. A. Shvets, V. B. Kazanskil, J. Catal. 1972, 25, 123-130; b) Y. B. Taarit, J. H. Lunsford, Chem. Phys. Lett. 1973, 19, 348-350.
- [21] a) X. Rozanska, R. A. van Santen, F. Hutschka, J. Hafner, J. Am. Chem. Soc. 2001, 123, 7655-7667; b) L. A. Clark, M. Slerka, J. Sauer, J. Am. Chem. Soc. 2003, 125, 2136-2141; c) E. G. Derouane, C. D. Chang, Microporous Mesoporous Mater. 2000, 35-36, 425-433; d) A. Pelmenschikov, J. Leszczynski, J. Phys. Chem. 8 1999, 103, 6886-6890.
- [22] B. R. Wood, J. A. Reimer, A. T. Bell. J. Catal. 2002, 209, 151-158.
- [23] L. Schlichting, J. Berendzen, K. Chu, A. M. Stock, S. A. Maves, D. E. Benson, R. M. Sweet, D. Ringe, G. A. Petsko, S. G. Silgar, Science, 2000, 287, 1615–1622.

[24] A.M. Valentine, S.S. Stahl, S.J. Uppard, J. Am. Chem. Soc. 1999, 121, 3876–3887.

- [25] S. P. Mehandru, A. B. Anderson, J. F. Brazdil, R. K. Grasselli, J. Phys. Chem. 1987, 91, 2930 – 2934.
- [26] H. van Koningveld, H van Bekkun, J. C. Jansen, Acta Crystallogr., Sect. 8: Struct. Sci. 1987, 43, 127 – 132.
- [27] M. Dolg, U. Wedig, H. Stoll, H. Preuss, J. Chem. Phys. 1987, 86, 866.
- [28] Gaussian 98 (Revision A.7), M. J. Frisch, G. W. Trucks, H. B. Schlegel, G. E. Scuseria, M. A. Robb, J. R. Cheeseman, V. G. Zakrzewski, J. A. Montgomery, R. E. Stratmann, J. C. Burant, S. Dapprich, J. M. Millam, A. D. Daniels, K. N. Kudin, M. C. Strain, O. Farias, J. Tomasi, V. Barone, M. Cossi, R. Cammi, B. Mennucci, C. Pomelli, C. Adamo, S. Clifford, J. Ochterski, G. A. Petersson, P. Y. Ayala, Q. Cul, K. Morokuma, D. K. Malick, A. D. Rabuck, K. Raghavachari, J. B. Foresman, J. Goslowski, J. V. Ortiz, B. B. Stefanov, G. Liu, A. Liashenko, P. Piskorz, L. Komaromi, R. Gomperts, R. L. Martin, D. J. Fox, T. Keith, M. A. Al-Laham, C. Y. Peng, A. Nanayakkara, C. Gonzalez, M. Challacombe, P. M. W. Gill, B. G. Johnson, W. Chen, M. W. Wong, J. L. Andres, M. Head-Gordon, E. S. Replogle, J. A. Pople, Gaussian, Inc., Pitts-

Received: April 12, 2004

burgh, PA, 2001.

Early View Article
Published online on November 12, 2004

Cation Mobility and Anion Reorientation in Sodium Trifluoromethyl Sulfonate

Leo van Wüllen, **** Natalia Sofina, *** and Martin Jansen***

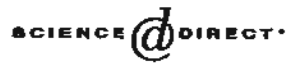
The study of solid electrolytes for use in all solid-state batteries remains an important facet of materials science. Mainly due to their low weight and flexibility, the vast majority of studies in this field has been devoted to polymer-based electrolytes. However, with respect to the key feature, a high ionic conductivity in combination with a more or less vanishing electronic contribution, crystalline materials might evolve as a promising alternative. One route to optimized conductivities in these materials follows a maximization of vacancies via aliovalent doping or replacement as successfully exemplified in $\text{Li}_{4-2x}\text{Si}_{1-x}\text{S}_2\text{O}_4$ (0.30 < x < 0.45), [II] $\text{Li}_{3x}\text{La}_{2(3)-y}\text{TiO}_3$ (0.04 < y < 0.14) [2-6] or $\text{Na}_{3-x}P_{1-x}\text{S}_x\text{O}_4$ (0 = z = 0.6), [2-6] The second route has its starting point with the observation that the phase transition of some alkali salts of complex anions (e.g., NO_2^- , SO_4^{2-} , PO_4^{3-} , Alf_6^{3-}) into the dynamically disordered high-temperature

- [a] Priv.-Doz. Dr. L. van Wüllen, N. Sofina, Prof. Dr. M. Jansen Max-Planck-Institut für Festkörperforschung Heisenbergstrasse 1, 70569 Stuttgart (Germany) Fax: (+ 49) 711-6891502 E-mail: wullen@unl-muenster.de
- m.jansen@mpi-stuttgart.mpg.de
 [b] Priv.-Ooz. Dr. L. van Wällen
 Institut für Physikalische Chemie
 Westfällische Wilhelms-Universität Münster
 Corrensstr. 30, 48149 Münster (Germany)

Fax: (+49) 251-8329159



Available online at www.sciencedirect.com



Journal of Catalysis 225 (2004) 523-530

JOURNAL OF CATALYSIS

www.elsevier.com/locate/jcat

Alkylation of benzene with ethylene over faujasite zeolite investigated by the ONIOM method

Supawadee Namuangruk, Piboon Pantu, and Jumras Limtrakul*

Laboratory for Computational and Applied Chemistry, Physical Chemistry Division, Kasetsart University, Bangkok 10900, Thailand
Received 30 March 2004; accepted 15 April 2004

Available online 2 June 2004

Abstract

The alkylation of benzene with ethylene over faujasite zeolite has been investigated using an 84T cluster of faujasite zeolite serving as a nanometer-sized chemical reactor modeled by the ONIOM3 (MP2/6-311++G(d,p):HF/6-31G(d):UFF) method, which gives accurate adsorption energies for the reactants and the product, indicating the accuracy of the model in representing interactions between the adsorbates and the zeolite. The computed adsorption energies are -8.73, -13.91, and -20.11 kcal/mol, which compared well with experimentally reported values of -9.0, -14.0, and -20.4 kcal/mol for ethylene, benzene, and ethylbenzene, respectively. Stepwise and concerted mechanisms of the alkylation reaction are considered. For the stepwise mechanism, the alkylation starts with the protonation of the adsorbed ethylene by an acidic zeolite proton leading to the formation of the ethoxide intermediate and, subsequently, the ethoxide reacts with a benzene molecule forming an ethylbenzene product. The computed activation energies are 30.06 and 38.18 kcal/mol for the first and second step, respectively. For the concerted mechanism, the alkylation of benzene takes place in a single reaction step without prior ethoxide formation. The concerted mechanism has an activation energy of 33.41 kcal/mol which is in between the two energy barriers of the stepwise mechanism.

@ 2004 Elsevier Inc. All rights reserved.

Keywords: Benzene alkylation; Density functional calculations; ONIOM, QM/MM; Zeolite; Reaction mechanism

1. Introduction

Ethylbenzene is an important raw material in the petrochemical industry for the manufacture of styrene, which is one of the most important industrial monomers. Worldwide capacity of ethylbenzene production is about 23 million metric tons per year [1]. Conventionally, ethylbenzene is produced by benzene alkylation with ethylene using mineral acids such as aluminum chloride or phosphoric acid as catalysts. However, these corrosive catalysts cause a number of problems concerning handling, safety, corrosion, and waste disposal. An immense endeavor has been put into developing alternative catalytic systems that are more environmentally friendly. As a result, the ethylbenzene production technology has been progressively moved toward zeolite-based processes. In the past couple of decades, zeolite-based processes have been introduced and licensed by several

manufactures, Mobil-Badger, Lummus-UOP, CDTech, and Dow Chemical [1].

Zeolite catalysts also offer an advantage of high selectivity toward the desired product due to the shape-selective properties of their microcrystalline pore structures. Several types of zeolites have been reported to have high activity for benzene alkylation, for example, faujasite, beta, H-ZSM-5, and MCM-22 [1-11]. Elucidation of the reaction mechanism of benzene alkylation on zeolite catalysts is of great interest. From an industry point of view, understanding the alkylation mechanism could help in optimizing the reaction conditions and designing a new catalyst for a more efficient process. However, the reaction mechanism of alkylation of aromatics with short-chain olefins on zeolites is not yet clearly understood. Venuto et al. [2] and Weitkamp [3] suggested that alkylation of benzene with ethylene over acidic faujasite and ZSM-5 zeolites followed the Eley-Rideal mechanism. Corma et al. [4] reported the Eley-Rideal mechanism for alkylation of benzene with propylene over MCM-22. While the Langmuir-Hinshelwood mecha-

^{*} Corresponding author.

E-mail address: fscijri@ku.ac.th (1. Limtrakul).

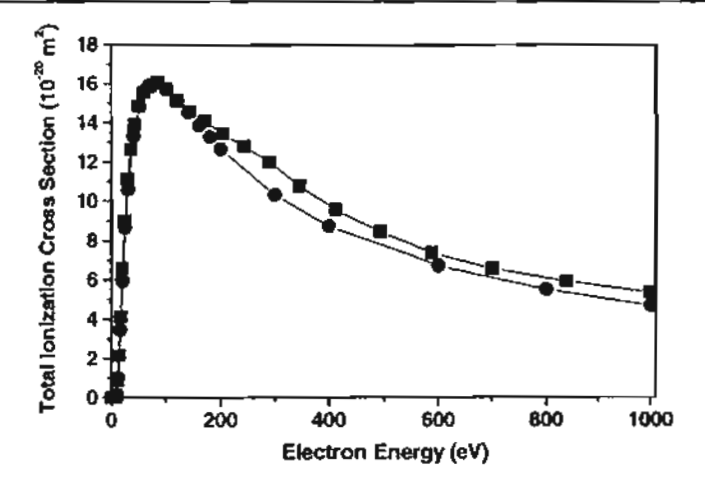


Figure 3. Total single tracil ionization cross section as a function of electron energy. The relative measured cross section was put on an absolute scale by normalization to a calculated cross section using the DM formalism of 15.7×10^{-20} m² at 100 eV. The normalized measured cross section (filled squares) is compared with the calculated DM cross section (filled circles) over the entire range of impact energies studied here (threshold to 1000 eV).

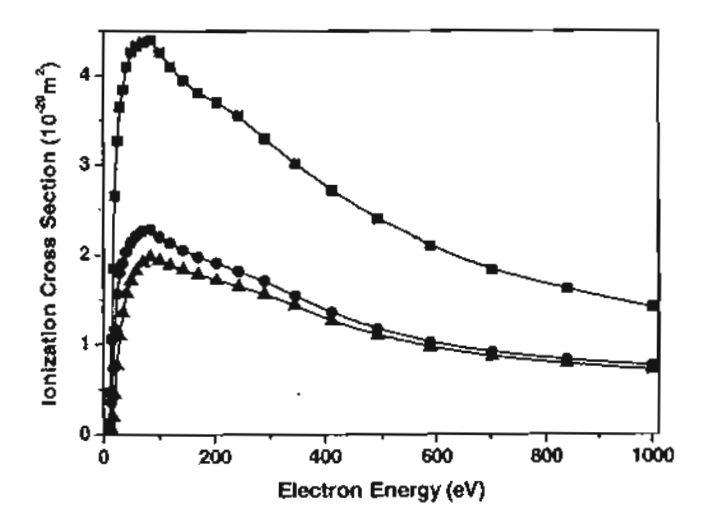


Figure 4. Absolute partial ionization cross sections for the formation of the parent uracil $C_4H_4N_2O_2^*$ ion (squares) and two fragment ions $C_3H_3NO^*$ (circles) and OCN* (triangles) as a function of electron energy following electron impact on uracil.

measured cross section tends to lie slightly above the calculated cross section. The maximum discrepancy in the two cross sections of slightly more than 10% is found in the energy range between 250 and 350 eV. At impact energies from 150 eV to 250 eV and above 400 eV, the deviation between the two curves is generally less than 5%.

Figure 4 shows the three absolute partial ionization cross sections for the parent uracil ion $C_4H_4N_2O_2^+$ and two fragment ions, $C_3H_3NO^+$ and OCN^+ . As one would expect on the basis of the mass spectrum depicted in figure 1, the parent ionization cross section has the

The reaction profile involving the reaction between the alkoxide intermediate with benzene to produce ethylbenzene is shown in Fig. 3a and selected structural parameters are tabulated in Table 2. A benzene molecule diffuses into the vicinity to react with the alkoxide. The alkylation of benzene involves concerted bond forming between the carbon atoms of ethylene and benzene and the breaking of a benzene proton giving the proton back to the zeolite-bridging oxygen. The vibrational motion corresponding to the imaginary frequency at the transition is explicitly shown in Fig. 3b, which clearly demonstrates that the C-C bond forming between the ethyl and benzene occurs via interactions of surface ethoxide and benzene. During the transformation, the C-O covalent bond of the surface ethoxide is breaking while the bond between the ethyl and benzene begins to form and a benzene proton is leaving toward the zeolite framework. The activation energy is evaluated to be 38.18 kcal/mol. The adsorbed ethylbenzene product is subsequently desorbed endothermically, requiring energy of 20.11 kcal/mol.

3.3.2. Concerted mechanism for benzene alkylation with ethylene

Alternatively, benzene alkylation can proceed via concerted interactions in the coadsorbed complex of ethylene and benzene without the formation of an alkoxide intermediate. The reaction steps can be written as follows:

$$C_{2}H_{4} + H-FAU \rightleftharpoons C_{2}H_{4}-H-FAU, \qquad (5)$$

$$C_{6}H_{6} + C_{2}H_{4}-H-FAU \rightleftharpoons (CH_{3}CH_{2})C_{6}H_{5}-H-FAU, \qquad (6)$$

$$(CH_{3}CH_{2})C_{6}H_{5}-H-FAU \rightleftharpoons (CH_{3}CH_{2})C_{6}H_{5} + H-FAU. \qquad (7)$$

Very recently, DFT cluster calculations of ethylbenzene formation via the concerted reaction of the coadsorbed complex have been reported using DFT quantum cluster calculations by Vos et al. [53] and Arstad et al. [54]. Therefore, a comparison will be made and the effect of inclusion of the extended framework of the zeolite by the ONIOM method will be discussed.

The reaction energy profile is presented in Fig. 4a and the selected geometrical parameters of intermediates and transition state are tabulated in Table 3. The reaction is initiated by coadsorption of benzene on the adsorbed ethylene at the acid site of the zeolite. The coadsorption energy is evaluated to be -16.79 kcal/mol, which is significantly higher than the values previously reported by Vos et al. and Arstad et al. (7.3 and 7.8 kcal/mol, respectively). The difference results mainly from Van der Waals interactions between the adsorbed complex and the zeolite walls, which in this study were taken into account by using the UFF force field to model the extended framework of the zeolite [30-37]. At the transition state, there is an imaginary frequency associated with the transition complex (Fig. 4b) which indicates that the zeolitic proton (H1) is moving toward the ethylene carbon (C1) and the other ethylene carbon (C2) starts forming a bond with the benzene carbon (C3) and, simultaneously, the

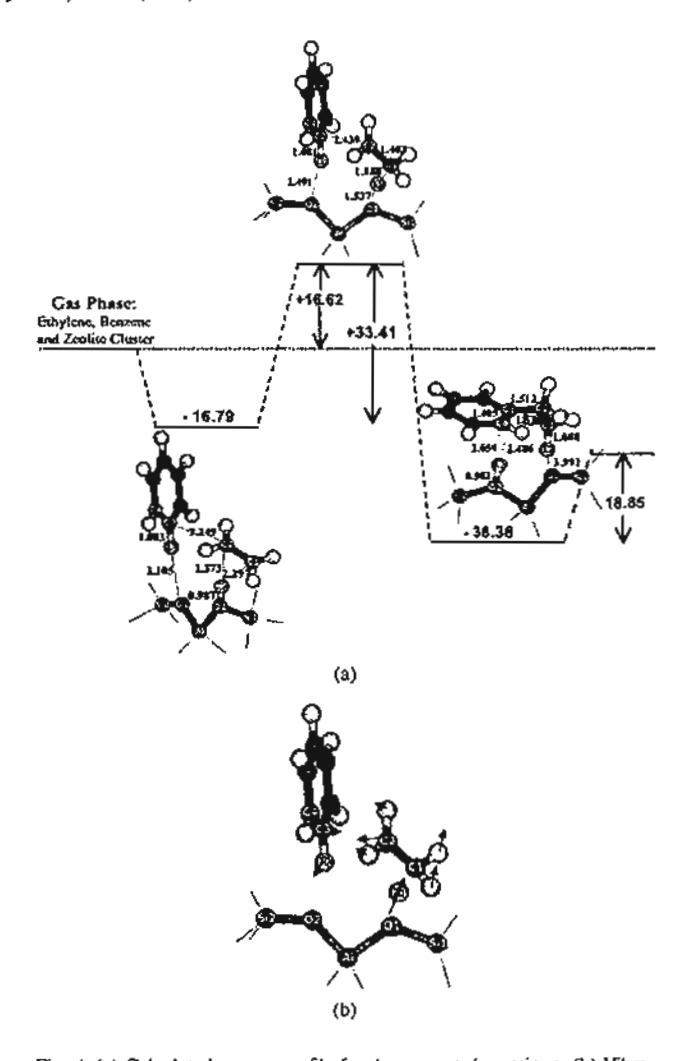


Fig. 4. (a) Calculated energy profile for the concerned reactions. (b) Vibrational movement corresponding to the imaginary frequency at the transition structure.

benzene proton is leaving toward the zeolite-bridging oxygen (O2). The vibrational motion of the transition state complex clearly indicates the concerted mechanism of the alkylation of benzene. The structure of the transition state shows that the Brønsted acid O1-HI distance is greatly lengthened from 0.987 to 1.537 Å and the distance between the zeolitic proton (H1) and the ethylene carbon (C1) becomes 1.188 Å. The ethylene C-C bond distance is significantly lengthened from 1.342 to 1.403 Å, whereas the structure of the benzene molecule does not significantly differ from that of the coadsorbed structure except that the distance between the benzene proton (H2) and the zeolite-bridging oxygen (O2) is shortened from 3.105 to 2.491 Å. The transition-state structure obtained in this model is similar to that of reported by Arstad et al., but slightly different from that reported by Vos et al. in which the ethylene is completely protonated at the transition state. The activation energy is calculated to be 33.41 kcal/mol, very close to the numbers reported by Vos et al. and Arstad et al. (31.6 and 31.3 kcal/mol, respectively).

Table 3

The optimized geometric parameters of isolated molecule, coadsorption complex, transition state (TS), and product of concerted reaction of benzene alkylation on FAU using ONIOM3 (distances are in angestroms and angles are in degrees)

Parameters	Isolated cluster	Coadsorption complex	Transition state	Product
Distances		<u> </u>	<u> </u>	
A)-H1	2.462			
C1-C2	1.335	1.342	1.403	1.529
C2-C3	-	3.249	2,439	1.512
C3-C4	-	1.398	1.408	1.405
C3-H2	_	1.083	1.081	2.486
C4-H2	-	2.147	2.159	2.659
O2-H2	-	3.105	2.491	0.982
CI-HI	-	2.297	1.188	1.088
C2-H1		2.373	2.030	2,165
O1–K1	0.970	0.987	1.537	3.992
A}-O1	1.876	1.861	1.773	1.701
A1-O2	1.694	1.699	1.741	1.886
\$i1-O1	1.669	1.667	1.612	1.601
Si2-O2	1.606	1.602	1.598	1.683
Angles				
ZSilOtAl	123.7	122.9	121.7	116.9
∠\$i2Q2A!	130.4	131.5	134.9	135.1

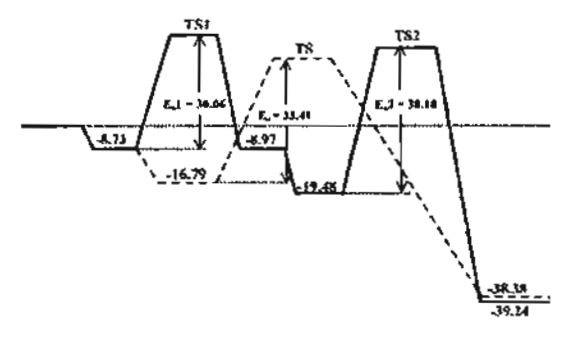


Fig. 5. Calculated energetic profiles for the stepwise (solid line) and concerted (dashed line) reaction mechanisms.

The complete energetic profiles of the two mechanisms are drawn on the same diagram (Fig. 5) for easy comparison. For the stepwise mechanism, the alkoxide formation has a smaller activation energy of 30.06 kcal/mol and the surface reaction step is the rate-determining step with the activation energy of 38.18 kcal/mol. The activation barrier of the concerted mechanism of 33.41 kcal/mol is in between the barriers of the stepwise mechanism. It might appear that the concerted mechanism should dominate the overall alkylation reaction due to the smaller activation energy. However, the stepwise mechanism could also contribute significantly because, from an energetic point of view, the alkoxide formation will occur relatively easily, and after the alkoxide intermediate is formed the stability of the adsorbed benzenealkoxide adduct makes the reverse reaction more difficult to occur than the forward reaction to the ethylbenzene product. When it is considered that both mechanisms can take place under the reaction conditions, the calculated apparent activation energy for the alkylation of benzene with ethylene would be in a range of 16.62-27.67 kcal/mol. Although, there is no experimental value of the activation energy for alkylation of benzene with ethylene in zeolites to compare with, our computed apparent activation energy range seems reasonable when compared with the apparent activation energies (10–18 kcal/mol) for alkylation of benzene with propylene in zeolites [4,6,46]. Because ethylene is a poorer alkylating agent than propylene, and the rate of benzene alkylation with ethylene is much slower than that with propylene and generally it requires a higher reaction temperature to obtain the same conversion level as that of the alkylation with propylene [1,4,47,53], the activation energy of the alkylation with ethylene is expected to be higher than the activation energy of the alkylation with propylene.

4. Conclusion

The alkylation of benzene with ethylene over faujasite zeolite has been investigated using the ONIOM3 model. The model is shown to be accurate in predicting adsorption energies of the adsorbed reactants and product compared to experimental estimates. Two alkylation mechanisms, stepwise and concerted, are considered. For the stepwise mechanism, the alkylation starts with protonation of the adsorbed ethylene which leads to the formation of the active surface ethoxide intermediate. Benzene alkylation takes place via interactions between the ethoxide species and a benzene molecule. The rate-determining step is found to be the reaction step where concerted bond forming between the carbon of the ethyl fragment and benzene and bond breaking of a benzene proton occur. The activation energy of 38.18 kcal/mol is predicted. For the concerted mechanism, the alkylation of benzene takes place in a single reaction step of the coadsorbed reactants without prior alkoxide formation. The activation energy is calculated to be 33.41 kcal/mol.

The results derived in the present study suggest that the ONIOM approach yields an accurate and practical model

for exploring the structure, adsorption, and reaction mechanisms of zeolites.

Acknowledgments

This work was supported in part by grants from the Thailand Research Fund (TRF Senior Research Scholar to J.L.) and the Kasetsart University Research and Development Institute (KURDI), as well as the Ministry of University Affairs under the Science and Technology Higher Education Development Project (MUA-ADB funds). The support from the Dow Chemical Company (USA) is also acknowledged.

References

- T.F. Degnan Jr., C.M. Smith, C.R. Venkat, App. Catal. A 221 (2001) 283.
- [2] P.B. Venuto, L.A. Hamilton, P.S. Landis, J. Catal. 5 (1966) 484.
- [3] J. Weitkamp, Int. Sympos. in Zeolite Catalysis, Siofok, Hungary, Acta Phys. Chem. 217 (1985).
- [4] A. Corma, V. Martinez-Soria, E. Schnoeveld, J. Catal. 192 (2000) 163.
- [5] Y. Morita, H. Matsumoto, T. Kimura, F. Kato, M. Takayasu, Bull. Jpn. Pet. Inst. 15 (1) (1973) 37.
- [6] K.A. Becker, H.G. Karge, W.-D. Streubel, J. Catal. 28 (1973) 403.
- [7] P.G. Smirniotis, E. Ruckenstein, Ind. Eng. Chem. Res. 34 (1995) 1517.
- [8] W.W. Kaeling, R.E. Holland, J. Catal. 19 (1988) 212.
- [9] N.Y. Chen, W.E. Garwood, Catal. Rev.-Sci. Eng. 28 (1986) 185.
- [10] K.S.N. Reddy, B.S. Rao, U.P. Shiralkar, Appl. Catal. A 95 (1993) 53.
- [11] A. Corma, Chem. Rev. 95 (1995) 559.
- [12] R. Shab, J.D. Gale, M.C. Payne, J. Phys. Chem. B 101 (24) (1997) 4787.
- [13] Y. Jeanvoine, J.G. Angyan, G. Kresse, J. Hafner, J. Phys. Chem. B 102 (1998) 5573.
- [14] I.H. Hillier, J. Mol. Struct. (Theochem.) 463 (1999) 45.
- [15] J. Limtrakut, S. Jungsuttiwong, P. Khongpracha, J. Mol. Struct. 525 (2000) 153.
- [16] J. Sauer, M. Sierka, J. Comput. Chem. 21 (2000) 1470.
- [17] J. Sauer, P. Ugliengo, E. Garrone, V.R. Saunders, Chem. Rev. 94 (1994) 2095.
- [18] J. Sauer, Chem. Rev. 89 (1989) 199.
- [19] J. Limtrakul, Chem. Phys. 193 (1995) 79.
- [20] J. Limtrakul, P. Treesukol, C. Ebner, M. Probst, Chem. Phys. 215 (1997) 77.
- [21] P.E. Sinclair, A.H. de Vries, P. Sherwood, C.R.A. Catlow, R.A. van Santen, J. Chem. Soc., Faraday Trans. 94 (1998) 3401.
- [22] M. Brandle, J. Saucr, J. Am. Chem. Soc. 120 (1998) 1556.
- [23] S.P. Greatbanks, I.H. Hillier, N.A. Burton, P. Sherwood, J. Chem. Phys. 105 (1996) 3370.
- [24] R.Z. Khaliullin, A.T. Bell, V.B. Kazansky, J. Phys. Chem. A 105 (2001) 10,454.
- [25] J. Limtrakul, T. Nanok, P. Khongpracha, S. Jungsuttiwong, T.N. Truong, Chem. Phys. Lett. 349 (2001) 161.

- [26] A.H. de Vries, P. Sherwood, S.J. Cotlins, A.M. Rigby, M. Rigutto, G.J. Kramer, J. Phys. Chem. B 103 (1999) 6133.
- [27] M. Svensson, S. Humbel, R.D.J. Froese, T. Matsubara, S. Sieber, K. Morokuma, J. Phys. Chem. 100 (1996) 19357.
- [28] C. Raksakoon, J. Limtrakul, J. Mol. Struct. (Theochem.) 631 (2003) 147.
- [29] W. Panjan, J. Limtrakul, J. Mol. Struct. 654 (2003) 35.
- [30] S. Kasuriya, S. Namuangruk, P. Treesukol, M. Tirtowidjojo, J. Limtrakul, J. Catal. 219 (2003) 320.
- [31] K. Bobuatong, J. Limtrakul, Appl. Catal. A 253 (2003) 49.
- [32] A. Pelmenschikov, J. Leszczynski, J. Phys. Chem. B 103 (1999) 6886.
- [33] T.A. Wesolowski, O. Parisel, Y. Ellinger, J. Weber, J. Phys. Chem. A 101 (1997) 7818.
- [34] E.G. Derouane, C.D. Chang, Mesopor. Mater. 35-36 (2000) 425.
- [35] L. A. Clark, M. Sierka, J. Sauer, J. Am. Chem. Soc. 125 (2003) 2136.
- [36] A.M. Vos, X. Rozanska, R.A. Schoonheydt, R.A. van Santen, F. Hutschka, J. Hafner, J. Am. Chem. Soc. 123 (2001) 2799.
- [37] X. Rozanska, R. A van Santen, F. Hutschka, J. Hafner, J. Am. Chem. Soc. 123 (2001) 7655.
- [38] D.H. Olson, E. Dempsey, J. Catal. 13 (1969) 221.
- [39] J.R. Hill, C.M. Freeman, B. Delley, J. Phys. Chem. A 103 (1999) 3772.
- [40] A.K. Rappe, C.J. Casewit, K.S. Colwell, W.A. Goddard, W.M. Skiff, J. Am. Chem. Soc. 114 (1992) 10,024.
- [41] M.J. Frisch, G.W. Trucks, H.B. Schlegel, G.E. Scuseria, M.A. Robb, J.R. Cheeseman, V.G. Zakrzewski, J.A. Montgomery, R.E. Stratmann Jr., J.C. Burant, S. Dapprich, J.M. Millam, A.D. Daniels, K.N. Kudin, M.C. Strain, O. Farkas, J. Tornasi, V. Barone, M. Cossi, R. Cammi, B. Mennucci, C. Pomelli, C. Adamo, S. Clifford, J. Ochterski, G.A. Petersson, P.Y. Ayala, Q. Cui, K. Morokuma, P. Salvador, J.J. Dannenberg, D.K. Malick, A.D. Rabuck, K. Raghavuchari, J.B. Foresman, J. Cioslowski, J.V. Ortiz, A.G. Baboul, B.B. Stefanov, G. Liu, A. Liashenko, P. Piskorz, I. Komaromi, R. Gomperts, R.L. Martin, D.J. Fox, T. Keith, M.A. Al-Laham, C.Y. Peng, A. Nanayakkara, M. Challacombe, P.M.W. Gili, B. Johnson, W. Chen, M.W. Wong, J.L. Andres, C. Gonzalez, M. Head-Gordon, E.S. Replogle, J.A. Pople, Gaussian B. Gaussian, Pinsburgh, PA, 2001.
- [42] D. Freude, J. Klinowski, H. Hamdan, Chem. Phys. Lett. 149 (1988) 355.
- [43] N.W. Cant, W.K. Hail, J. Catal. 25 (1972) 161.
- [44] D. Barthomeuf, B.H. Ha, J. Chem. Soc., Faraday Trans. 112 (1973) 2158.
- [45] D.M. Ruthven, M. Goddard, Zeolites 6 (1978) 275.
- [46] S. Siffert, L. Gaillard, B.-L. Su, J. Mol. Catal. A 153 (2000) 267.
- [47] Y. Du, H. Wang, S. Chen, J. Mol. Catal. A 179 (2002) 253.
- [48] P.B. Venuto, P.S. Landis, Adv. Catal. 18 (1968) 259.
- [49] C. Flego, I. Kiricsi, C. Perego, G. Bellussi, Stud. Surf. Sci. Catal. 94 (1995) 405.
- [50] E.M. Evleth, E. Kassab, H. Jessri, M. Allavena, L. Montero, L.R. Sierra, J. Phys. Chem. 100 (1996) 11,368.
- [51] X. Rozanska, Th. Demuth, F. Hutschka, J. Hafner, R.A. van Santen, J. Phys. Chem. B 106 (2002) 3248.
- [52] M. Boronat, C.M. Zircovich-Wilson, P. Viruela, A. Corma, J. Phys. Chem. B 105 (2001) 11,169.
- [53] A.M. Vos, R.A. Schoonheydt, F.D. Proft, P. Geerlings, J. Phys. Chem. B 107 (2003) 2001.
- [54] B. Arstad, S. Kolboe, O. Swang, J. Phys. Chem. B 108 (2004) 2300.



Available online at www.sciencedirect.com





Journal of Molecular Catalysis A: Chemical 207 (2004) 137-146

www.elsevier.com/locate/molcata

Density functional theory study of the ethylene epoxidation over Ti-substituted silicalite (TS-1)

Jumras Limtrakula, i, Chan Inntama, Thanh N. Truongb,*

Computational & Applied Chemistry Laboratory, Physical Chemistry Division, Kasetsart University, Bangkok 10900, Thailand b Department of Chemistry, Henry Eyring Center for Theoretical Chemistry, University of Utah, 315 S 1400 E, Room 2020, Salt Lake City, UT 84112, USA

Received 2 January 2003; received in revised form 10 June 2003; accepted 10 June 2003

Abstract

The mechanism of ethylene epoxidation with hydrogen peroxide over Ti-substituted silicalite (TS-1) catalyst was investigated by using both the cluster and embedded cluster approaches at the B3LYP/6-31G(d) level of theory. The complete catalytic cycle was determined. The epoxidation of ethylene consists of three steps. First, the chemisorption of H₂O₂ at the Ti active site forms the oxygen donating Ti-OOH species and then the transfer of an oxygen atom from the Ti-OOH species to the adsorbed ethylene. The final step is the dehydration of the Ti-OH species to regenerate to active center. The oxygen atom transfer step was found to be the rate-limiting step with the zero-point energy corrected barrier of 17.0 kcal/mol using the embedded cluster model at B3LYP/6-31G(d) level of theory, which is in agreement with the experimental estimate of about 16.7 kcal/mol. Regeneration of the active center by dehydration of the Ti-OOH species was found to have a rather small barrier and the overall process is exothermic. Our results also show that inclusion of the effects of the zeolite crystal framework is crucial for obtaining quantitative energetic information. For instance, the Madelung potential increases the barrier of the oxygen atom transfer step by 5.0 kcal/mol.

@ 2003 Elsevier B.V. All rights reserved.

Keywards: Density functional theory; Ethylene epoxidation; Ti-substituted silicalite

1. Introduction

Ti-substituted silicalite (TS-1) has been widely used as a catalyst for several important oxidation reactions such as the olefin epoxidation, the phenol hydroxylation, cyclohexanone amoxidation, as well as the conversions of ammonia to hydroxylamine, of secondary alcohol to ketone, and of secondary amine to dialkylhydroxylamine [1-7]. In particular, its use in alkene epoxidation reactions with hydrogen peroxide as oxidant has been experimentally [4-7] and theoretically [8-15] studied. The characterization of TS-1 structure and the nature of its active site have been studied experimentally by using X-ray diffraction, IR, Raman, UV-Vis spectroscopy and EXAFS [16-21].

There have been several previous theoretical studies on the oxidation of ethylene over TS-1 catalysts using quan-

culations are often computationally demanding if it is still

feasible. The embedded cluster methodology provides a cost

tum chemistry methods. These studies provided useful information on the mechanism and energetic properties of

the reaction, though complete catalytic cycle has not been

determined and the rate determining step has not been well

understood. Furthermore, all of these studies used the clus-

ter models to represent the reactive center and thus did not include the effects of the zeolite framework. In our previous study, we found that the Madelung potential from the zeolite framework can increase the adsorption energy of ethylene in H-ZSM-5 zeolite by about 50% and bring the predicted results in much closer agreement with experimental observations [22]. This indicates that the Madelung potential could be an important factor in stabilizing the adsorption complexes and transition states for the ethylene epoxidation over TS-1 catalyst. To accurately include the effects of the extended zeolite framework on the catalytic properties, one can employ periodic electronic structure methods, such as the periodic density functional theory methodology. However, due to the large unit cells of typical zeolites, such cal-

^{*} Corresponding author.

E-mail addresses: [scijr]@ku.ac.th (J. Limtrakul), truong@chem.utah.edu (T.N. Truong).

¹ Co-corresponding author.

effective computational strategy for including the effects of the zeolite framework [23–32]. In this approach, the effects of the zeolite framework can be modeled either by a classical molecular mechanic force field or by a set of point charges.

In this study, we investigated the complete catalytic cycle for the alkene oxidation over TS-1 catalysts in the presence of hydroperoxides and the influence of a zeolitic framework, particularly the Madelung potential on the structural and energetic information. The surface charge representation of the external embedded potential (SCREEP) embedded cluster methodology was used. This method has been found to be rather accurate in representing the Madelung potential for studying adsorptions and reactions in zeolites [22,26-31].

2. Method

The active site of TS-1 is modeled by a five-tetrahedral (ST) cluster (OH)₂Ti[OSi(OH)₂OSiH₃]₂ selected from the ZSM-5 zeolite structure where the Ti atom is located at the T12 site. To have a more accurate description of the active site, OH terminations were used for Si atoms closed to the Ti atom. The T12 site has been used as an active site of ZSM-5 in many theoretical studies since it was predicted to be among the most stable Brønsted acid sites [33,34]. It is located at the intersection of main and sinusoidal channels and is accessible to adsorbates. It should be noted that the preferred Ti-substitution sites in TS-1 are still not known for certain and thus require further detailed study. The 5T cluster used in this study (see Fig. 1) is one half of the 10T ring and is the largest cluster that has been used previously. For the embedded cluster model, (see Fig. 1), this 5T cluster is embedded in a set of point charges according to the surface charge representation of external embedded potential method [23]. Accuracy of this method for modeling adsorption processes in zeolites has already been addressed in

several previous studies [22,26-31]. These models consist of three layers. The center layer is a five-tetrahedral (5T) quantum chemical cluster. The next layer of the model is a set of explicit point charges located at the lattice positions. Their magnitudes were derived from periodic population analyses of zeolite systems. To minimize the interaction that occurs between the quantum mechanical terminating hydrogens and the neighboring point charges, the layer of explicit point charges nearest to the quantum cluster is moved out and combined with the next layer of point charges. The charge values of the moved point charges are fitted to minimize deviation from the original external electrostatic field. The outermost layer of the model is the SCREEP surface represented by a set of surface point charges to model the remaining Madelung potential from the extended zeolite crystal.

All geometry optimizations were done at the B3LYP/6-31G(d) level. The two SiH₃ groups and H atoms of the six OH groups bonded to the Ti and Si atoms were fixed along the Si-O crystal framework (see Fig. 2) while other atoms in the quantum cluster were allowed to relax in all geometry optimizations. Normal mode analyses were carried out to verify the transition states to have one imaginary frequency whose mode correspond to the designated reaction. All calculations were done using the Gaussian98 program [35].

3. Results and discussion

For the purpose of clarity, we separate the discussion below into two sub-sections. In one sub-section we discuss only the mechanisms of ethylene epoxidation by the TS-1 zeolite using the embedded cluster model. In the other section we focus only on the effects of the Madelung potential on structural and energetic information of this reaction by comparing the differences in the results predicted by the embedded and bare cluster models.

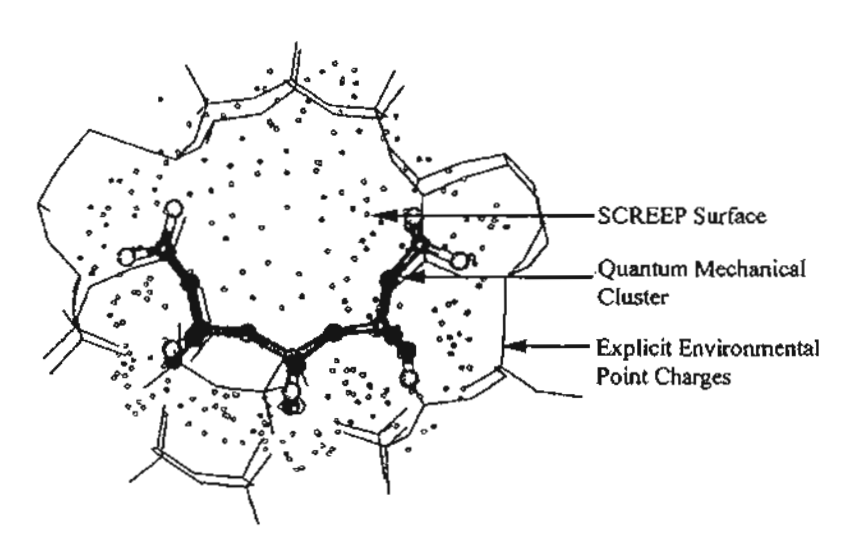


Fig. 1. SCREEP embedded cluster model for studying adsorption or reaction in zeolites.

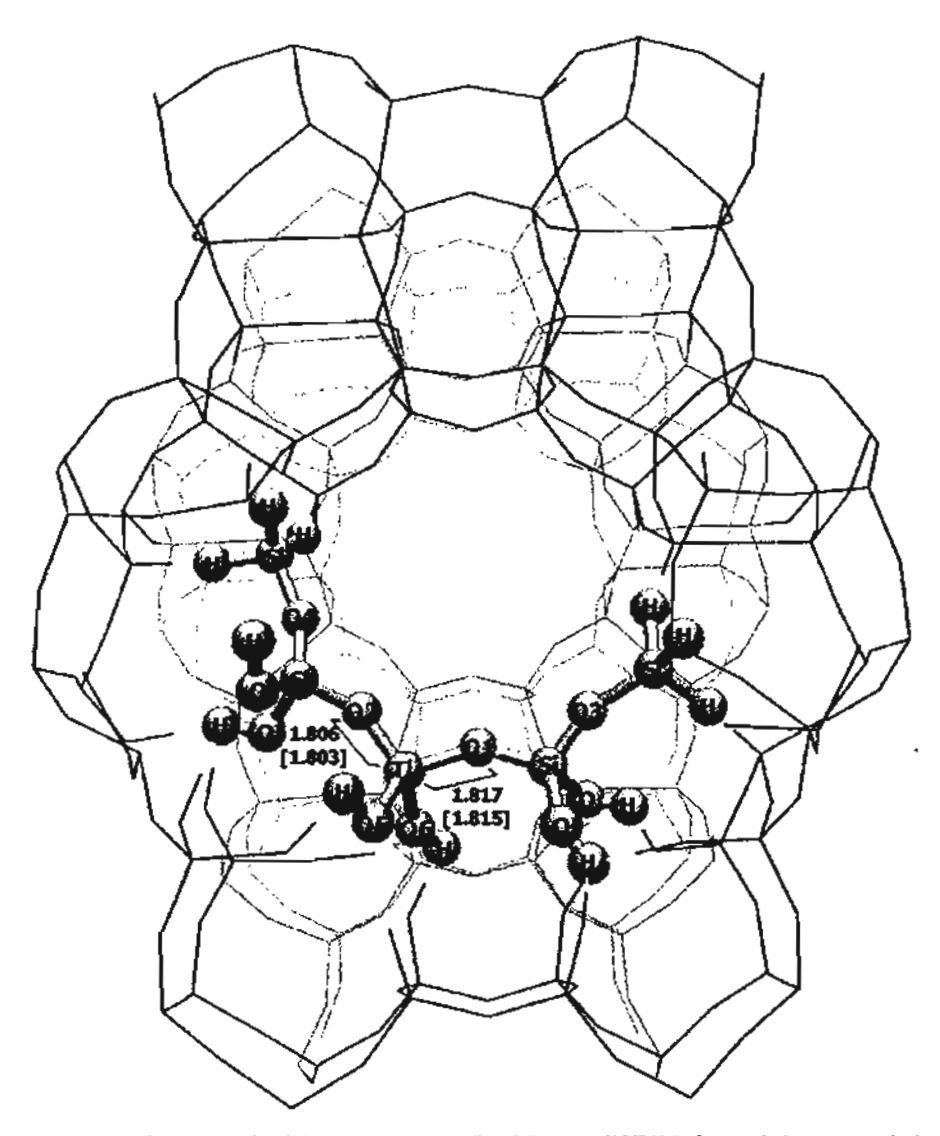


Fig. 2. Embedded ST cluster model of the active site Ti(IV) of the TS-1 zeolite. Selected B3LYP/6-31G(d) optimized geometrical parameters using both the bare cluster and embedded cluster models are also given. The values in parentheses are obtained from the cluster model.

3.1. Chemistry of ethylene epoxidation by TS-1 zeolite

The complete catalytic cycle of the ethylene epoxidation by hydrogen peroxide is known to consist of three steps: (1) chemisorption of hydrogen peroxide to form Ti-OOH active species; (2) epoxidation of ethylene by the Ti-OOH species and the desorption of the adsorbed ethylene epoxide; and (3) dehydration to regenerate the active center [8-15]. It is informative to first discuss the nature of the active site in comparison with known experimental data. This would provide indication on the accuracy of the computational method.

3.1.1. The active site

In this study, the active site of TS-1 is modeled by a Ti(IV) atom located at the T12 site of the ZSM-5 zeolite framework as shown in Fig. 2. Selected optimized geometrical parameters are reported in Table 1, and also depicted in Fig. 2.

Table 1
Selected optimized geometrical parameters of the active site of TS-1 using both the bare cluster and embedded cluster models at the B3LYP/6-31G(d) level of theory

Bond (Å) or angle (°)	Embedded	Bare cluster	Expt.
Ti-O1	1.817	1.815	-
Ti-O2	1.806	1.803	-
Ti-O5	1.804	1.805	-
Ti-06	1.766	1.790	_
(Ti-O)	1.798	1.803	1.79°, 1.80–{.81°
Si-O1	1.630	1.642	-
\$i-O2	1.633	1.646	-
(Si-O)	1.635	1.650	_
∠Ti-O1-Si	150.7	152.4	
∠Ti-O2-\$i	140.6	144.7	
∠O1-Ti-O2	108.3	110.5	-

^{*} XRD data is taken from [36].

b EXAFS data are taken from [19,37,38].

The calculated average Ti-O bond lengths of 1.798 Å is in good agreement with that of 1.79 Å obtained from XRD experiments [36] and of 1.80-I.81 \pm 0.01 Å from EXAFS [19,37,38] experiments.

3.1.2. Chemisorption of H₂O₇

 H_2O_2 chemisorbs on the Ti active site to form two possible active oxygen donor species, Ti-OOH denoted as Ti(η_1 -OOH) and Ti(η_2 -OOH). In the former, the terminal oxygen atom of the OOH group binds to the Ti atom whereas in the latter both oxygen atoms of the OOH group bind to the Ti atom resembling a bidentate configuration.

The $Ti(\eta_2\text{-OOH})$ species was found to be more stable than the $Ti(\eta_1\text{-OOH})$ by about 9.2 kcal/mol. This is slightly larger than that of 8.0 kcal/mol from the DFT/DNP done by Karlsen and Schoeffel [9]. For this reason, we focused only on the formation of the $Ti(\eta_2\text{-OOH})$ species and its interaction with ethylene in the second step of the epoxidation process.

Fig. 3 shows structures of the stationary points for the dissociative chemisorption of H_2O_2 on the active site of TS-1 to form the $Ti(\eta_2\text{-OOH})$ species. Selected optimized geometrical parameters are listed in Table 2. H_2O_2 first molecularly adsorbs to the active site with the O_a atom binding to the Ti atom at the distance of 2.469 Å. The corresponding adsorption energies for the $H_2O_2/5T$ complex is -10.8 kcal/mol. This is lower than that of -7.4 kcal/mol from non-local GGA/BP DFT single-point energy calculations at the optimized local LDA/VWN geometries done by Munakata et al. [15]. The difference is partly due to the inclusion of H-bonding such as between H_a - O_3 in our adsorbed complex (see Fig. 3a) but not in the model used by Munakata et al. [15].

The transition structure for chemisorption of H₂O₂ on TS-1 zeolite is shown in Fig. 3b. The chemisorption of the H₂O₂ molecule occurs over both the Ti and O1 atoms rather than just over the Ti atom. As the adsorption complex approaches the transition state the Ti-Oa bond is shortened from 2.469 to 2.151 Å, and the Ha atom migrates to the OI atom with the Oa-Ha bond elongated from 0.976 to 1.249 Å. Due to the change in the valancy of the O1 atom as Ha migrating over, the Ti-O1 bond distance is elongated from 1.826 to 2.043 Å. Continuing trends are observed as the system moves from the transition state to form the dissociated product, Ti(n2-OOH). Note that this complex plays a major role as an oxidizing agent in the oxidation reaction of unsaturated hydrocarbons. The optimized structure of Ti(n2-OOH) is in agreement with available experimental data [10] found in the crystal structure of $\{[(\eta_2-tert-buty|peroxo)titanatrane]_2-3-dichrolomethane\}$ $Ti-O_a = 1.97 \text{ Å}$ versus 1.91 Å, $Ti-O_b = 2.21 \text{ Å}$ versus 2.27 Å and O_a - O_b = 1.48 Å versus 1.47 Å (the latter numbers are the experimental results).

The barrier height, $\Delta E_a^{\rm I}$, for the chemisorption of H_2O_2 is predicted to be 13.6 kcal/mol. Our finding is consistent with the previously reported barrier of 11.9 kcal/mol ob-

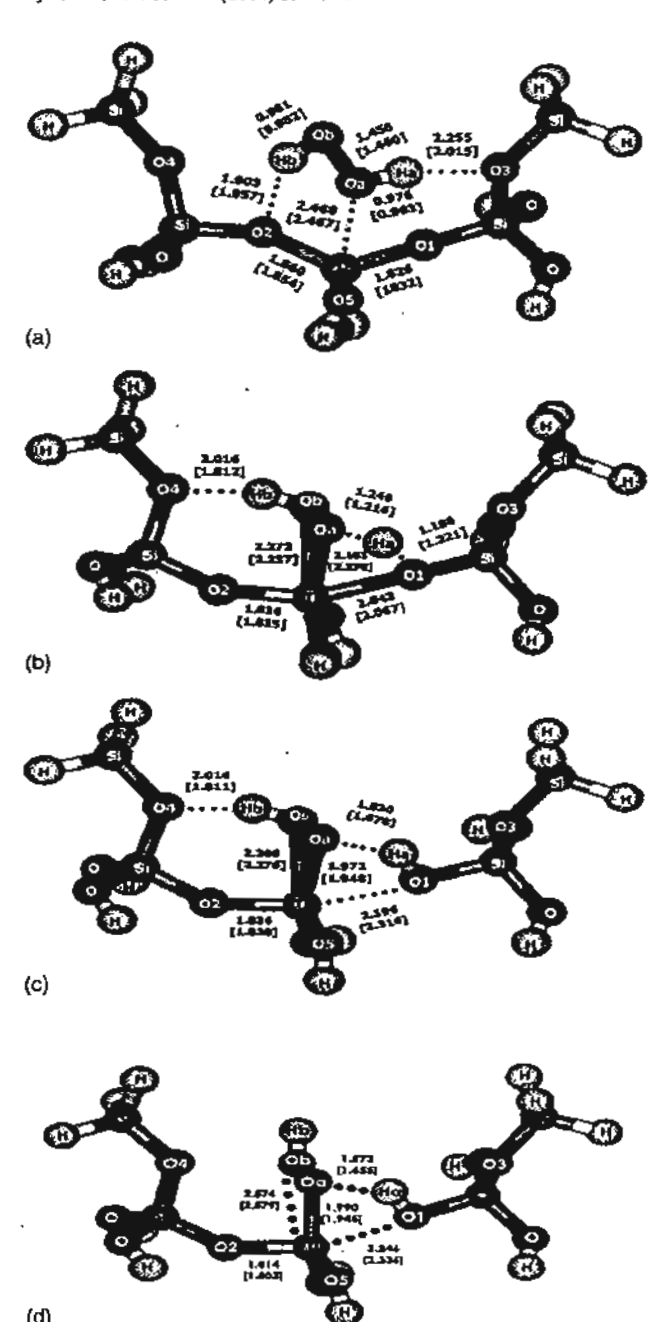


Fig. 3. Structures of the $H_2O_2/TS-1$ complexes: (a) physisorbed complex; (b) transition state structure; (c) chemisorbed $Ti(\eta_2\text{-OOH})$ complex; (d) chemisorbed $Ti(\eta_1\text{-OOH})$ complex. Selected B3LYP/6-31G(d) optimized geometrical parameters using both the bare cluster and embedded cluster models are also given. The values in parentheses are obtained from the cluster model.

tained from BP86/DZVP calculations but with a smaller cluster [11]. The formation of $Ti(\eta_2\text{-OOH})$ active species (Fig. 3c) is found to be energetically favorable with the reaction energy calculated to be -3.2 kcal/mol. Our predicted reaction energy is lower than that of Munakata et. al. [15] by 5.8 kcal/mol which may be due to the inclusion

Table 2 Selected optimized geometrical parameters for the $H_2O_2/TS-1$ system: (3a) physisorbed complex; (3b) transition state; (3c) chemisorbed product at the B3LYP/6-31G(d) level of theory

Bond (Å) or	Physisorbed con	hysisorbed complex (Fig. 3a)		Transition state (Fig. 3b) Ti(Ti(η2-OOH) complex (Fig. 3c)		Ti(η ₁ -OOH) complex (Fig. 3d	
angic (°)	Embedded cluster	Bare cluster	Embedded cluster	Bare cluster	Embedded cluster	Bare cluster	Embedded cluster	Bare cluster	
Ti-O.	2.469	2.467	2.151	2.170	1.972	1.948	1.990	1.945	
11-O₀	_	-	2.272	2.237	2.208	2.276	2.574	2.579	
ฑ-0เ	1.826	1.832	2.043	2.067	2.196	2.316	2.246	2.336	
Ti-O2	1.860	1.854	1.836	1.835	1.836	1.820	1.814	1.803	
O _a -O _b	1.455	1.460	1.478	1.477	1.479	1.475	1.476	1.470	
O ₆ -H ₆	0.981	0.982	0.983	0.992	0.983	0.990	0.974	0.972	
O ₄ -H ₄	0.976	0.983	1.249	1.216	1.830	1.678	1.573	1.655	
OI-H.	2,543	2.495	1.188	1.222	0.987	0.999	1.015	1.000	
03-H,	2.255	2.015	_	_	_	-	_	-	
02~Hb	1.903	1.957	_	_	_	_		-	
04-H _b	2.509	2.434	2.016	2.016	2.016	1.811	3.126	3.068	
∠Ti-O1-Si	157.3	155.1	138.9	154.9	137.0	177.5	171.8	178.4	
∠TiO2-Si	138.6	144.3	154.4	1527	143.7	146.1	141.6	144.7	
∠Ti-O₁-O₀	113.6	110.8	75.0	72.9	78.1	82.1	94.8	97.1	
∠O1-Ti-O2	116.2	119.2	156.2	155.9	163.1	158.4	154.8	155.5	

of additional hydrogen bonding in our physical model, as mentioned earlier.

3.1.3. Epoxidation of ethylene by $Ti(\eta_2\text{-}OOH)$ and desorption of ethylene epoxide

Fig. 4 shows the structures of the oxygen atom transfer from the active $Ti(\eta_2\text{-OOH})$ species to the absorbed ethylene and of the adsorbed product ethylene epoxide. Selected optimized geometrical parameters for these two stationary points are given in the figure and are also listed in Table 3. The ethylene molecule preferably attacks the $Ti(\eta_2\text{-OOH})$ at the O_a position yielding the product of ethylene epoxide

Table 3 Selected B3LYP/6-31G(d) optimized geometrical parameters for the $C_2H_4/Ti(\gamma_2\text{-OOH})$ complexes

Bond (Å) or angle (°)	Transition st (Fig. 5a)	nucture	Epoxide coπ (Fig. 5b)	plex
	Embedded cluster	Bare cluster	Embedded cluster	Bare cluster
Ti-O _a	2.037	2.053	2.314	2.461
Ti-O _b	2.087	2.043	1.988	1.932
Ti-OI	2.323	2.333	2.327	2.341
Ti-O2	1.830	1.818	1.818	1.815
O ₄ -O ₆	1.791	1.807	2.636	2.622
O_b-H_b	0.974	0.979	0.970	0.972
O4-Hb	2.300	1.993	2.679	2.320
Ob-Ha	2.227	2.204	1.483	1.590
O _a -H _a	1.638	1.709	2.760	2.789
OI-H.	200.1	0.997	1.038	1.013
O _a Cl	2.149	2.107	1.458	1.448
O,-C2	2.265	2.152	1.458	1.450
C1-C2	1.355	1.358	1.467	1.466
∠Ti-O1-Si	173.9	{71.6	167.5	176.5
∠3ĭ-O2-Si	144.0	142.8	142.6	143.1
∠1ĭ-0,-C	122.8	122.8	112.8	114.2
∠O1~1ĭ~O2	160.6	161.5	162.7	162.8
∠C1~Oa~C2	60.3	60.8	35.6	52.4

(see Fig. 4a). A similar finding has also recently been reported [10]. At the transition state, the Ti-O_a distance (see Fig. 4a) is elongated from 1.972 to 2.037 Å. The C1-C2 distance is calculated to be 1.355 Å which is only slightly larger than the corresponding C-C distance of the isolated C₂H₄ (1.331 Å) and is significantly smaller than that of the isolated epoxide OC₂H₄ species (1.430 Å). This indicates that the transition state is closer to the reactant than the product. Since the reaction is rather exothermic of 42.4 kcal/mol, this result is consistent with the Hammond postulate (Table 4).

The barrier for the ethylene epoxidation, ΔE_a^{II} , is predicted to be 18.5 kcal/mol. As compared to the chemisorption of H_2O_2 step, the ethylene epoxidation is the rate-limiting step in this catalytic process. Including the zero-point energy correction lowers this barrier to 17.0 kcal/mol. This result is particularly encouraging since it compares well with the experimental estimate for the activation barrier of 16.7 kcal/mol [39]. Fig. 4b illustrates the product, OC_2H_4 , adsorbed on the Ti-OH complex. We found that O-C1 and O-C2 distances of the OC_2H_4 molecule are virtually identical (1.448 Å versus 1.450 Å). These distances are slightly different from those of the isolate OC_2H_4

Table 4
Energies (kcal/mol) of stable complexes and transition states for the ethylene epoxidation reaction relative to the separated reactants

	B3LYP/6-31G(d)		
	Embedded cluster	Bare cluster	
Physisorption complex (Fig. 3a)	~10.8	-16.3	
Transition state I (Fig. 3b)	2.8	-4.7	
Ti(η2-OOH) complex (Fig. 3c)	-3.2	-6.7	
Transition state II (Fig. 4a)	15.3	6.8	
Epoxide complex (Fig. 4b)	-45.6	-53.6	
Transition state III (Fig. 5b)	-41.6	-46.2	
Water adsorption complex (Fig. 5c)	-67.6	-64.5	

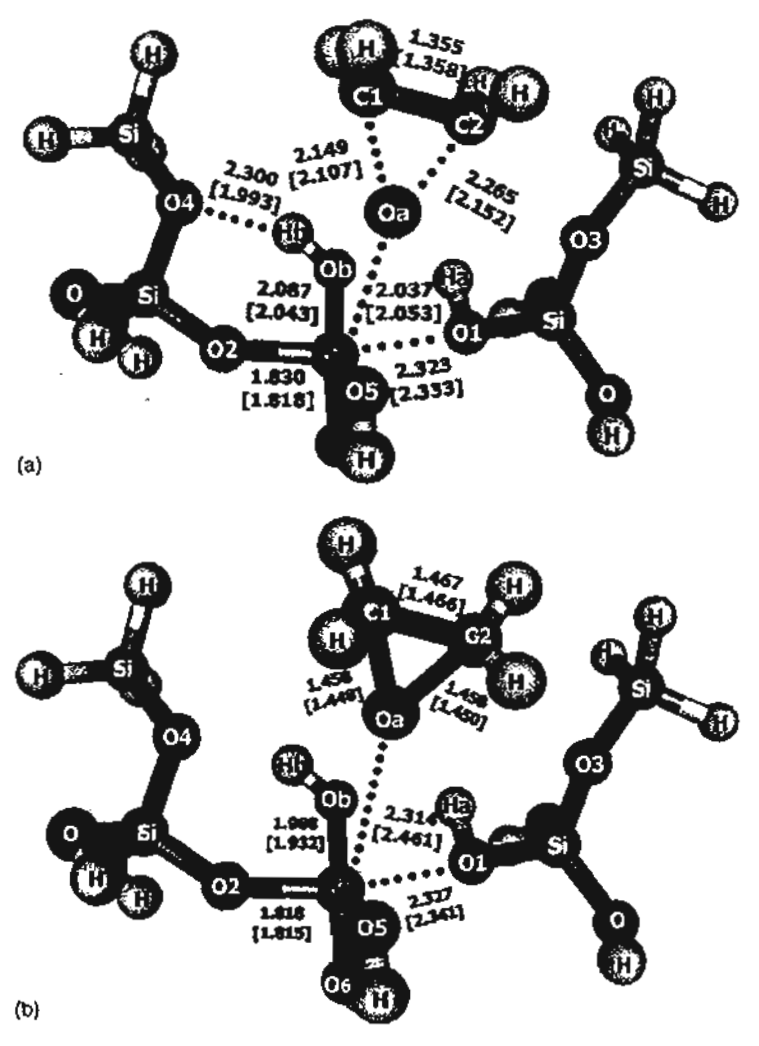


Fig. 4. Similar to Fig. 3, except for the geometries of (a) the transition state structure of the epoxidation step and (b) the adsorbed ethylene epoxide complex.

species, C-O = 1.431 Å. The reaction energy for formation of the $OC_2H_4/TiOH$ complex is -45.6 kcal/mol with respect to the separated reactants. In addition, we found that the calculated desorption energy of OC_2H_4 from the Ti-OH complex is predicted to be 3.3 kcal/mol.

3.1.4. Dehydration to regenerate the active site

Previous studies have not considered the regeneration the active site by dehydration of the Ti-OH species. As shown in Fig. 5a-c, we found that this step involves the migration of a hydrogen atom H1 bound to the zeolite frame-work oxygen atom O3 to the oxygen of the Ti-OH species and the strengthening of Ti-O3 bond. In particular, the Ti-O2 from 1.903 to 2.266 Å. The concerted motion of the hydrogen migration and the shortening of the Ti-O3 bond lead to a rather small barrier to dehydration step of 0.6 kcal/mol relative to the energy of the Ti-OH species. The product of this step is the adsorbed water on the Ti active site. The step is also rather exothermic with the reaction energy of -25.4 kcal/mol with respect to the Ti-OH species. Desorp-

tion of the adsorbed water to regenerate the Ti active site requires 21.1 kcal/mol.

3.1.5. Discussion

Figs. 6 and 7 illustrate the catalytic cycle and schematic energy profile along this cycle with respect to the overall zero of energy, namely the energies of the separated reactants. It is clear that the rate-limiting step is the oxygen migration from the Ti-OOH active species to the adsorbed ethylene. This step has the barrier of 15.3 kcal/mol relative to the overall zero and of 18.5 kcal/mol relative to the stable intermediate of adsorbed ethylene on the Ti-OOH species. The overall energy of the catalytic cycle is -46.5 kcal/mol. It is interesting to compare our present results with those from previous studies. Wu and Lai [8] reported a BLYP study using the HOOTi(OH)3 cluster model to study the epoxidation step and found the barrier height to be 10.7 kcal/mol. Karlsen and Schoffel [9] used a rather small Ti(OH)4 cluster with the B88LYP/DNP method and found the corresponding barrier height to be 22.9 kcal/mol. Hillier and co-workers

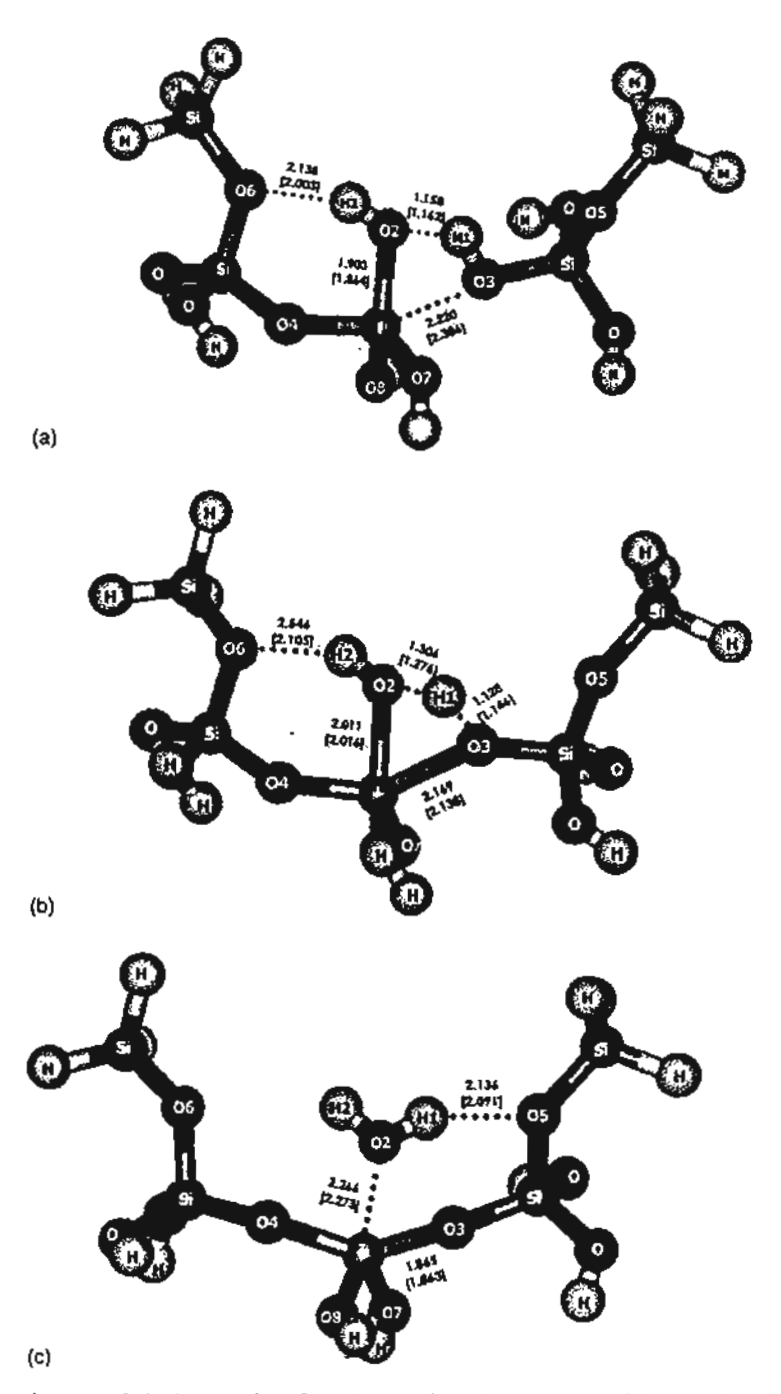


Fig. 5. Similar to Fig. 3, except for the optimized geometries of (a) the Ti-OH species; (b) the transition state for the dehydration step; and (c) the adsorbed water on the Ti active site.

[10] employed the B3LYP/3-21G(d) level of theory with the (H₃SO)₃Ti(IV)-O(1)O(2)H/MeOH cluster model and found that the corresponding barrier beight was estimated to be 11.9 kcal/mol. Using a different 4T cluster model with the BP86 DFT method, Sinclair and Catlow [11] found that the chemisorption of H₂O₂ is the rate-limiting step instead of the epoxidation step with the barrier of 13.3 kcal/mol whereas the epoxidation step has a lower barrier of 10.2 kcal/mol.

Munakata et al. [15] performed BP//VWN calculations with a different 5T cluster to model the Ti active site. The authors modeled the epoxidation reaction with an additional water molecule in coordination with the adsorbates, H₂O₂ and C₂H₄ and found the barrier, relative to the complex [active site-H₂O·C₂H₄], is about 18.3 kcal/mol. The estimated barrier of the epoxidation step is 15.8 kcal/mol with respect to the separated reactants. Our study does not consider such

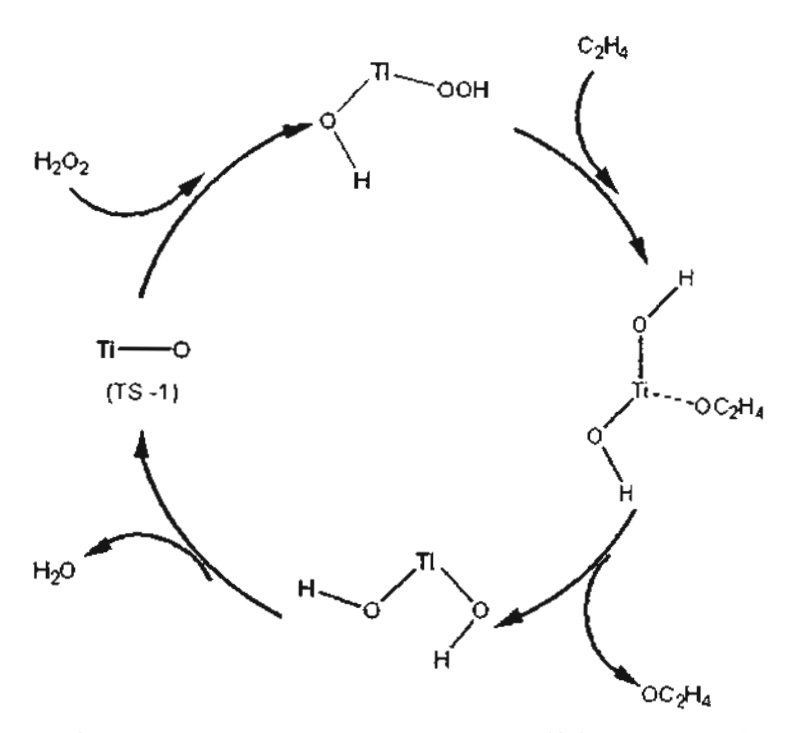


Fig. 6. Schematic diagram to illustrate the catalytic cycle for the epoxidation of ethylene by TS-1 zeolite.

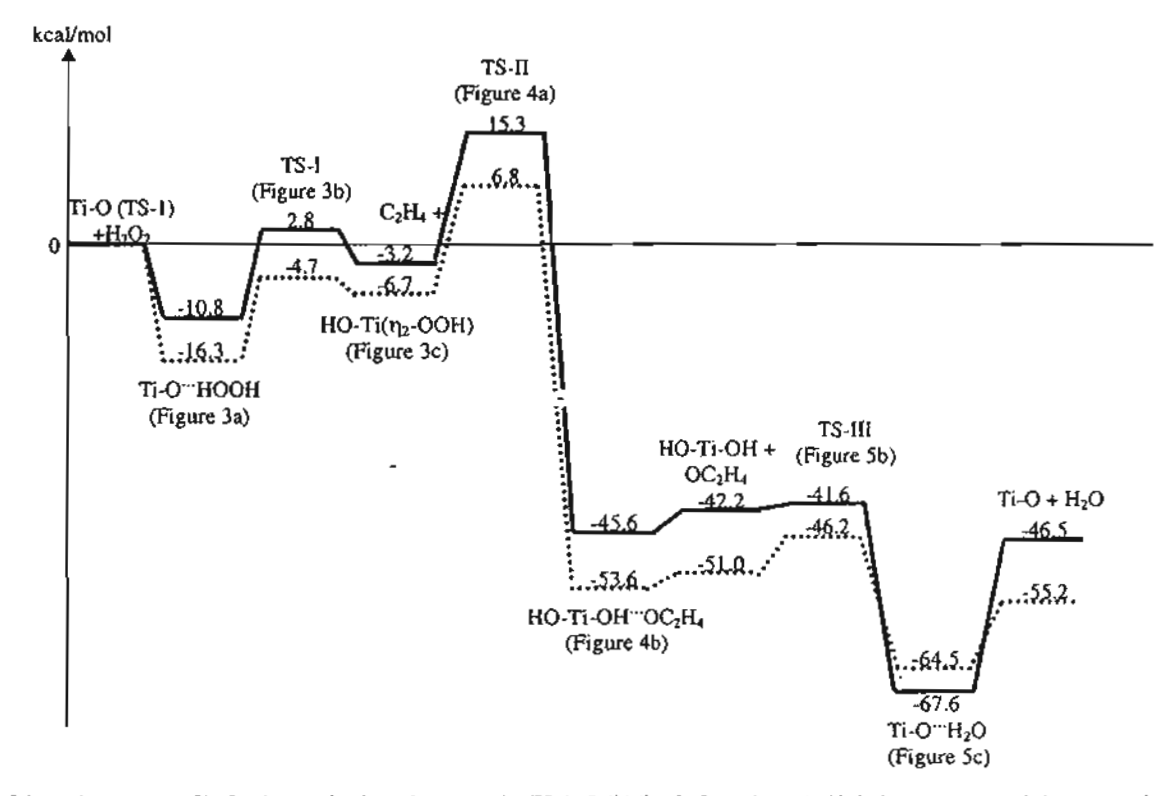


Fig. 7. Schematic energy profile for the epoxidation of ethylene by TS-1. Solid line is from the embedded cluster results and the dashed line is from the bare cluster results using the B3LYP/6-31G(d) level of theory.

additional water and our results are also consistent with available experimental data. Thus, it is not clear what are the roles of the water in overall mechanism for the ethylene epoxidation by hydrogen peroxide in TS-1 zeolite. Though water is produced in the dehydration step with the adsorption energy of -21.1 kcal/mol that is almost twice larger than the adsorption of the hydrogen peroxide on the Ti active site. However, the overall exothermicity of the catalytic cycle of -46.5 kcal/mol would have sufficient energy to regenerate the active center. More study is certainly needed to further understand the roles of water in the mechanism of this reaction.

3.2. Effects of the Madelung potential

We found that the local structure of the active site of the TS-1 model is not very sensitive to the inclusion of the Madelung potentials. It is noted that the Madelung potential has an effect of destabilizing $Ti(\eta_1\text{-OOH})$ and $Ti(\eta_2\text{-OOH})$ by about 3.5 kcal/mol for the n2 structure (Fig. 3c) and 2.1 kcal/mol for the η_1 structure (Fig. 3d) does not change the order of relative stability of the two complexes. The Madelung potential from the zeolite framework has a significant effect on the adsorption structure, particularly the hydrogen H_b-O₂ and H_a-O₃ bonds where it shortens the former by 0.05 Å and elongates the latter by 0.3 Å. Consequently, it lowers the adsorption energy (or increases the binding energy) by 5.5 kcal/mol. We found that the effects of the Madelung potential on the structure increase as the reaction proceeds toward the product. In fact at the dissociated product, Ti(n2-OOH) as shown in Fig. 3c, such effects were found to be noticeably large. The Ti-O1 bond is shortened by 0.12 Å while Ti-O_a is elongated by 0.03 Å. For the transition state to oxygen migration step to form ethylene epoxide, the Ti-O₂ bond distance is shortened by 0.16 Å. As a result, the Madelung potential increases the barrier for this rate-limiting step by 5.0 kcal/mol. The largest effect of the Madelung potential is seen in the desorption energy of water to regenerate the Ti active site. It increases the water desorption energy by 11.8 kcal/mol.

A general observation from these results and from the differences between our cluster and embedded cluster results is that the effects of the Madelung potential are rather large and thus the embedded cluster model used in this study appears to provide more quantitative information on the energetic properties as compared with experimental observation.

4. Conclusion

We have carried systematic ab initio cluster and embedded cluster studies on the mechanism of the ethylene epoxidation by hydrogen peroxide over the Ti-substituted silicalite zeolite. B3LYP/6-31G(d) level of theory was employed. The active site of the TS-1 zeolite was modeled by a 5T cluster. The effects of the Madelung potential from extended zeolite framework on the structural and energetic properties of this process were investigated. The complete catalytic cycle was determined. The reaction involves three steps: (a) the chemisorption of hydrogen peroxide to form Ti-OOH active species; (b) the oxygen atom transfer from the Ti-OOH active species to the adsorbed ethylene to form the produce ethylene peroxide and Ti-OH species; and (c) the dehydration of Ti-OH species to regenerate the Ti active site. The chemisorption of the H₂O₂ molecule on the TS-1 catalyst has the barrier of 13.6 kcal/mol to form dominantly oxygen donor species, Ti(η2-OOH) using the embedded cluster model. For the epoxide formation, the ethylene molecule interacts with the oxygen atom close to the Ti atom of the Ti(n2-OOH) complex. The epoxidation step is found to be the rate-limiting step where the oxygen atom from the Ti-OOH group transfer to the adsorbed ethylene molecule. The predicted activation energy including the zero-point energy correction for this step is 17.0 kcal/mol. Our predicted results are in agreement with the experimental estimate for the activation barrier of 16.7 kcal/mol. The dehydration of the Ti-OH species to regenerate the Ti active site has rather small barrier. We found that the Madelung effects are rather large, in particular they increase the activation energy of the rate-limiting step by 5.0 kcal/mol.

Acknowledgements

This work is supported by grants from the Thailand Research Fund (senior TRF research scholar), the Development and Promotion for Science and Technology Talents project (DPST), the Kasetsart University Research and Development Institute (KURDI) and the Ministry of University Affairs under the Science and Technology Higher Education Development Project (MUA-ADB funds). It is also supported in part by the ACS-PRF fund to TNT. The computer support from the University of Utah Center for High Performance Computing and Kasetsart 72 clusters is gratefully acknowledged. Our sincere thanks are due to Professor R. Ahlrichs (Karlsruhe, Germany) for his continued support of this work.

References

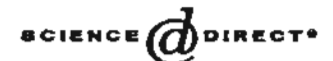
- [1] M. Taramasso, G. Perego, B. Notari, U.S. Patent 4,410,501 (1983).
- [2] B. Notari, Adv. Catal. 41 (1996) 253.
- [3] I.W.C.E. Arends, R.A. Sheldon, M. Wallau, U. Schuchardt, Angew. Chem. 36 (1997) 1144.
- [4] M.G. Clerici, P. Ingallina, J. Catal, 140 (1993) 71.
- [5] M.G. Clerici, G. Bellussi, U. Romano, J. Catal. 129 (1991) 159.
- [6] C.B. Khouw, C.B. Daru, J.A. Labinger, M.E. Davis, J. Catal. 149 (1994) 195.
- [7] G. Bellussi, A. Catari, M. Clerici, G. Maddinelli, R. Millim, J. Catal. 133 (1992) 220.
- [8] Y.D. Wu, D.K.M. Lai, J. Org. Chem. 60 (1995) 673.
- [9] E. Karlsen, K. Schoffel, Catal. Today 32 (1996) 107.

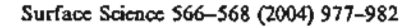
- [10] D. Tantanak, M.A. Vincent, I.H. Hillier, Chem. Commun. (1998) 1031.
- [11] P.E. Sinclair, C.R.A. Catlow, J. Phys. Chem. B 103 (1999) 1084.
- [12] P.E. Sinclair, C.R.A. Catlow, Chem. Commun. (1997) 1881.
- [13] M. Neurock, L.E. Manzer, Chem. Commun. (1996) 1133.
- [14] G.N. Vayssilov, R.A. van Santen, J. Catal. 175 (1998) 170.
- [15] H. Munakata, Y. Oumi, A. Miyamoto, J. Phys. Chem. B 105 (2001) 3493.
- [16] G. Ricchiardi, A. Damin, S. Bordiga, C. Lamberti, G. Spano, F. Rivetti, A. Zecchina, J. Am. Chem. Soc. 123 (2001) 11409.
- [17] J. Sudhakar Reddy, S. Sivasanker, P. Ratnasarny, J. Mol. Catal. 69 (1991) 383.
- [18] T. Blasco, M.A. Camblor, A. Corma, J. Perez-Pariente, J. Am. Chem. Soc. 115 (1993) 11806.
- [19] S. Bordiga, S. Collucia, C. Lamberti, L. Marchese, A. Zecchina, F. Boscherini, F. Buff, F. Genoni, G. Leofanti, G. Petrini, G. Vlaic, J. Phys. Chem. 98 (1994) 4125.
- [20] F.J. Feher, D.A. Newman, J.F. Walzner, J. Am. Chem. Soc. 111 (1989) 1741.
- [21] A. Zecchina, S. Bordiga, C. Lamberti, G. Ricchiardi, D. Scaranto, G. Petrini, G. Leofanti, M. Mantegazza, Catal. Today 32 (1996) 97.
- [22] J. Limtrakul, T. Nanok, P. Khongpracha, S. Jungsuttiwong, T.N. Truong, Chem. Phys. Lett. 349 (2001) 161.
- [23] E.V. Stefanovich, T.N. Truong, J. Phys. Chem. B 102 (1998) 3018.
- [24] S.P. Greatbanks, I.H. Hillier, N.A. Burton, P. Sherwood, J. Chem. Phys. 105 (1996) 3370.
- [25] R.Z. Khaliullin, A.T. Bell, V.B. Kazansky, J. Phys. Chem. A 105 (2001) 10454.
- [26] P. Treesukol, J. Limurakul, T.N. Truong, J. Phys. Chem. B 105 (2001) 2421.
- [27] J. Limtrakul, P. Khongpracha, S. Jungsuttiwong, T.N. Truong, J. Mol. Catal. A 153 (2000) 2469.
- [28] S. Jungsuttiwong, S. Nokbin, P. Chuichay, P. Khongpracha, T.N. Truong, J. Limtrakul, Stud. Surf. Sci. Catal. 135 (2001) 2518.
- [29] J. Limtrakul, P. Khongpracha, S. Jungsuttiwong, J. Mol. Struct. 525 (2000) 153.
- [30] J. Limtrakut, S. Nokbin, P. Chuichay, J. Mol. Struct. 560 (2001) 169.
- [31] J. Limtrakul, S. Nokbin, S. Jungsuttiwong, P. Khongpracha, T.N. Truong, Stud. Surf. Sci. Catal. 135 (2001) 2469.

- [32] (a) R. Vetrivel, C.R.A. Catlow, E.A. Colbourn, Proc. R. Soc. London A 417 (1998) 81;
 - (b) M. Allavena, K. Seiti, E. Kassab, G. Ferency, J.G. Angyan, Chem. Phys. Lett. 168 (1990) 461;
 - (c) G. Aloisi, P. Barnes, C.R.A. Catlow, R.A. Jackson, A.J. Richard, J. Phys. Chem. 93 (1990) 3573;
 - (d) J.C. White, A.C. Hess, J. Phys. Chem. 97 (1993) 8730;
 - (e) E.H. Teunisson, A.P.J. Jansen, R.A. van Santen, R. Orlando, R. Dovesi, J. Phys. Chem. 101 (1994) 5865;
 - (f) A. Kyrlidis, S.J. Cook, A.K. Chakraborty, A.T. Bell, D.N. Theodorou, J. Phys Chem. 99 (1995) 1505;
 - (g) E.H. Teunissen, A.P.J. Jansen, R.A. van Santen, J. Phys. Chem. 99 (1995) 1873;
 - (h) U. Eichler, M. Brandle, J. Sauer, J. Phys. Chem. B 99 (1997) 1873:
 - (i) M. Brandle, J. Sauer, J. Am. Chem. Soc. 120 (1998) 1556.
- [33] E.G. Derouane, J.G. Fripat, Zeolites 5 (1985) 165.
- [34] A.E. Alvaradoswaisgood, M.K. Baw, P.T. Hay, A. Redondo, J. Phys. Chem. 95 (1991) 10031.
- [35] M.J. Frisch, G.W. Trucks, H.B. Schlegel, G.E. Scuseria, M.A. Robb, J.R. Cheeseman, V.G. Zakrzewski, J.A. Montgomery, R.E. Stratmann, J.C. Burant, S. Dapprich, J.M. Millam, A.D. Daniels, K.N. Kudin, M.C. Strain, O. Parkas, J. Tomasi, V. Barone, M. Cossi, R. Cammi, B. Mennucci, C. Pomelli, C. Adamo, S. Clifford, J. Ochterski, G.A. Petersson, P.Y. Ayala, Q. Cui, K. Morokuma, P. Salvador, J.J. Dannenberg, D.K. Malick, A.D. Rabuck, K. Raghavachari, J.B. Foresman, J. Cioslowski, J.V. Ortiz, A.G. Baboul, B.B. Stefanov, G. Liu, A. Liashenko, P. Piskorz, I. Komaromi, R. Gomperts, R.L. Martin, D.J. Fox, T. Keith, M.A. Al-Laham, C.Y. Peng, A. Nanayakkara, M. Challacombe, P.M.W. Gill, B. Johnson, W. Chen, M.W. Wong, J.L. Andres, C. Gonzalez, M. Head-Gordon, E.S. Replogle, J.A. Popte, Gaussian '98, Gaussian, Inc., Pittsburgh, PA, 2001.
- [36] G. Bellussi, V. Fatore, Stud. Surf. Sci. Catal. 69 (1991) 79.
- [37] S. Pei, G.W. Zajak, J.A. Kaduck, J. Faber, B.I. Boyanov, D. Duck, D. Fazzini, T.I. Morrison, D.S. Yang, Catal. Lett. 21 (1993) 333.
- [38] R.J. Davis, Z. Liu, J.E. Tabora, W.S. Wielband, Catal. Lett. 34 (1995) 101.
- [39] A. van der Pol, J.H.C. van Hooff, Appl. Catal. A 106 (1993) 97.



Available online at www.sciencedirect.com







DFT plane-wave calculations of the Rh/MgO(001) interface

Somkiat Nokbin a,b, Jumras Limtrakul b, Kersti Hermansson a,*

Materials Chemistry, The Angström Laboratory, Box 538, SE-751 21 Uppsala, Sweden
 Laboratory for Computational and Applied Chemistry, Department of Chemistry, Kasetsart University, Bangkok 10900, Thailand
 Available online 15 June 2004

Abstract

The Rh/MgO(001) system has been studied by periodic plane-wave density functional calculations using the VASP code and PAW potentials. Four different adsorption sites (which were reduced to three after optimization) and three different surface coverages were investigated. For the most stable site, above O, the adhesion energy was found to decrease as a function of coverage (from 2.0 to 1.1 eV as the coverage increases from 1/8 to 1 ML), while the adsorption energy was found to increase with surface coverage. Electron density difference plots were calculated to display some of the electron rearrangement responsible for the Rh-oxide adhesion energy, and the features of the Mg and O adsorption sites were compared.

© 2004 Elsevier B.V. All rights reserved.

Keywords: Density functional calculations; Magnesium oxides; Rhodium; Chemisorption; Electron density, excitation spectra calculations

1. Introduction

The role of the metal oxide support in metal/ oxide catalytic systems is intriguing. The activity and reactivity of metal-metal oxide catalysts depend on the nature and structure of both the metal and the metal oxide support and on their interplay. Even the very stable MgO system appears to play a decisive role in heterogeneous catalysis, and then not only as an inactive support or as a model system. The present study is concerned with the Rh/MgO system. The functionality of Rh/MgO catalysts has been studied intensively experimentally (see, for example, [1-12]). Only rather few

As for theoretical studies, to the best of our knowledge, only a small number of Rh/MgO studies have been published. Wu and Freeman [15] investigated the possible magnetism of Pd, Rh and Ru monolayers on MgO(001) using full-potential linearized augmented-plane-wave (FLAPW) periodic calculations (see [15] for details); there, five-layer MgO slabs were used with the metal atoms

E-mail address: kersti@mkem.uu.se (K. Hermansson).

studies have been directly concerned with the structural characterization of Rh/MgO systems at an atomic level. One such example is the work by Emrich et al. [13], who used EXAFS (Extended X-ray absorption fine structure spectroscopy) to investigate the structure of highly dispersed Rh particles on MgO under reduced conditions and determined the Rh-O bond length to be 1.95 Å (under these conditions). The ionic state of reduced Rh particles has also been investigated by X-ray photoelectron spectroscopy (XPS) [14].

^{*}Corresponding author. Tel.: +46-18-471-3767; fax: +46-18-

placed on top of every O atom on each side of the slab (i.e. the coverage was 100%, using the definition that full coverage, i.e. I ML, is when either each cation or each anion is covered by one metal atom). They found an adhesion energy (see definition later) of 0.84 eV and an optimized Rh-O distance of 2.34 Å. Periodic DFT (density functional theory) calculations with the BLYP functional and a local atom-based basis set (LCAO) were reported by Stirling et al. [16] for Rh adsorbed over two different adsorption sites (O or Mg) on one side of a one-layer MgO slab, with a surface coverage of 1/8 ML. The reactivity with NO and NO2 was also investigated. It was found that Rh prefers to bind to O rather than to Mg, with an optimized Rh-oxide interaction energy of 1.8 eV for a Rh-O distance of 2.1 A. Very recently, Bogicevic et al. [17] calculated the energy of adhesion for a number of transition metals, including Rh, on the MgO(100) surface, with and without oxygen vacancies present. These authors used periodic, plane-wave DFT calculations with the GGA (generalized gradient approximation) treatment of the exchange-correlation functional and the systems consisted of five-layer oxide slabs with the metal atom placed on one side of the slab only, and a coverage of 1/18 ML. The adhesion energy for Rh on top of O was reported to be 1.93 eV.

If we try to summarize the adsorption information resulting from the three theoretical studies just described, we arrive at the following picture: the Rh atoms prefer to reside above the oxygen atoms on MgO(001) and the adhesion energy is approximately 1.9 [17], 1.8 [16] and 0.8 [15] eV per ad-atom for a coverage of 1/18, 1/8 and 1 ML, respectively. The values display a strongly decreasing trend as a function of surface coverage, which may or may not be a consequence of the fact that different DFT methods were used in the studies compared. In the current study we present optimized geometries and interaction energies for the Rh/MgO(001) interface system for three different coverages, calculated with one and the same theoretical method, namely, plane-wave DFT calculations at the GGA level with the projector augmented-wave (PAW) method to describe the core electrons [18]. Four different adsorption sites were investigated.

2. Computational details

The Rh/MgO(001) system in our calculations was described with a periodic slab model, where each slab was infinite in the x and y directions and finite along the z direction, and then repeated periodically along the z direction with a vacuum gap between nearest slab images. In the present calculations, each slab consisted of 4 MgO(001) layers with one Rh layer placed on only one side of the slab and the vacuum gap was approximately 15 A (7 Mg-O distance intervals). All Mg-O distances in the x and y directions were kept fixed at the optimized bulk value (2.125 A; the experimental value is 2.105 Å [19]) and the Rh layer was placed epitaxially on top of the oxide slab. Four different adsorption sites and three different coverages (1/8, 1/2 and 1 ML) were explored and will be further discussed in Section 3.1. A 1×1 crystallographic supercell was selected as a model for the 1/2 and 1 ML calculations, whereas a 2×2 supercell was used for the 1/8 ML case. Both the Mg-O and Rh-oxide distances along the z direction were allowed to relax, but two different relaxation schemes were used, namely either all Mg-O distances were allowed to relax in the z direction, or the bottom two oxide layers were kept fixed at the optimized bulk structure value. The two relaxation models gave virtually identical structural and energetical results and only the fully optimized (in the z direction) slab results are reported here. Moreover, test calculations with an 8layer oxide slab confirmed that a four-layer oxide slab was thick enough for our interface study.

The calculations were performed within the framework of periodic DFT using the Vienna Ab initio Simulations package (VASP) [20,24]. Here, non-spin polarized calculations are reported, since we also performed spin polarized calculations and found the effect on the calculated adsorption energy to be 0.2 eV or less. The valence electron configurations used in our calculations were Rh(4p⁶, 5s¹, 4d⁸), Mg(2p⁶, 3s²) and O(2s², 2p⁴) and the projector augmented-wave method (PAW) [18,22] was used to treat the core electrons. The GGA functional PW91 [23] was used. An energy cut-off of 500 eV and a Gaussian smearing factor with $\sigma = 0.1$ eV were applied in all cases.

For the bulk and surface systems, respectively, $(6 \times 6 \times 6)$ and $(6 \times 6 \times 1)$ meshes of k-points, selected according to the Monkhorst-Pack (MP) algorithm [24], were used in the Brillouin zone sampling. All structures were optimized until the forces on all unconstrained atoms were less than 0.01 eV/ Å.

3. Results and discussions

3.1. Rh/MgO(001) structure

As mentioned, four different adsorption sites were investigated for surface coverages of 1/8, 1/2 and 1 ML: (i) on top of O, (ii) on top of Mg, (iii) above the middle of the Mg-O bond and (iv) above a hollow site (see Fig 1a). It turned out that when Rh was placed above the middle of the Mg-O bond, the Rh atoms moved towards the O site and found the same equilibrium positions as for a starting position above the O atoms. Therefore only the results for three sites are reported in Table 1.

We find that a Rh overlayer placed over the O atoms induces an "inverse buckling" (inverse rumpling) of the oxide surface, compared to the relaxed surface structure of the isolated MgO(001) slab. Thus, with the Rh atoms present on top of the O atoms, the Mg atoms in the surface layer lie further out from the slab center than the (Rh-covered) O atoms. For the 1 ML case, this inverse rumpling is as large as 0.13 Å and smaller values of 0.02 and 0.03 are found for the 1/2 and 1/8 coverages, respectively. The optimized atomic positions reported in [15] also bear evidence of this inverse rumpling.

The optimized vertical distances between the Rh atoms and the MgO surface are reported in Table 1. As seen in the table, Rh prefers to bind to the O atom, in agreement with experimental [13] and previous theoretical [15-17] results. Our optimized Rh-O distance is 1.99 Å for 1/8 ML coverage, in good agreement with the reported low-coverage theoretical values in the literature (2.09 Å [16] and 2.01 Å [17]). We find that the distance increases with higher coverage, reaching a value of 2.10 Å for 1 ML coverage. The only experimental distance reported in the literature (see Section 1) is 1.95 Å [13].

3.2. Rh/MgO(001) energetics

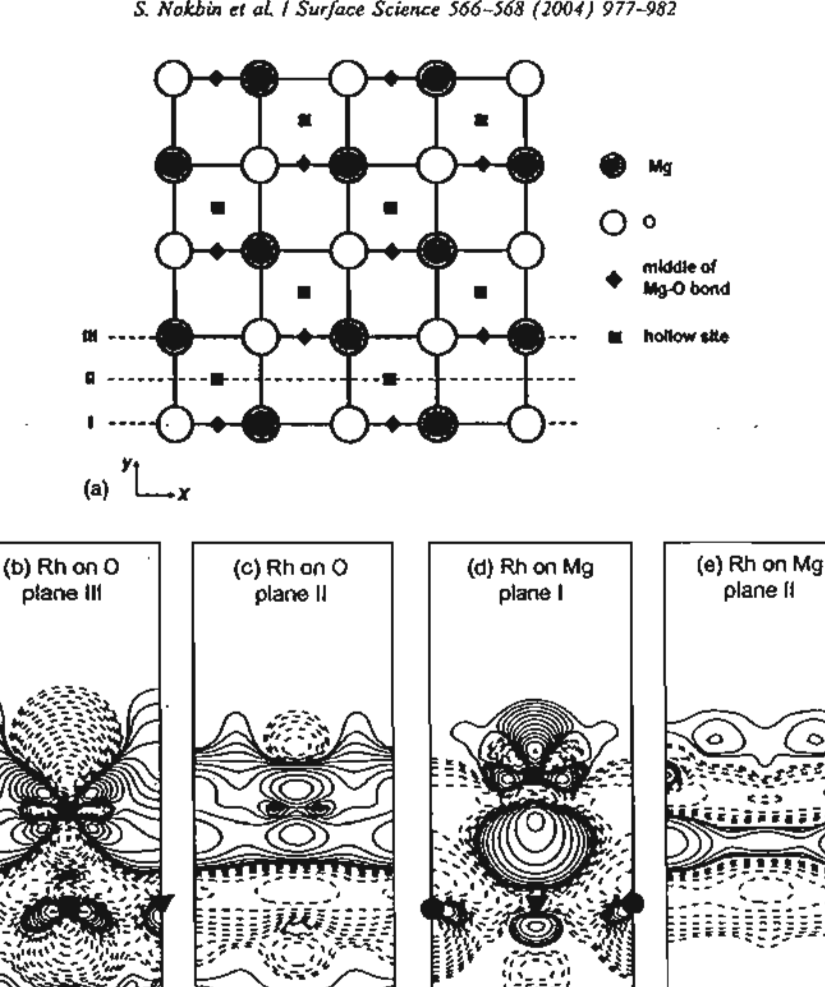
Two types of metal-metal oxide interaction energies were calculated, namely the adsorption energy E_{ads} and the adhesion energy E_{adh} defined in (2) and (3) below. The formation of the metal/oxide interface (3) can be thought of as consisting of two consecutive steps, (1) and (2), according to

- (1) $Rh(g) \rightarrow Rh$ -layer $\Delta E_1 = -\Delta E_{formation-of-layer}$
- (2) Rh-layer + MgO-slab \rightarrow Rh/MgO-slab $\Delta E_2 = -E_{adh}$
- (3) Sum: Rh(g) + MgO-slab \rightarrow Rh/MgO-slab $\Delta E_3 = \Delta E_1 + \Delta E_2 = -E_{ads}$

These definitions of $E_{\rm ads}$ and $E_{\rm adh}$ follow the usual convention in the literature, but also step (I) has been highlighted above, since this energy contribution becomes particularly interesting when adsorption energies at different coverages are compared. $\Delta E_{\rm formation-of-layer}$ is thus the energy required or gained when an isolated overlayer is produced from the isolated metal atoms. All systems in the definitions above have the same atomic positions, namely those of the total (geometry-optimized) Rh/MgO interface system.

The $E_{\rm ads}$ and $E_{\rm adh}$ values for the optimized structures are also presented in Table 1. $\Delta E_{\rm formation-of-layer}$ is not included in the table since it is constant for each coverage and is less than 0.001 eV for 1/8 coverage, equal to 0.55 for 1/2 ML coverage and 2.88 eV for 1 ML. The Rh layer is thus stabilized by an increased number of Rh-Rh interactions.

The adhesion energy, however, is seen to become less stabilizing for larger coverages, in agreement with the trends suggested by the existing data in the literature (see Section 1). The magnitude of $\Delta E_{\text{formation-of-layer}}$ is larger than the magnitude of E_{adh} , however, and the combined effect of $\Delta E_{\text{formation-of-layer}}$ and E_{adh} is that the total adsorption energy E_{ads} increases with surface coverage (see Table 1). Given the larger value of $\Delta E_{\text{formation-of-layer}}$ compared to the E_{adh} one might expect "island formation" of Rh to be important. We have not made any attempt to study this phenomenon in the present paper.



▼ Mg ■ Rh O Fig. 1. (a) Top view of the clean MgO(001) surface, indicating the various adsorption sites as described in the text. The figure shows a 2×2 crystallographic supercell where the left and right edges are thus identical, as well as the upper and lower edges. The adsorption pattern corresponds to 1 ML coverage in each case. The labels I, II and III indicate the xz sections [(010) plane] used for the electron density plots. (b)-(e) Difference electron density, $\Delta \rho = \rho_{Rh/MgO} - [\rho_{MgO,dub} + \rho_{Rh,layer}]$, for the optimized interface system with four oxide layers and 1 ML Rh coverage. Rh over O in (b)-(c) and over Mg in (d)-(e). Solid contour lines denote electron excess, dashed lines electron loss. The contour levels are at ±0.0005, ±0.0008, ±0.0013, ... e/a.u. increasing by a factor of 1002 for every contour line.

Our E_{adh} result for the low coverage, 2.05 eV, shows quite similar result as compared to other low-coverage studies in the literature, i.e. 1.82 eV

[16] and 1.93 eV [17], and our 1 ML E_{adh} value of . 1.1 eV is in reasonable agreement with the highcoverage value of 0.8 eV reported in [15].

Table 1
Interaction energies (in eV) and vertical Rh-surface distance (in Å) for the optimized Rh/MgO(001) system at different coverages

Coverage	Adsorpt	ion site					_			
	0			Hollow	Hollow			Mg		
	r	E _{state}	E_{ada}	r	Each	Eads	r	$E_{\rm adh}$	Eads	
1/8 ML	1.99	2.05	2.05	1.80	1.91	1.91	2.55	0.60	0.60	
1/2 ML	2.07	1.71	2.25	1.93	1.18	1.72	2.70	0.39	0.94	
1 ML	2.10	1.11	3.99	2.48	0.35	3.23	2.92	0.16	3.04	

The adhesion energy and adsorption energy are defined in the text.

As for the other adsorption sites, the hollow site is a fairly good one, whereas the Mg ion is not. This is reflected both by the Rh-surface distance and by $E_{\rm ads}$.

3.3. Rh/MgO(001) electronic charge density

Fig. 1b-e shows the electron density redistribution corresponding to 1 ML adsorption over the O and Mg sites (Fig. 1b-c and d-e, respectively). More exactly, the quantity plotted is $\Delta \rho \approx$ $\rho_{Rh/MgO} - [\rho_{MgO slab} + \rho_{Rh layer}]$, which is the electron redistribution occurring when an isolated Rh layer and an isolated MgO slab combine to form the interface system (all components at the optimized interface system geometry). This difference density is thus the "density-equivalent" of ΔE_{*dh} . The difference density has been plotted in three different xz planes, defined in Fig. 1a. From Fig. 1b, for example, we see that the O ion in the topmost layer induces strong electron density rearrangements in the Rh atom lying just above it. The electron density "spills over" to the region above the Mg ions, giving a stabilizing effect. The electron density rearrangement induced by the Rhsurface interaction is seen to extend quite far down into the slab, although it of course decreases as a function of depth. Electron density maps were also presented in [15], where the authors emphasized that the electron density rearrangement was essentially confined to the Rh atoms and the outermost oxide layer, a conclusion supported by their electron density maps. As usual, however, the choice of contour levels may be crucial in steering the scientific conclusions drawn from the analysis of electron density maps. It is clear from our results that also the atoms a few layers down into the slab are significantly affected by the Rh overlayer. Fig. 1c shows that also in the region "between and below" the Rh atoms there are some effects of the Rh layer present, although relatively very small.

In Fig. 1e, no such features are visible (with the current choice of contour levels). This is one manifestation of the fact that the Rh-Mg interaction is weaker than the Rh-O interaction. Fig. 1d shows the plane containing the Rh atom and the Mg atom directly below it (plus all the other atoms in that plane). A comparison with Fig. 1b shows that, overall, the polarization features are more enhanced for Rh adsorption at the O site than at the Mg site. The fact that we obtained a much larger $E_{\rm adh}$ value for the O site supports this conclusion, although it must be borne in mind that any interaction energy also contains components which are not visible in a difference electron density map, namely truely electrostatic contributions.

4. Conclusion

The structural and energetic properties of Rh atoms on MgO(001) were studied by periodic DFT plane-wave calculations. Our results show that Rh prefers to bind to the surface O site, which exhibits both relatively large adhesion energy and a short Rh-surface distance. Also the hollow site is a rather attractive site for Rh. Our calculated adhesion energies over O are in good agreement with the scarce literature data existing. The adhesion energy is found to decrease with coverage and the adsorption energy increases with coverage. Rh adsorption at the O site introduces more electron density rearrangement in the oxide slab than adsorption at the Mg site.

Acknowledgements

Financial support from the Swedish Foundation for International Cooperation in Research and Higher Education (STINT) and the Swedish Research Council (VR) are gratefully acknowledged. S.N. and J.L. wish to thank the Thailand Research Fund (TRF) for a Royal Golden Jubilee Ph.D. fellowship (3.C.KU/43/A.2) and a TRF Senior Research Scholar.

References

- [1] D. Qin, J. Lapszewicz, Catal. Today 21 (1994) 551.
- [2] H.Y. Wang, E. Ruckenstein, J. Catal, 186 (1999) 181.
- [3] M. Baerns, O.V. Buyevskaya, L. Mieczko, D. Wolf, Stud. Surf. Sci. Catal. 107 (1997) 421.
- [4] D. Qin, J. Lapszewicz, X. Jiang, J. Catal. 159 (1996) 140.
- [5] T. Iizuka, Y. Tanaka, K. Tanabe, J. Catal. 76 (1982) 1.
- [6] J. Wang, J.A. Lercher, G.L. Haller, J. Catal. 88 (1984) 18.
- [7] F. Solymosi, A. Erdohelyi, J. Catal. 91 (1985) 327.
- [8] Y.W. Chen, J. Chin. Inst. Chem. Engrs. 19 (1988) 53.

- [9] A.M. Efstathiou, J. Mol. Catal. 69 (1991) 105.
- [10] A. Ualikhanova, A.E. Temirbulatova, Z. Prikladnoi Khimii (Sankt-Peterburg, Russian Federation) 64 (1991) 2393.
- [11] T. Lopez, J. Mendez-Vivar, R. Juarez, J. Non-Cryst. Solids 147-148 (1992) 778.
- [12] F. Solymosi, J. Cserenyi, L. Ovari, J. Catal, 171 (1997) 476.
- [13] R.J. Emrich, A.N. Mansour, D.E. Sayers, S.T. McMillan, J.R. Katzer, J. Phys. Chem. 89 (1985) 4261.
- [14] M.A. Baltanas, J.H. Onuferko, S.T. McMillan, J.R. Katzer, J. Phys. Chem. 91 (1987) 3772.
- [15] R. Wu, A.J. Freeman, Phys. Rev. B 51 (1995) 5408.
- [16] A. Stirling, I. Gunji, A. Endou, Y. Oumi, M. Kubo, A. Miyamoto, J. Chem. Soc. Faraday Trans. 93 (1997) 1175.
- [17] A. Bogicevic, D.R. Jennison, Surf. Sci. 515 (2002) L481.
- [18] P.E. Bloechl, Phys. Rev. B 50 (1994) 17953.
- [19] R.W.G. Wyckoff, Crystal Structures, 2nd ed., vol. 2, Interscience, New York, 1964.
- [20] G. Kresse, J. Hafner, Phys. Rev. B 47 (1993) 558.
- [21] G. Kresse, J. Furthmueller, Phys. Rev. B 54 (1996) 11169.
- [22] G. Kresse, D. Joubert, Phys. Rev. B 59 (1999) 1758.
- [23] J.P. Perdew, J.A. Chevary, S.H. Vosko, K.A. Jackson, M.R. Pederson, D.J. Singh, C. Fiolhais, Phys. Rev. B 46 (1992) 6671.
- [24] H.J. Monkhorst, J.D. Pack, Phys. Rev. B 13 (1976) 5188.





Journal of Molecular Structure 733 (2005) 239-246



www.elsevier.com/locate/molstruc

The adsorption of benzene on industrially important nanostructured catalysts (H-BEA, H-ZSM-5, and H-FAU): confinement effects

Ratana Rungsirisakun, Bavornpon Jansang, Piboon Pantu, Jumras Limtrakul*

Laboratory for Computational and Applied Chemistry, Physical Chemistry Division, Department of Chemistry, Faculty of Science,
Kasetsart University, 50 Phahonyothin Road, Lat Yao Sub., Bangkok 10900, Thailand

Received 1 June 2004; revised 26 August 2004; accepted 1 September 2004

Abstract

The structure of industrially important zeolitic catalysts (H-BEA, H-ZSM-5, and H-FAU) and their interactions with benzene have been investigated within the framework of our-own-N-layered integrated molecular orbital + molecular mechanics (ONIOM) approach utilizing the three-layer ONIOM scheme (B3LYP/6-31G(d,p):HF/3-21G:UFF). Inclusion of the extended zeolitic framework covering the nanocavity has an effect on adsorption properties and leads to differentiation of different types of zeolite, unlike the small cluster models which are not able to make this differentiation. The ONIOM adsorption energies of benzene on ZSM-5, BEA, and FAU zeolites are ~19.23, ~16.11, and ~15.22 kcal/mol, respectively, which agrees well with the known adsorption trend of these three zeolites. On the other hand, the small cluster models underestimate the adsorption energies and even yield an unreasonable trend of adsorption energies (~8.09, ~8.48, and ~8.93 kcal/mol for ZSM-5, BEA, and FAU, respectively). With the inclusion of basis set superposition error (BSSE) and the MP2 corrections, the ONIOM3(MP2/6-31G(d,p):HF/3-21G:UFF) adsorption energies are predicted to be ~18.96, ~16.34, and ~15.18 kcal/mol, for ZSM-5, BEA, and FAU, respectively. The last value can be compared well with the experimental data (~15.31 kcal/mol) for benzene adsorption on a FAU zeolite. The results derived in this study suggest that the ONIOM3(MP2/6-31G(d,p):HF/3-21G:UFF) scheme provides a more accurate method for investigating the adsorption of aromatic hydrocarbons on these zeolites.

© 2004 Elsevier B.V. All rights reserved.

Keywords: BEA zeolite; Faujasite zeolite; ZSM-5 zeolite; DFT-study; Benzene adsorption; ONIOM

1. Introduction

Zeolite is one of the most important heterogeneous catalysts for environmental and industrial applications [1,2]. Many petrochemical processes take advantage of the high activity of the protonic form of these aluminosilicates [3-12]. It has been shown that the difference in catalytic activity can be ascribed to different acid strengths of the acid sites and to the confinement effect, i.e. interactions between adsorbed molecules and the nanostructured zeolitic pores [13]. Derouane et al. [14,15] found that the confinement effects are results of van der Waals interactions which are major factors for determining the strength of interactions between the adsorbed molecule and the zeolite Brønsted

sites. The understanding and rational utilization of confinement effects will undoubtedly contribute to increase the productivity, selectivity and specificity of such chemical transformations [13–16].

Numerous theoretical models, including the periodic electronic structure methods, have been proposed to study the interactions in extended systems such as crystals or surfaces [17-24]. For nanostructured materials, such as zeolites, that have a high impact in industrial processes usually possess hundreds of atoms per unit cell. This makes the use of accurate periodic structure calculations computationally too expensive and even impractical when very large zeolites are concerned. Alternatively, hybrid methods, such as embedded cluster or combined quantum mechanics/molecular mechanics (QM/MM) [25-31] methods, as well as the more general our-own-N-layered integrated molecular orbital+molecular mechanics (ONIOM) method

Corresponding author,
 E-mail address: fscijrl@ku.ac.th (J. Limtrakul).

[32,33], have brought a larger system within reach of obtaining accurate results.

In this study we present the ONIOM method that takes advantage of the density functional theory for the accurate treatment of the interactions of adsorbed molecules with the acid site of zeolite and of the universal force fields (UFF) for rigorous presentation of the van der Waals interaction due to the confinement of the extended zeolitic structure [34-40]. This efficient scheme has been demonstrated to yield adsorption energies close to the experimental estimates [34,35,41,42], suggesting that the ONIOM approach is a sufficiently accurate and practical model in studying adsorption of unsaturated hydrocarbons on zeolites. In this study, the effects of the zeolite environments on the adsorption properties of benzene in three different zeolites. (H-BEA, H-ZSM-5, and H-FAU), are examined and compared in order to address the confinement effect in these nanostructurted materials.

2. Methods

Two different strategies have been employed to model the different types of zeolites and their complexes with benzene. First, small quantum cluster (B3LYP/6-31G(d,p):HF/3-21G) of 10T H-ZSM-5, 12T H-BEA, and 12T H-FAU zeolites are modeled to represent the active sites of the H-ZSM-5, H-BEA and faujasite (H-FAU) zeolites. The second strategy employs the ONIOM3(-B3LYP/6-31G(d,p):HF/3-21G:UFF) approach for the more realistic models of 46T-H-ZSM-5, 78T-H-BEA and 84T-H-FAU zeolites.

The cluster models of H-ZSM-5, H-BEA and H-FAU were obtained from their crystal lattice structures of H-ZSM-5, H-BEA and H-FAU, respectively [10,43,44]. The 12T-BEA cluster is the 12-membered-ring representing the main gateway to the intersection of two perpendicular 12MR channel systems (Fig. 1a). The 10T-ZSM-5 cluster is the 10-membered-ring window representing the zigzag gateway of the ZSM-5 zeolite that is large enough to allow the probe molecule to move freely (Fig. 2a). The 12T-FAU cluster is the 12-membered-ring window connecting two supercages of FAU zeolite (Fig. 3a).

The effect of the extended framework structure of zeolites cannot be totally neglected if accurate results are required. Thus, realistic clusters were proposed for representing the systems of H-ZSM-5, H-BEA and H-FAU using the ONIOM scheme. In the ONIOM scheme, for computational efficiency, only the active region is treated accurately with the ab initio method, while interactions in the rest of the model is approximated by a less accurate method. As for Beta zeolite, the 78T cluster is used for representing nanocavity at the intersection of the two perpendicular 12MR channels (Fig. 1b). The ONIOM3 scheme, in which the whole model is subdivided into three layers, is adapted. The active region consisting of the 3T

cluster, H3SiOAl(OH)2O(H)SiH3, which is considered the smallest unit required to represent the acid site of zeolite, and the reactive molecules is treated with the B3LYP/6-31G(d,p) or MP2/6-31G(d,p) method. A silicon atom at a T5 position in Beta zeolite is substituted by an aluminum atom, and a proton is added to the bridging oxygen atoms bonded directly to the aluminum atom, conventionally called O5 position [10]. The extended framework environment is included using less expensive levels of theories, the Hartree-Fock, and molecular mechanics force field (UFF) methods [45]. The HF/3-21G method is used for the 9T ring fragment connecting the 3T acidic site to complete the 12T pore opening of the Beta zeolite (Fig. 1). The remainder of the 78T extended framework is treated with the UFF force field to reduce computational time and to practically represent the confinement effect of the zeolite pore structure.

In order to observe the interactions of the adsorbed molecule with different environments of the zeolite framework, comparison is made with a similar ONIOM3 scheme for H-ZSM-5 and H-FAU zeolites. We utilize the MP2 or B3LYP method for the 3T cluster of Brønsted acid site and the benzene. In the intermediate layer, the Hartree-Fock method is employed to complete the remainder of the 10T and 12T membered-ring windows of the H-ZSM-5 and H-FAU zeolites, respectively. The selected outermost layers include the extended framework up to 46T and 84T tetrahedral atoms for the H-ZSM-5 (Fig. 2b) and H-FAU (Fig. 3b) zeolites, respectively, which cover all the important frameworks—where the reaction normally takes place.

All calculations have been performed using the GAUSSIAN 98 code [46]. The 6-31G(d,p) basis set is used for the B3LYP and MP2 calculations, while the basis set for the Hartree–Fock calculations is 3-21G. During the structure optimization, only the active site region $\{ \equiv SiO(H)Al(O)_2. OSi \equiv \}$, and the adsorbates are allowed to relax while the remainder is fixed at the crystallographic coordinates [10,43,44].

In order to obtain more reliable interaction energies, basis sets superposition error (BSSE) corrections were also taken into account. It is known that DFT does not account for the dispersion component of the interactions. Single point MP2/6-31G(d,p) calculations for the high-level active region were carried out at the B3LYP optimized geometries to improve the energetic information between benzene and the zeolite framework.

3. Results and discussion

3.1. Comparisons of small cluster with extended zeolitic cluster models

The 12T and 78T cluster models for H-BEA zeolite are shown in Fig. 1. Selected geometrical structures for all

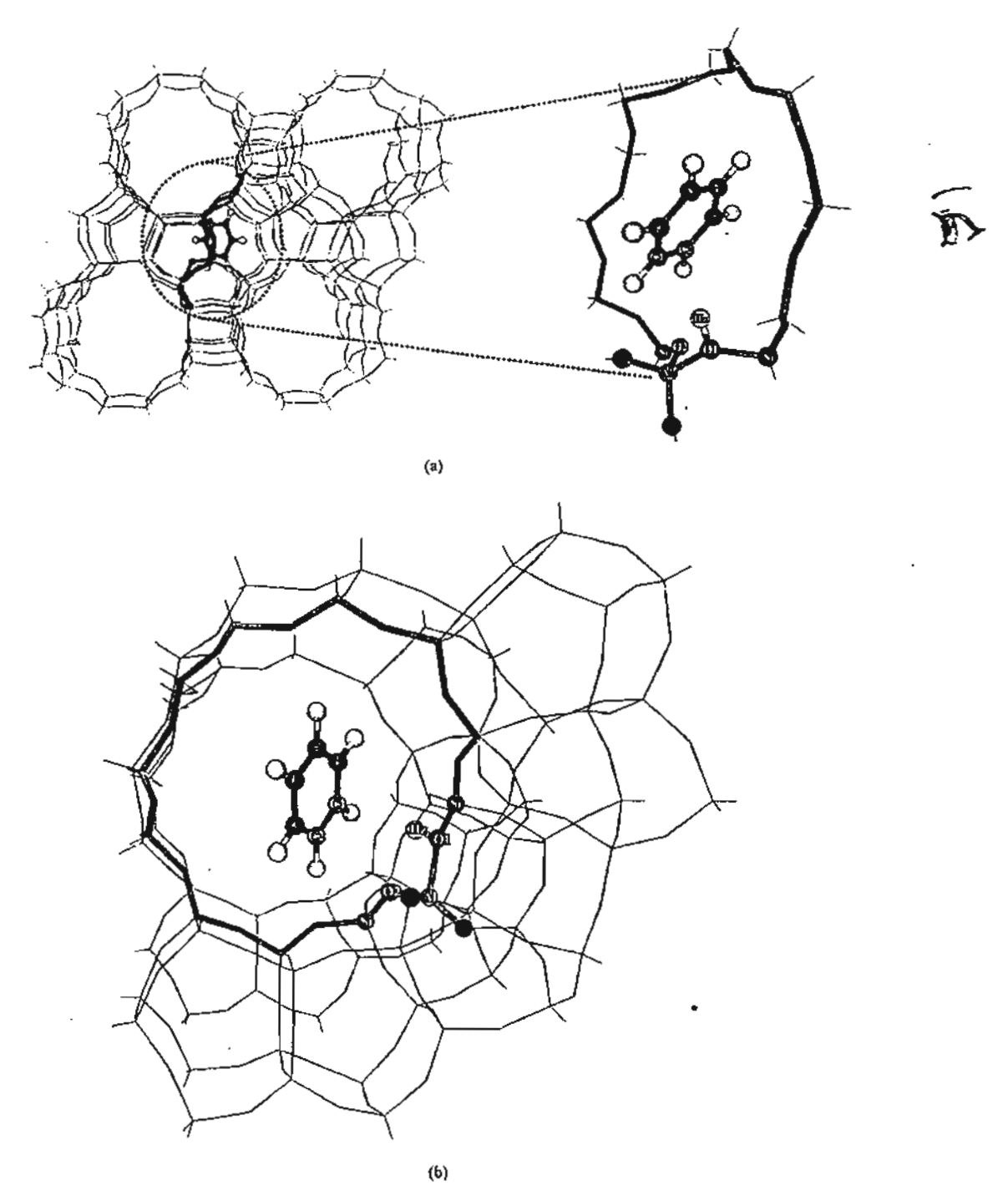


Fig. 1. The oval dashed line encloses an intersection of two perpendicular 12MR channel systems of Beta zeolite which is modeled by the 78T cluster-serving as a nanoreactor, where the benzene molecule is favorably adsorbed. (a) The 12T-BEA cluster is the 12-membered-ring representing the main gateway to the intersection of Beta zeolite and is viewed along [100] as indicated by the eye's sign. (b) The 78T cluster model viewed from the main channel. The atom belonging to the 12T quantum cluster is drawn as a sphere.

cluster models are documented in Tables 1 and 2. The extended structure included in the ONIOM3(B3LYP/6-31G(d,p):HF/3-21G:UFF) scheme was found to have a small effect on the structure of BEA zeolite. In the most realistic model of the 78T cluster model, Si-O1, Al-O1 bond

lengths decrease slightly. On the other hand, this model slightly elongates the O1-Hz bond distance (Brønsted acid site) by 0.1 pm for BEA zeolite. There is also a slight increase in the Si-O1-Al bond angle as compared to the small cluster model (131.1 vs. 135.5 pm).

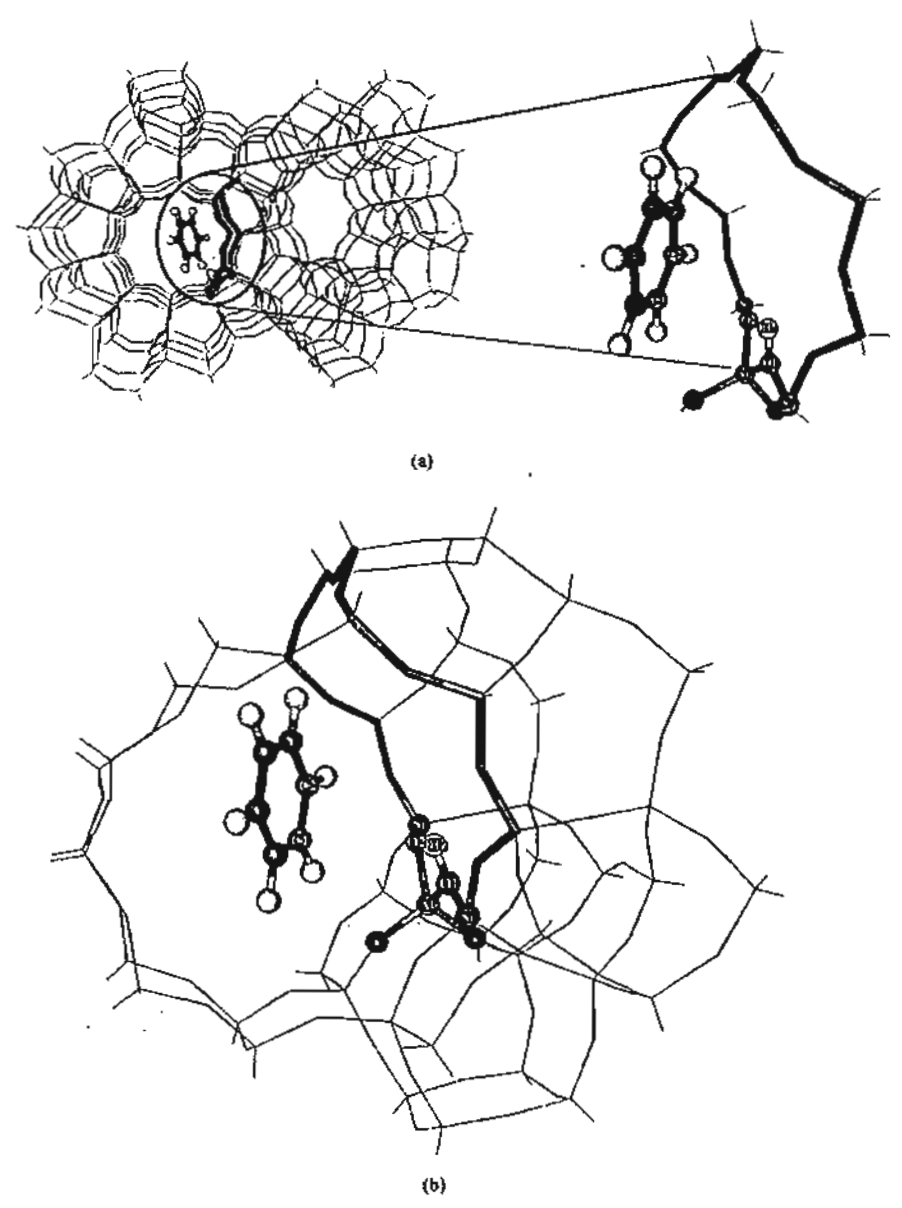


Fig. 2. Optimized structures of C₆H₆ adsorbed on H-ZSM-5 zeolite. (a) The IOT cluster model of H-ZSM-5/C₆H₆ complex is the IO-membered-ring window representing the zigzag gateway of the ZSM-5 zeolite. (b) The 46T cluster model of the H-ZSM-5/C₆H₆ complex; both are viewed from the direction of the straight channel of the H-ZSM-5 zeolite. The atom belonging to the IOT quantum cluster is drawn as a sphere.

Further support for the reliability of the active site subunit, \equiv Si-OH-Al \equiv , by our model calculations is given from NMR studies. Klinowski et al. have estimated the internuclear distance between the aluminum and proton nuclei in the Brønsted acid site, Al···Hz, of different zeolites [47,48] to be in the range of 234-252 pm, and our computed Al···Hz distances of the most realistic models of 78T-H-BEA, 46T-H-ZSM-5 and 84T-H-FAU zeolites are in the range of 233-245 pm.

Despite the small magnitude, the changing of distances and angles at the active region with the ONIOM model, one can expect that adsorption of probe molecules on the zeolites will be affected by the presence of the long-range interaction of the framework, and this will be discussed in the following text.

3.2. The interactions of benzene with the BEA zeolite

The C-C and C-H bond lengths of a benzene molecule were ascertained experimentally to be 139.7 and 108.4 pm, respectively. The B3LYP/6-31G(d,p) level of theory predicted the bond lengths of 139.6 and 108.6 pm which are in excellent agreement with the experimental observation. For the bare 12T quantum cluster, the changes of geometrical parameters upon the adsorption of benzene are in accordance with Gutmann's rule [49,50], i.e. a lengthening of

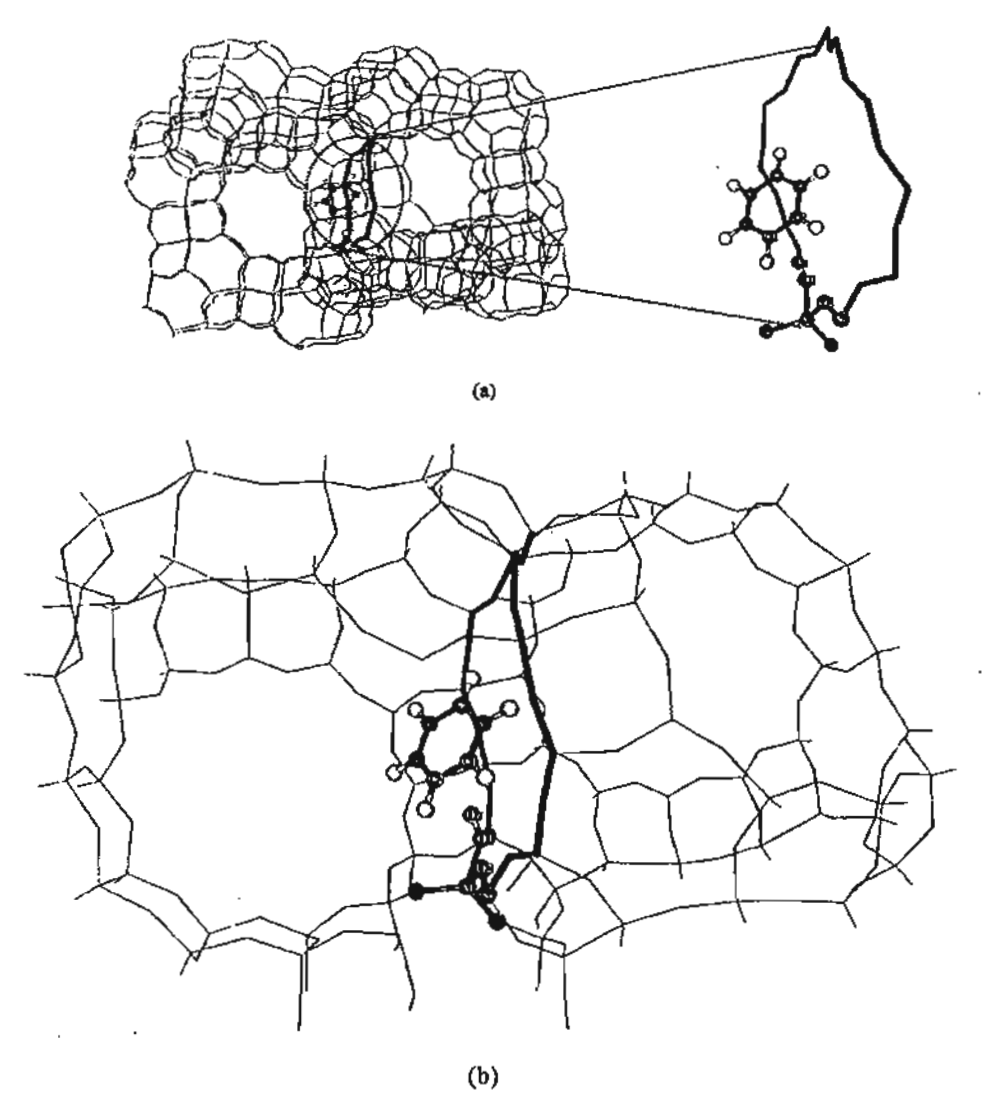


Fig. 3. Optimized structures of C_6H_6 adsorbed on H-FAU zeolite. (a) The L2T-FAU cluster model of H-FAU/ C_6H_6 complex is the 12-membered-ring window connecting two supercages of FAU zeolite. (b) The 84T cluster model of the H-ZSM-5/ C_6H_6 complex, which includes two supercages. The atom belonging to the 12T quantum cluster is drawn as a sphere.

Table 1 Structure parameters for various zeolites and their complexes with C_6H_6 are obtained at small clusters

Parameters	10T ZSM-5		12T BEA		12T FAU	
	Isolated	Complex	Isolated	Complex	Isolated	Complex
O1-Hz	97.2	97.5	96.9	98.4	97.1	98.5
Si-O1	1.66.1	166.2	168.3	168.2	168.6	168.4
AI-O1	183.7	183.0	187.9	187.0	190.6	189.4
AI-02	167.4	167.3	168.7	169.5	169.7	170.0
AlHz	238.8	238.7	236.2	237.3	250.6	248.8
∠Si-O1-AI	134.0	133.3	131.1	129.6	125.6	124.7
CIHz	~	300.1	_	227.7	_	233.5
C2···Hz	-	319.0	-	259.0	-	258.0
C1-C2	139.6	140.1	139.6	140.2	139.6	140.2
CI-HI	108.6	108.7	108.6	108.7	108.6	108.6

Bond lengths are in picometer and bond angles are in degree.

Table 2 Structure parameters for various zeolites and their complexes with C_6H_6 are obtained at large clusters

Parameters	46T ZSM-5		78T BEA		84T FAU	
	Isolated	Complex	Isolated	Complex	Isolated	Complex
 01-Нг	97.2	97.4	97.0	'98.3	97.2	98.7
Si-O1	164.6	164.7	166.5	165.7	166.5	166.1
Al-Ol	184.3	183.6	184.9	185.6	187.1	186.1
A!-02	166.0	165.9	169.2	170.2	168.9	169.1
Al···Hz	232.6	232.8	- 234.4	234.6	245.0	243.9
∠\$i-O1-A1	135.0	134_3	135.5	135.2	123.5	123.6
C1···Hz	-	333.1	-	253.5	-	220.4
C2···Hz	-	398.4	-	300.8	-	257.6
C1-C2	139.6	139.8	139.6	139.9	139.6	140.3
CI-HI	108.6	108.7	108.6	108.6	108.6	1.801

Bond lengths are in picometer and bond angles are in degree.

the O1-Hz (96.9 vs. 98.4 pm) along with a corresponding slight decrease in Al-O1 and lengthening of Al-O2 (not adjacent to the bridging OH). The distances of Brønsted proton (Hz) and C1 and C2 atoms of benzene are calculated to be 227.6 and 259.0 pm, respectively. Benzene adsorption results in a slight elongation of the C-C bonds as compared to the isolated molecule (140.2 vs. 139.6 pm). However, no significant change is observed in the lengths of the C-H bonds. Our calculated adsorption energy from the 12T cluster models is estimated to be ~8.48 kcal/mol at B3LYP/6-31G(d,p) level, which is significantly lower than the adsorption energy of benzene obtained from the ONIOM model (-16.11 kcal/mol). After BSSE correction, the adsorption energy (ΔE_{Ads}^{BSSE}) predicted by the ONIOM model is -13.54 kcal/mol, which is reasonably close to the experimental estimate of -15.31 kcal/mol for related zeolite [51]. The large deviation observed in the 12T model is due to the fact that the small cluster model neglects longrange interactions of the extended framework, which is important for adsorption-desorption in zeolites [52,53].

3.3. The effect of the different types of zeolite framework (FAU, BEA and ZSM-5) on the adsorption properties of benzene

In order to demonstrate that ONIOM3 can be employed to explore the different types of zeolites, adsorption of benzene on other industrially important zeolites, FAU and ZSM-5, are also studied using the same ONIOM3 scheme. Similar trends about the adsorption energies have also been observed (ΔE_{Adx}^{BSSE} reported in Table 3), in which the adsorption energies (ΔE_{Ads}^{BSSE}) for small cluster models (-5.78 and -6.46 for the H-ZSM-5 and H-FAU complexes, respectively) are significantly lower than the corresponding values obtained from the large ONIOM cluster models. Therefore, in order to keep this article short, we will discuss mainly the effect of the different pore sizes in these zeolites on adsorption properties. The structural parameters of these complexes are documented in Tables 1 and 2. A pronounced effect of the zeolite framework of H-ZSM-5 is observed in adsorption of benzene. The 10T ring

Table 3
Adsorption energies for C₆H₆/H-zeolites obtained from various models and methods

Zcolite	Mode)	Method	Adsorption energy (kcal/mol)		
			∆E _{Ads}	ΔE8SSE.	
ZSM-5	10T	B3LYP/6-31G(d,p):HF/3-21G	-8.09	-5.78	
	IOT	MP2/6-31G(d,p):HF/3-21G //B3LYP/6-31G(d,p):HF/3-21G	-11.50	-8.02 (-9.31) ⁶	
	46T	B3LYP/6-31G(d,p):HF/3-21G:UFF	-19.23	-17.24	
	46T	MP2/6-31G(d,p):HF/3-21G:UFF //B3LYP/6-31G(d,p):HF/ 3-21G:UFF	-21.88	-18.96	
BEA	12T	B3LYP/6-31G(d,p):HF/3-21G	-8.48	5.41	
	12T	MP2/6-31G(d,p):HF/3-21G //B3LYP/6-31G(d,p):HF/3-21G	-11.64	-6.94 (-8.74)b	
	78T	B3LYP/6-31G(d,p):HF/3-21G:UFF	- 16.11	-13.54	
	78T	MP2/6-31G(d,p):HF/3-21G:UFF //B3LYP/6-31G(d,p):HF/ 3-21G:UFF	-20.36	-16.34	
FAU	12 T	B3LYP/6-31G(d,p):HF/3-21G	-8.93	~6.46	
	12T	MP2/6-31G(d.p):HF/3-21G //B3LYP/6-31G(d.p):HF/3-21G	- 12.06	$-8.27 (-10.34)^{6}$	
	84T	B3LYP/6-31G(d,p):HF/3-21G:UFF	-15.22	- 12.22	
	84T	MP2/6-31G(d,p):HF/3-21G:UFF //B3LYP/6-31G(d,p):HF/ 3-21G:UFF	-18.86	15.18	

 ^{\(\}Delta E^{\text{BSSE}} \) is the calculated adsorption energy with the BSSE correction.

With additional columbic interactions due to a set of point charges located on the positions of zeolite framework [23].

of H-ZSM-5 zeolite is apparently too constricted for the benzene molecule to form a complex within the 10 membered-ring. The benzene molecule is moved toward the intersection of the pore channels, which is more spacious (see Fig. 2). This finding is supported by the neutron and Xray diffraction measurement [54]. Unlike H-ZSM-5, the FAU consists of a 12 membered-ring which allows the benzene to be trapped within its window. The small cluster models significantly underestimate the adsorption energies of benzene/ZSM-5 and benzene/FAU. Inclusion of the extended framework results in higher adsorption energies, i.e. -17.24 and -12.22 kcal/mol for benzene/ZSM-5 and benzene/FAU complexes, respectively. The interaction energies of benzene adsorbed on zeolites, calculated from the ONIOM models, are much larger than from the bare quantum cluster models and better in agreement with experimental results. This difference is mainly attributed to 'non-local interactions' which are the van der Waals interactions due to confinement of the zeolite microporous structure, and the long range electrostatic interactions. The interactions of benzene with the zeolite acidic site are small as reflected by the small interaction energies obtained from the cluster calculations and minute changes in structure of adsorbed benzene. Since benzene is a non-polar molecule the long range electrostatic interactions are not expected to be significant. Indeed, by using columbic calculations with the quantum cluster directly interacted with the potential due to a set of point charges located on the positions of zeolite framework [23], we can demonstrate that for benzene adsorbed on the different types of zeolite, (ZSM-5, BEA and FAU), inclusion of the long range electrostatic interactions only increases the interaction energy by 1-2 kcal/mol compared to the quantum cluster calculations (cf. Table 3). On the other hand, the van der Waals interactions, accounted for by the UFF force field, with the zeolite pore walls should contribute significantly to the adsorption of benzene because the size of benzene molecule is comparable to the nanometer-sized zeolite pores [34, 36-40]. The results also suggest that the large extended zeolite framework covering nanocavity is needed for accurate representation of the different types of zeolite, which cannot be drawn from the typical small quantum cluster. The difference in interaction energies of benzene in the H-ZSM-5, H-BEA, and H-FAU zeolites may be due to the combination of the acidity and confinement effects of the zeolites. Due to the smaller pore size of H-ZSM-5 (540 pm) than that of H-BEA (640 pm) and H-FAU (740 pm for cage window and 1250 pm for supercage) zeolites, the confinement effect (mainly van der Waals interactions) is stronger in ZSM-5 zeolite. Since the van der Waals interactions dominate the adsorption of non-polar molecules, the adsorption energy of benzene in H-ZSM-5 is higher than those of H-BEA and H-FAU zeolites. In the ONIOM3(B3LYP:HF:UFF) scheme, the acidity of zeolite is sufficiently accounted for by the quantum cluster of the active region treated by the density functional theory

(B3LYP) and the van der Waals interaction is reasonably described by the UFF force field [45]. Therefore, the ONIOM3 scheme proposed here can provide a better estimate of adsorption energies than the typical small quantum cluster calculations.

It is known that DFT does not account for the dispersion component of the interactions. Single point MP2/6-31G(d,p) calculations for the high-level active region were carried out at the B3LYP optimized geometries to improve the energetic information between benzene and the zeolite framework. Using the MP2 in place of the B3LYP for the active region in the ONIOM3(MP2/6-31G:HF/3-21G:UFF) scheme, the models yield the adsorption energies (ΔE_{AA}^{BSSE}) of -18.96, -16.34, and -15.18 kcal/mol, for the H-ZSM-5. H-BEA, and H-FAU complexes, respectively. The last value is in excellent agreement with the experimental estimate of -15.31 kcal/mol obtained by Coker et al. [51], indicating that our combined approach is considered to be one of the best combinations for the ONIOM scheme. This efficient scheme provides a cost effective computational strategy for treating the effects of a large extended framework structure.

Thus, the studies of the zeolite framework structure revealed that adsorption properties of zeolite do not depend only on the acidic site center, but also on the framework structure where the acidic site is located.

4. Conclusion

We have carried out systematic ONIOM studies on the adsorption of benzene on industrially important H-BEA, H-ZSM-5, and H-FAU zeolites. The effects of the extended zeolite framework covering the nanocavity on the adsorption properties were investigated using ONIOM3 schemes. We found that the zeolite environ ment significantly enhances the adsorption energies of benzene on zeolites. The efficient ONIOM schemes, the ONIOM3(B3LYP/6-31G(d,p):HF/3-21G:UFF) and ONIOM3(MP2/6-31G(d,p):HF/3-21G:UFF) superbly in comparison to the known adsorption trend of these three zeolites. Conversely, the small cluster models yield very low adsorption energies for these three zeolites and even yield an unreasonable trend of adsorption energies for these zeolites/benzene complexes (-8.09; -8.48, and -8.93 kcal/mol for benzene adsorption on H-ZSM-5, H-BBA, and H-FAU zeolites, respectively). With the inclusion of basis set superposition error (BSSE) and the MP2 corrections, the ONIOM3(MP2/6-31G(d,p):HF/3-21G:UFF) adsorption energies are predicted to be -18.96, -16.34, and -15.18 kcal/mol, for benzene adsorption on H-ZSM-5, H-BEA, and H-FAU zeolites, respectively. The computed adsorption energy for benzene/H-FAU can be compared well with the experimental observation of -15.31 kcal/mol for benzene adsorption on an H-FAU zeolite. The results derived in this study suggest that the ONIOM3(MP2/6-31G(d,p):HF/3-21G:UFF) scheme provides a more accurate method for investigating the adsorption of aromatic hydrocarbons on these zeolites.

Acknowledgements

This work was supported in part by grants from the Thailand Research Fund (TRF Senior Research Scholar to J.L.) and the Kasetsart University Research and Development Institute (KURDI), as well as the Ministry of University Affairs under the Science and Technology Higher Education Development Project (MUA-ADB funds). The support from the Dow Chemical Company (USA) is also acknowledged.

References

- C.R.A. Catlow, Modeling of Structure and Reactivity in Zeolites, Academic Press, San Diego, 1992.
- [2] R.A. van Santen, G.J. Kramer, Chem. Rev. 95 (1995) 637.
- [3] N.O. Gonzales, A.T. Bell, A.K. Chakraborty, J. Phys. Chem. B 101 (1997) 10058.
- [4] S. Bordiga, G. Ricchiardi, G. Spoto, D. Scarano, L. Carnelli, A. Zecchina, C.O. Arean, J. Chem. Soc. Faraday Trans. 89 (1993) 1843.
- [5] J. Sauer, P. Ugliengo, E. Garrone, V.R. Saunders, Chem. Rev. 94 (1994) 2095.
- [6] M. Sierka, J. Sauer, J. Phys. Chem. B 105 (2001) 1603.
- [7] Y. Huang, H. Wang, Langmuir 19 (2003) 9706.
- [8] J. Limtrakul, Chem. Phys. 193 (1995) 79.
- [9] W.H. Chen, A. Pradhan, S.J. Jong, T.Y. Lee, I. Wang, T.C. Tsai, S.B. Liu, J. Catal. 163 (1996) 436.
- [10] A.H. de Vries, P. Sherwood, S.J. Collins, A.M. Rigby, M. Rigutto, G.J. Krarner, Phys. Chem. B 103 (1999) 6133.
- [11] J. Pardillos, D. Brunel, B. Coq. P. Massiani, L.C. De Ménorval, F. Figueras, J. Aro. Chem. Soc. 112 (1990) 1313.
- [12] G. Bellussi, G. Pazzuconi, C. Perego, G. Girotti, G. Terzoni, J. Catal. 157 (1995) 227.
- {13} E.G. Derouane, J.M. Andre, A.A. Lucus, J. Catal, 110 (1988) 58.
- [14] E.G. Derouane, C.D. Chang, Microporous Mesoporous Mater. 35–36 (2000) 425.
- [15] E.G. Derouane, J. Mol. Catal. A 29 (1998) 134.
- [16] S.M. Babitz, B.A. Williams, J.T. Miller, R.Q. Snurr, W.O. Haag, H.H. Kung, Appl. Catal. A 179 (1999) 71.
- [17] R. Shah, J.D. Gale, M.C. Payne, Chem. Commun. 1997; 131.
- [18] Y. Jeanvoine, J.G. Angyan, G. Kresse, J. Hafner, J. Phys. Chem. B 102 (1998) 5573.
- [19] J. Limtrakul, S. Nokbin, S. Jungsuttuwong, P. Khongpracha, Stud. Surf. Sci. Catal. 135 (2001) 2469.
- [20] P. Treesukol, J. Limtrakul, T. Truong, J. Phys. Chem. B 105 (2001) 2421.
- [21] J. Sauer, M. Sierka, J. Comput. Chem. 21 (2000) 1470.
- [22] E.H. Teunissen, A.P. Jansen, R.A. van Santen, R. Orlando, R. Dovesi, J. Chem. Phys. 101 (1994) 5865.
- [23] V. Dungsrikaew, J. Limtrakul, K. Hermansson, M. Probst, Int. J. Quantum Chem. 96 (2003) 17.

- [24] S. Ketrat, J. Limtrakul, Int. J. Quantum Chem. 94 (2003) 333.
- [25] H.I. Hillier, J. Mol. Struct. (Theochem) 463 (1999) 45.
- [26] J. Limtrakul, S. Jungsuttuwong, P. Khongpracha, J. Mol. Struct. 525 (2000) 153.
- [27] P.E. Sinclair, A.H. de Vries, P. Sherwood, C.R.A. Catlow, R.A. van Santen, J. Chem. Soc. Faraday Trans. 94 (1998) 3401.
- [28] M. Brandle, J. Sauer, J. Am. Chem. Soc. 120 (1998) 1556.
- [29] S.P. Greatbanks, L.H. Hillier, N.A. Burton, P. Sherwood, J. Chem. Phys. 105 (1996) 3770.
- [30] R.Z. Khaliullin, A.T. Bell, V.B. Kazansky, J. Phys. Chem. A 105 (2001) 10454.
- [31] J. Limtrakul, T. Nanok, P. Khongpracha, S. Jungsuttiwong, T.N. Truong, Chem. Phys. Lett. 349 (2001) 161.
- [32] S. Dapprich, I. Komaromi, K.S. Byun, K. Morokuma, M.J. Frisch, J. Mol. Struct. (Theochem) 461 (1999) 1.
- [33] M. Svensson, S. Humbel, R.D.J. Froese, T. Matsubara, S. Sieber, K. Morokuma, J. Phys. Chem. 100 (1996) 19357.
- [34] S. Kasuriya, S. Namuangruk, P. Treesukol, M. Tirtowidjojo, J. Limtrakel, J. Catal. 219 (2003) 320.
- [35] K. Bobuatong, J. Limtrakul, App. Catal. A, Gen. 253 (2003) 49.
- [36] A. Pelmenschikov, J. Leszczynski, J. Phys. Chem. B 103 (1999) 6886.
- [37] T.A. Wesolowski, O. Parisel, Y. Ellinger, J. Weber, J. Phys. Chem. A 101 (1997) 7818.
- [38] L.A. Clark, M. Sierka, J. Sauer, J. Am. Chem. Soc. 125 (2003) 2136.
- [39] A.M. Vos, X. Rozanska, R.A. Schoonheydt, R.A. van Santen, F. Hutschka, J. Hafner, J. Am. Chem. Soc. 123 (2001) 2799.
- [40] X. Rozanska, R. van Santen, F. Hutschka, J. Hafner, J. Am. Chem. Soc. 123 (2001) 7655.
- [41] C. Raksakoon, J. Limtrakill, J. Mol. Struct. (Theochem) 631 (2003) 147.
- [42] W. Panjan, J. Limtrakul, J. Mol. Struct. 654 (2003) 35.
- [43] H. van Koningveld, H. van Bekkum, J.C. Jansen, Acta Crystallogr. B 43 (1987) 127.
- [44] D.H. Olson, B. Dempsey, J. Catal. 13 (1969) 221.
- [45] A.K. Rappe, C.J. Casewit, K.S. Colwell, W.A. Goddard, W.M. Skiff, J. Am. Chem. Soc. 114 (1992) 10024.
- [46] M.J. Frisch, G.W. Trucks, H.B. Schlegel, G.E. Scuseria, M.A. Robb, J.R. Cheeseman, V.G. Zakrzewski, J.A. Montgomery, R.E. Stratmann, Jr., J.C. Burant, S. Dapprich, J.M. Millam, A.D. Daniels, K.N. Kudin, M.C. Strain, O. Farkas, J. Tomasi, V. Barone, M. Cossi, R. Cammi, B. Mennucci, C. Pomelli, C. Adamo, S. Clifford, J. Ochterski, G.A. Petersson, P.Y. Ayala, Q. Cui, K. Morokuma, P. Salvador, J.J. Dannenberg, D.K. Malick, A.D. Rabuck, K. Raghavachari, J.B. Foresman, J. Cioslowski, J.V. Ortiz, A.G. Baboul, B.B. Stefanov, G. Liu, A. Liashenko, P. Piskorz, I. Komaromi, R. Gomperts, R.L. Martin, D.J. Fox, T. Keith, M.A. Al-Laham, C.Y. Peng, A. Nanayakkara, M. Challacombe, P.M.W. Gill, B. Johnson, W. Chen, M.W. Wong, J.L. Andres, C. Gonzalez, M. Head-Gordon, E.S. Replogle, J.A. Pople, Gaussian, Inc., Pittsburgh, PA, 2001.
- [47] D. Frende, J. Klinoski, H., Harnden, Chem. Phys. Lett. 149 (1988) 355.
- [48] J. Klinowski, Chem. Rev. 91 (1991) 1459.
- [49] V. Gutmann, The Donor-Acceptor Approach to Molecular Interaction, Plenum Press, New York, 1978.
- [50] V. Gutmann, G. Resch, W. Linert, Coord, Chem. Rev. 43 (1982) 133.
- [51] E.N. Coker, C. Jia, H.G. Karge, Langmuir 16 (2000) 1205.
- [52] J. Xie, M. Bousmina, G. Xu, S. Kaliaguine, J. Mol. Catal. A 135 (1998) 187.
- [53] B. Coughlan, M.A. Keane, J. Chem. Soc. Faraday Trans. 86 (1990) 3961
- [54] R. Goyal, A.N. Fitch, H. Jobic, J. Phys. Chem. B 102 (2000) 2878.

THE INFLUENCE OF THE FRAMEWORK TO STRUCTURES AND ENERGETIC PROFILES OF THE VAPOR PHASE OF THE BECKMANN REARRANGEMENT ON DIFFERENT TYPES OF ZEOLITE

Jakkapan Sirijaraensre, and Jumras Limtrakul*

Computational & Applied Chemistry Laboratory, Physical Chemistry Division, Kasetsart University, Bangkok, Thailand

Introduction

The Beckmann rearrangement¹⁻⁶ is an industrially important reaction for the production of -caprolactam, a raw material for the production of Nylon-6, where the market consumption was millions of tons in 1998.7 Caprolactam is produced by the Beckmann rearrangement of cyclohexanone oxime with oleum or concentrated sulfuric acid as a reaction medium. Although this procedure is convenient from the chemical standpoint, difficulties in manufacturing anticorrosion equipment and eliminating a large amount of the ammonium sulfate formed during the neutralization process make the process environmentally unacceptable. However, using a heterogeneous catalyst in this reaction, usually called the vapor phase of the Beckmann rearrangement, can solve these problems. Zeolite proves to be an excellent candidate 8-40 for taking over the catalytic function since the use of a zeolitic catalyst has the benefit not only from an economical point of view, but also from an ecological viewpoint.

The Beckmann rearrangement of oxime compound has been widely investigated, especially on solid catalysts such as H-ZSM5⁸⁻¹⁸, FAU¹⁹⁻²⁰, and B-ZSM5²³⁻²⁶ etc. Zecchina et al¹⁷ studied the vapor phase of the Beckmann rearrangement in H-Faujasite, H-ZSM-5 and silicalite-1 by using IR-spectroscopy and found that: a) both internal silanols and strong acid sites in zeolite can catalyze the Beckmann rearrangement of cyclohexanone oxime; b) a stable protonated intermediate is formed on a strong acid site; c) the reaction at weak acid sites has a higher activation energy through a mechanism not involving a protonated intermediate. Rhee et al²¹⁻²² studied the Beckmann rearrangement of cyclohexanone oxime over an H-beta catalyst using FT-IR spectroscopy. They suggested that the initial step of the rearrangement involved the N-protonated complex of oxime, not the O-protonated complex. Recently, Nguyen et al⁴¹⁻⁴¹ used MP2 to investigate the

Recently, Nguyen et al. used MP2 to investigate the mechanism of the Beckmann rearrangement in the gas phase. The reaction path was proposed in two key steps. The first step is called 1,2 H-shift, which connects the N-protonated complex and the O-protonated complex. The second step, called the Beckmann rearrangement, is a migration of the alkyl group to the nitrogen atom and an elimination of water molecule, giving a nitrilium cation. The first step was found to be the rate-determining step with an energy barrier of 54 kcal/mol. It is noted that in their calculations they used a proton to model the Brønsted acid of the catalyst interacting with the oxime molecule, thus the effect of the catalytic framework was omitted.

To the best of our knowledge, no theoretical works regarding the interaction of oxime and zeolite catalysts have been published. In this work, the formaldehyde oxime was chosen as a model for simplicity (small oxime molecule). The interaction of the ZSM-5 and FAU zeolites with the N-, O-formaldehyde oxime have been carried out at both the cluster and the embedded cluster approaches with the aim of: a) investigating the mechanism of the Beckmann rearrangement on both zeolites; b) determining the effects of the zeoltic framework, particularly the effect of the Madelung potential to the reaction mechanism and the energetic profile.

Methods

The bare cluster and embedded cluster models were used to determine the adsorbed structure of oxime molecules on zeolite (active site) as well as their possible N-protonated and O-protonated species. For the ZSM-5 system, the 10T cluster model (Figure 1(a)) was taken from the crystal structure of ZSM-5 to model the ZSM-5 system. The Si atom at T12 position, at the intersection between the straight channel and the zigzag channel, was replaced by Al atom and the negative charge was counter balanced by a proton which is sitting on the oxygen bridging atom. 34-40 While in the FAU system, the 12T cluster model (Figure 1(b)) which is surrounded by two supercages was taken from the crystal structure of the FAU to model the FAU system.

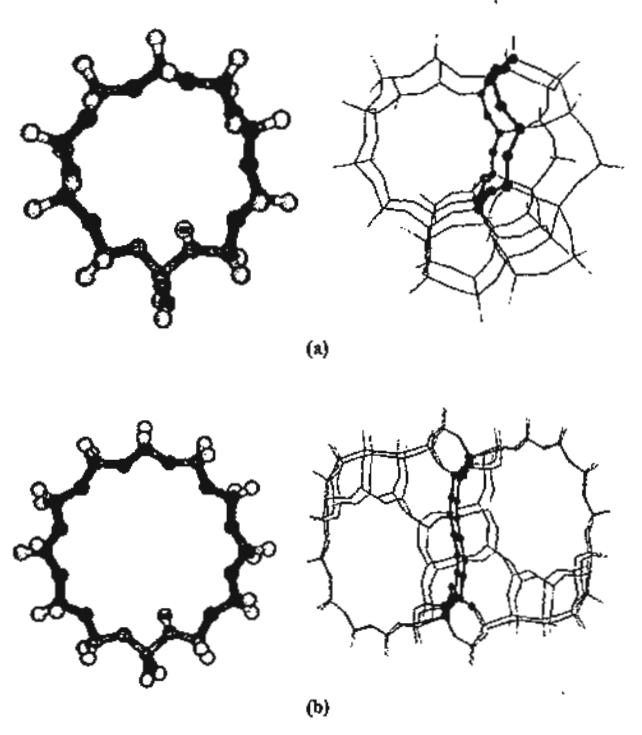


Figure 1. Presentation of the bare cluster models of zeolite. (a) 10T bare cluster model of H-ZSM-5 zeolite illustrating the zigzag gateway of the ZSM-5 zeolite (b) 12T bare cluster model of H-FAU zeolite showing the two supercages.

In the embedded cluster model, the static Madelung potential from the infinite lattice of zeolite can be mimicked by point charges surrounding the cluster. More details on this method can be found elsewhere. 44-47 With this small number of point charges, the additional computational cost is often less than 5% when compared to bare cluster calculations.

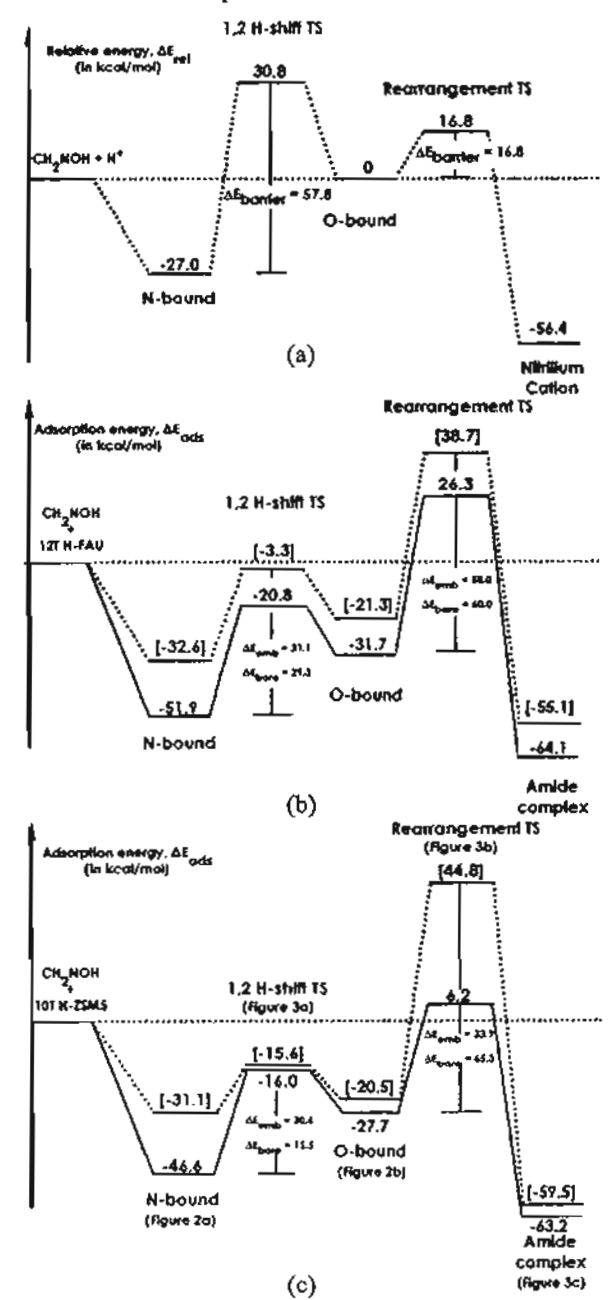


Figure 2. Comparison of the energetic profiles along the pathway of the Beckmann rearrangement of formaldehyde oxime adsorbed on different acid catalysts: gas phase model (a), H-FAU (b) and H-ZSM-5 (c) zeolites, respectively, at the B3LYP level of theory. The energetic changes for the embedded cluster (solid line) and the bare cluster (dash line) complexes are in keal/mol.

In the present work, the calculations of 10T and 12T models have been done at the B3LYP level of theory. In both models. only the active site (H2Si1OAl(OH)2O(H)Si2H2) had been treated at B3LYP/6-31G(d,p) while a lower basis set, 3-21G basis set had been applied to the rest of the cluster models. In all geometrical optimizations, the Si, Al, O bridging atoms and HI (Brønsted acid site) of the active site region of the quantum cluster were allowed to relax, while other atoms were kept fixed at the experimental structure. All calculations were performed using the Gaussian98 program. 46 The computations were performed using the computer resources at the Laboratory for Computational and Applied Chemistry (LCAC) at Kasetsart University.

Results and Discussion

The vapor-phase Beckmann rearrangement reaction. The vapor-phase Beckmann rearrangement is investigated on the industrial catalysts, FAU and ZSM-5 zeolites. This study is the investigation the reaction mechanism and the energetic profile of the Beckmann rearrangement at the strong acid site of both zeolites by using bare cluster and embedded cluster models. The energetic profiles of the Beckmann rearrangement on both zeolites are shown in Figure 2. The proposed reaction mechanism is divided into two steps. The first step is the 1,2 H-shift step which is the transformation from the N-bound configuration structure (interactions of formaldehyde oxime via its nitrogen-end with proton from the acid catalyst) to the O-bound configuration structure (interactions of formaldehyde oxime via its oxygen-end with proton from acid catalyst). After that, the second step is the Beckmann rearrangement step (BR) which is the transformation from the oxime compound to the amide compound by the migration of the tran-alkyl group (or hydride group) at the carbon atom of the oxime compound concurrently with the releasing of the water molecule. Next, the water molecule is released and this reacts with the nitrilium cation to form the amide compound (eq 1).

The reaction mechanism on the embedded cluster model of Faujasite and ZSM-5 zeolites. In order to take into account the long range interactions of the extended zeolite lattice beyond the bare cluster models, the embedded cluster models of 10T H-ZSM-5 and 12T H-FAU zeolites are employed. Comparing the result between the cluster and the embedded cluster models, the Madelung potential has the effect of lengthening the O1-H1 bond distance (Brønsted acid site) by about 0.7 pm and shortening the adjacent Al-O bond which is in accordance with Gutmann's rules. In addition, the Mulliken population on the H1 atom is slightly increased from 0.38 to 0.41 due to the Madelung potential effect.

The results obtained from the embedded cluster models of both zeolites still provided the reaction mechanism as found in the bare cluster model. The optimized structures are slightly changed, but the influence from the Madelung potential has a significant effect on the energetic profile, especially in the

H-ZSM-5 zeolite. In the 1,2 H-shift step, influence from Madelung potential has the effect of stabilizing the adsorption complexes, especially in both of the adsorption complexes (N-bound and O-bound complexes). The adsorption energy of the N-bound complex (Figure 3(a)) is enhanced to -51.9 and -46.6 kcal/mol for on H-FAU and H-ZSM-5 zeolites, respectively. The optimized structures in both zeolites are still in the form of a protonated complex. While in the O-bound complex (Figure 3(c)), the adsorption energy is increased to -31.7 and -27.7 kcal/mol for H-FAU and H-ZSM-5 zeolites, respectively. But the optimized structures are turned into protonated structures at the oxygen-end of oxime compound. The energy barrier of the 1, 2 H-shift step (Figure 3(b)) is calculated to be 31.1 and 30.6 kcal/mol for the H-FAU and H-ZSM-5 zeolites, respectively. The transition state structures obtained from cluster and embedded cluster calculations are quite similar. The OI-HI distance of the embedded cluster is slightly changed by about 3 pm. The transition state of the embedding calculation is more stable than that of the bare cluster. The higher energy barrier compared to the energy barrier of the bare cluster model can be explained by the fact that the N-protonated complex is effectively stabilized by the long-range electrostatic potential from the zeolite framework.

In the last step of this reaction, rearrangement step (Figure 3(d)), the activation energy is slightly changed in the case of the H-FAU zeolite, but significantly changed in H-ZSM-5 zeolite. The activation energy derived from the embedded calculation of the H-ZSM-5 zeolite was decreased from 65.3 to 33.9 kcal/mol. The difference in activation energies of H-ZSM-5 and H-FAU zeolites may be due to the combination of topology of TS structure at acid site and pore size of zeolites. Due to the smaller pore size of ZSM-5 than that of FAU zeolite, the Madelung effect is stronger in ZSM-5 zeolite and its effect is to significantly stabilize the TS structure of ZSM-5.

From these results, the embedded cluster model provides the different results to those obtained from the bare cluster model. This indicates that the influences from the zeolite lattice have an important effect on both the reaction mechanism and the energetic profile. Moreover, the embedded technique can differentiate the types of zeolite, unlike the bare cluster model which is not able to make this differentiation.

Conclusion

The vapor phase Beckmann rearrangement of formaldehyde oxime over both types of zeolite, FAU and ZSM-5 zeolites, have been studied by both the bare cluster and the embedded cluster methods at the B3LYP/6-31G (d,p) level of theory. The N-protonated species was obtained in both the cluster and the embedded cluster methods and was similarly found in both FAU and ZSM-5 zeolites. Regarding the interaction of zeolite with the oxygen atom of oxime (O-oxime) molecules, the cluster models yielded only hydrogen bonded adducts, while the O-protonated species were only obtained with the embedded cluster model and was the same in both zeolites. The embedded results indicate that the N-protonation of oxime is preferable to the O-protonation.

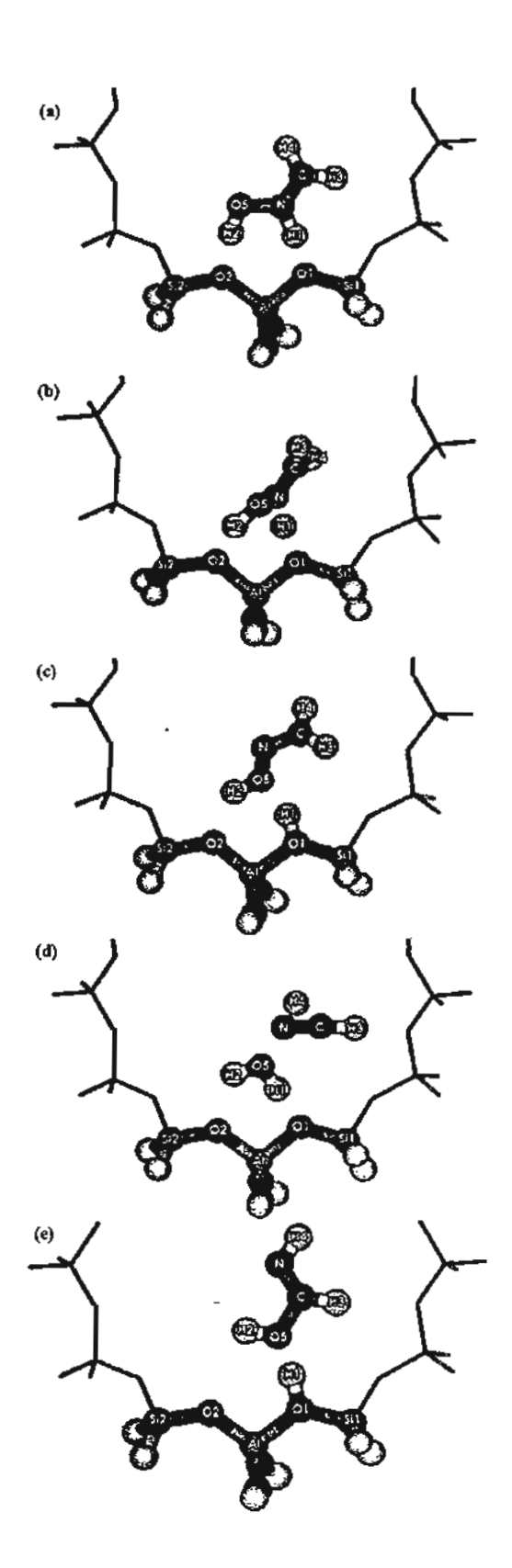


Figure 3. Presentation of the structure of each step in the Beckmann rearrangement on zeottic; (a) N-bound complex, (b) 1,2 H-shift TS, (c) O-bound complex (d) rearrangement of TS and (e) Arnide complex.

This study suggests that the initial structure of the Beckmann rearrangement reaction is not the O-protonation but the N-protonation of oxime. From the results of both types of zeolite, the energies barrier for the 1,2 H-shift connecting N, O protonated species is lower than that of the rearrangement step. Comparing the difference between the types of zeolite from the energetic profile, it is indicated that the H-ZSM5 zeolite is a better acid catalyst for the Beckmann rearrangement reaction of formaldehyde oxime than the H-FAU zeolite. Our finding may be good supporting evidence for the newly proposed mechanism for the cyclohexanone oxime interacting with zeolites and finding the suitable zeolite for this reaction. This indicates that inclusion of the effects of the zeolite crystal framework is crucial for obtaining the mechanistic aspect of the Beckmann rearrangement.

Acknowledgements. This work was supported in part by grants from the Thailand Research Fund (TRF Senior Research Scholar to JL.) and the Kasetsart University Research and Development Institute (KURDI), as well as the Ministry of University Affairs under the Science and Technology Higher Education Development Project (MUA-ADB funds). The support from the Dow Chemical Company (USA) is also acknowledged.

References

- (1) Beckmann, E. Chem. Ber. 1886, 89, 988.
- (2) Blatt, A.H. Chem. Rev. 1933, 12, 215.
- (3) Jones, B. Chem. Rev. 1944, 35, 335.
- (4) Heldt, W.Z. J. Org. Chem. 1961, 26, 1695.
- (5) Ungnade, H.E.; McLaren, A.D. J. Org. Chem. 1945, 10, 29.
- (6) Pearson, D.E.; Bruton, J.D. J. Org. Chem. 1954, 19, 957.
- (7) European Chemical News 1999, 18.
- (8) Takahashi, T.; Nishi, M.; Tagawa, Y.; Kai, T. Micropor. Mater. 1995. 3. 467.
- (9) Takahashi, T.; Ueno, K.; Kai, T. Micropor. Mater. 1993, 1, 323.
- (10) Heitmann, G.P.; Dahlhoff, G.; Hölderich, W.F. J. Catal. 1999, 186, 12.
- (11) Ichihashi, H.; Kitamura, M. Catal Today 2002, 73, 23.
- (12) Yashima, T.; Oka, N.; Komatsu, T. Catal Today 1997, 38, 249.
- (13) Kath, H.; Gläser, R.; Weitkamp, J. Chem. Eng. Technol. 2001, 24, 150.
- (14) Misona, M.; Inui, T. Catal. Today 1999, 51, 369.
- (15) Takahashi, T.; Nasution, M.N.A.; Kai, T. Appl. Catal. A: General 2001, 210, 339.
- (16) O'Sullivan, P.; Forni, L.; Hodnett, B. K. Ind. Eng. Chem. Res. 2001, 40, 1471.
- (17) Fois, G. A.; Ricchiardi, G.; Bordiga, S.; Busco, C.; Dalloro, L.; Spano, G.; Zecchina, A. Stud. Surf. Sci. Catal. 2001, 135, 2477.
- (18) Ichihashi, H.; Sato, H. Appl. Catal. A: General 2001, 221, 359.
- (19) Dai, L.X.; Iwaki, Y.; Koyama, K.; Tatsumi, T. Appl. Surf. Sci. 1997, 121-122, 335.
- (20) Dai, L.X.; Koyama, K.; Miyamoto, M.; Tatsumi, T. Appl. Catal. A: General 1999, 189, 237.
- (21) Rhee, H. K.; Chung, Y. M. J. Mol. Catal. A: Chemical 2000, 159, 389.
- (22) Rhee, H. K.; Chung, Y. M. J. Mol. Catal. A: Chemical 2001, 175, 249.
- (23) Hölderich, W.F. Catal. Today 2000, 62, 115.

- (24) Röseler, J.; Heitmann, G.; Hölderich, W. F. Appl. Catal. A: General 1996, 144, 319.
- (25) Heitmann, G.P.; Dahlhoff, G.; Neiderer, J.P.M.; Hölderich, W.F. J. Catal. 2000, 194, 122.
- (26) Hölderich, W. F.; Röseler, J.; Heitmann, G.P.; Liebens, A.T. Catal. Today 1997, 37, 353.
- (27) Dal Pozzo, L.; Fornasari, G.; Monti, T. Catal. Commun. 2002, 3, 369.
- (28) Paker Jr., W. O. Magn. Reson. Chem. 1999, 37, 433.
- (29) Komatsu, T.; Maeda, T.; Yashima, T. Micropor. Mesopor. Mater. 2000, 35-36, 173.
- (30) Ko, A. N.; Hung, C. C.; Chen, C. W.; Ouyang, K. H. Catal. Lett. 2001, 71, 219.
- (31) Chaudhari, K.; Bal, R.; Chandwadkar, A.J.; Sivasanker, S. J. Mol. Catal. A: Chemical 2000, 77, 247.
- (32) Shouro, D.; Ohya, Y.; Mishima, S.; Nakajima, T. Appl. Catal. A: General 2001, 214, 59.
- (33) Singh, P.S.; Bandyopadhyay, R.; Hegde, S.G.; Rao, B.S. Appl. Catal. A: General 1996, 136, 249.
- (34) Limtrakul, J.; Nanok, T.; Khongpracha, P.; Jungsuttiwong, S.; Truong, T. N. Chem. Phys. Letts. 2001, 349, 161.
- (35) Treesukol, P.; Limtrakul, J.; Truong, T. N. Phys. Chem. B 2001, 105, 2421.
- (36) Limtrakul, J.; Nokbin, S.; Chuichay, P. J. Mol. Struct. 2001, 560, 169.
- (37) Limtrakul, J.; Nokbin, S.; Jungsuttiwong, S.; Khongpracha, P.; Truong, T. N. Stud. Surf. Sci. Catal. 2001, 135, 2469.
- (38) Jungsuttiwong, S.; Nokbin, S.; Chuichay, P.; Khongpracha, P.; Truong, T. N.; Limtrakul, J. Stud. Surf. Sci. Catal. 2001, 135, 2518.
- (39) Limtrakul, J.; Khongpracha, P.; Jungsuttiwong, S. J. Mol. Struct. 2000, 525, 153.
- (40) Limtrakul, J.; Khongpracha, P.; Jungsuttiwong, S.; Truong, T. N. J. Mol. Catal. A: Chemical 2000, 153, 2469.
- (41) Nguyen, M. T.; Raspoet, G.; Vanquickenborne, L. G. J. Chem. Soc., Perkin Trans. 2 1995, 9, 1791.
- (42) Nguyen, M. T.; Raspoet, G.; Vanquickenborne, L. G. J. Am. Chem. Soc. 1997, 119, 2552.
- (43) Nguyen, M. T.; Raspoet, G.; Vanquickenborne, L. G. J. Chem. Soc., Perkin Trans. 2 1997, 4, 821.
- (44) Stefanovich, E. V.; Truong, T. N. J. Phys. Chem. B 1998, 102,
- (45) Vollmer, J. M.; Stefanovich, E. V.; Truong, T. N. J. Phys. Chem.
- B 1999, 103, 9415.
 (46) Ketrat, S.; Limtrakul, I. Int. J. Quan. Chem. 2003, 96(6), 333.
- (47) DungSrikaew, V.; Limtrakul, J.; Hermansson, K.; Probst, M. Int. J. Quan. Chem. 2004, in press.
- (48) Frisch, M. J.; Trucks, G. W.; Schlegel, H. B.; Scuseria, G. E.; Robb, M. A.; Cheeseman, J. R.; Zakrzewski, V. G.; Montgomery, J. A.; Stratmann, R. E. Jr.; Burant, J. C.; Dapprich, S.; Millam, J. M.; Daniels, A. D.; Kudin, K. N.; Strain, M. C.; Farkas, O.; Tomasi, J.; Barone, V.; Cossi, M.; Cammi, R.; Mennucci, B.; Pomelli, C.; Adamo, C.; Ctifford, S.; Ochterski, J.; Petersson, G. A.; Ayala, P. Y.; Cui, Q.; Morokuma, K.; Salvador, P.; Dannenberg, J. J.; Malick, D. K.; Rabuck, A. D.; Raghavachari, K.; Foresman, J. B.; Cioslowski, J.; Ortiz, J. V.; Baboul, A. G.; Stefanov, B. B.; Liu, G.; Liashenko, A.; Piskorz, P.; Komaromi, I.; Gomperts, R.; Martin, R. L.; Fox, D. J.; Keith, T.; Al-Laham, M. A.; Peng, C. Y.; Nanayakkara, A.; Chaltacombe, M.; Gill, P. M. W.; Johnson, B.; Chen, W.; Wong, M. W.; Andres, J. L.; Gonzalez, C.; Head-Gordon, M.; Replogle, E. S.; Pople, J. A. Gaussian 98; Gaussian, Inc.; Pittsburgh, PA, 2001.



Fuel Processing Technology 85 (2004) 1623-1634



www.elsevier.com/locate/fuproc

Synthesis of ZSM-5 zeolite from lignite fly ash and rice husk ash

Metta Chareonpanich ^{a,*}, Teerapong Namto ^a, Paisan Kongkachuichay ^a, Jumras Limtrakul ^b

^aDepartment of Chemical Engineering, Kasetsart University, 50 Paholyothin Rd., Chatuchak,

Bangkok 10900, Thailand

bDepartment of Chemistry, Kasetsart University, Chatuchak, Bangkok 10900, Thailand

Accepted ! October 2003

Abstract

The lignite fly ash from the Mae-Moh power plant, Thailand, and rice husk ash were used as raw materials for ZSM-5 zeolite synthesis. Factors affecting the yield of ZSM-5 zeolite synthesized from fly ash, i.e., the SiO₂/Al₂O₃ mole ratio, the presence of tetrapropyl ammonium bromide (TPABr, the structure-directing material for ZSM-5 zeolite synthesis), the holding temperature and time, and the initial pressure were investigated. It was found that without TPABr only zeolite P could be synthesized at SiO₂/Al₂O₃ mole ratios of 2.8-200. In order to synthesize ZSM-5 zeolite, sodium silicate solution was added to adjust the SiO₂/Al₂O₃ mole ratio in raw ash. The yield of ZSM-5 zeolite was as high as 59 wt.% when following conditions were used: SiO₂/Al₂O₃ mole ratio, 40; the holding temperature, 210 °C; the holding time, 4 h and the initial pressure, 4 bar. The catalytic performance for CO₂ hydrogenation reaction of the ZSM-5 zeolite was preliminary tested and compared with that of commercial one. It was observed that there was no significant difference in the catalytic performance between these two catalysts.

© 2004 Elsevier B.V. All rights reserved.

Keywords: Fly ash; ZSM-5 zeolite; Rice husk ash; CO2 hydrogenation

1. Introduction

In Thailand, low quality lignite is found predominantly. Approximately 74% of coal produced are supplied to power station as energy source. The major problem in coal-fired power generation is that the plenty of solid waste so-called fly ash (of about 30% of raw

^{*} Corresponding author. Tel./fax: +662-579-2083. E-mail address: fengrate@ku.ac.th (M. Chareonpanich).

coal) is produced [1]. Previously, almost all the fly ash was disposed by landfill, which became increasingly expensive and caused an environmental problem. Therefore, fly ash utilization was considered by many investigators. Fly ash can be mainly used as building materials according to its pozzolanic properties [2-4]. However, due to the fluctuation of demand, the alternative utilization of fly ash as the raw material for zeolite synthesis was focused.

The synthesis of zeolites from fly ash can be classified into direct and non-direct synthesis. For the direct synthesis [5-13], fly ash was hydrothermally treated with an alkaline solution. At the temperature lower than 100 °C, zeolites P, X and Na-P1 were obtained with 2-4 M NaOH solution while hydroxy sodalite and zeolite Y were obtained with 4-10 M NaOH solution. At the temperature higher than 120 °C, zeolite Na-P1, hydroxy sodalite and analcime were obtained with 4-10 M NaOH solution.

For the non-direct synthesis [14,15], silica and alumina were firstly extracted from fly ash with hot alkaline solution and this resulted in the mixture of silicate and aluminate extracts. These extracts were used as the starting material for faujasite synthesis at as low a temperature as 60-90 °C and at a synthesis period of 2-5 days.

In this work, the direct synthesis of ZSM-5 zeolite using the Mae-Moh lignite fly ash as the main raw material was focused. However, the SiO₂/Al₂O₃ mole ratio in the raw fly ash is too low to synthesize ZSM-5 zeolite (SiO₂/Al₂O₃ mole ratio=2.8). In order to obtain the appropriate SiO₂/Al₂O₃ mole ratio, the sodium silicate solution was added to adjust the mole ratio of raw fly ash. From the economic point of view, the sodium silicate solution prepared from rice husk ash was used instead of the commercial ones because there is an abundant supply of rice husk in Thailand. The factors affecting the ZSM-5 zeolite yield, i.e., SiO₂/Al₂O₃ mole ratio, the presence of tetrapropyl ammonium bromide, temperature and initial pressure were investigated. In all cases, the most suitable condition that gave the maximum yield of ZSM-5 zeolite was focused.

2. Experimental

2.1. Raw feed and reagents

Lignite fly ash obtained from the Mae-Moh electric power station, Thailand, was ground and sieved to the diameter of lower than 0.074 mm. The sample was dried at 105 °C for 1 h and kept in the desiccator before use. Chemical compositions of fly ash were examined by X-ray Fluorescence Spectroscopy (XRF: Philips, PW 1400). Physical characteristics were analyzed by X-ray Diffraction Spectroscopy (XRD: Philips, PW 1830/40, Cu-α radiation) and BET surface area analysis (Quantachrome, NOVA 1200).

Sodium silicate solution (Na₂Si₃O₇: 4 wt.% NaOH; 27 wt.% SiO₂) was used to adjust the SiO₂/Al₂O₃ ratio of fly ash mixture. First, rice husk was treated with 1 M HCl for 2.5 h. The treated rice husk was washed thoroughly with distilled water, dried at 120 °C and pyrolyzed in oxygen atmosphere at 600 °C for 1 h. The residual ash with about 99.6 wt.% silica was dissolved in NaOH solution to obtain a desired composition of sodium silicate solution.

Tetrapropyl ammonium bromide (TPABr; C₁₂H₂₈BrN) of 98% purity from Fluka Chemicals was used as a structure-directing substance for ZSM-5 zeolite preparation.

2.2. Synthesis of ZSM-5 zeolite from lignite fly ash

Batch experiments were carried out to determine effects of the SiO₂/Al₂O₃ mole ratio, the presence of TPABr, the temperature and the initial pressure on the yield of crystalline ZSM-5 zeolite. The characteristics of products were determined by XRD and Scanning Electron Microscopy (SEM: Jeol, JSM-5600 LV). The yield of ZSM-5 zeolite was obtained by converting the peak intensity of ZSM-5 zeolite from XRD analysis to weight of zeolite using of standard curved. The product yield was reported as wt.% of pure ZSM-5 zeolite in the solid product.

2.2.1. Effect of SiO₂/Al₂O₃ mole ratio and the presence of TPABr

In this series of experiments, 3 g of lignite fly ash was mixed with 50 cm³ of 0.001 M NaOH solution and variable amounts of sodium silicate solution. The average SiO₂/Al₂O₃ mole ratio in raw fly ash was about 2.8 (data from XRF). Subsequently, the SiO₂/Al₂O₃ mole ratios were adjusted to 20, 40, 60, 80, 100 and 200 by adding the sodium silicate solution into the fly ash mixture. The TPABr (0.37 g, 20 mol% of alumina in fly ash) was added to the mixture. The 0.5 M H₂SO₄ solution was used to adjust the pH of the mixture (fixed at 11±0.2). With fast synthesis process, the mixture was placed in the autoclave, pressurized at 3 bar by using nitrogen gas (99.99% purity) and then heated up from room temperature to 210 °C within 2 h. During this period, the pressure in the autoclave was autogeneously increased. The temperature was kept constant here for 2 h. By using this process, ZSM-5 zeolite can be synthesized in 4 h. The crude product was then separated from the solution, washed thoroughly with distilled water and dried in the oven at 110 °C for 2.5 h before analysis.

The experimental conditions in Sections 2.2.2 and 2.2.3 were the same as that of Section 2.2.1 unless otherwise indicated.

2.2.2. Effect of temperature

The effect of reaction temperature was examined using the same experimental conditions as those of Section 2.2.1 except the temperature and the holding time. The mixture was heated up from room temperature to 150, 180 and 210 °C with the heating rate of 1.5 °C/min and held there for 2 h. For the study of the effect of the holding time, the synthesis temperature was fixed at 210 °C and the holding time was varied from 0 to 4.0 h.

2.2.3. Effect of initial pressure

The optimum SiO₂/Al₂O₃ mole ratio and temperature determined in Sections 2.2.1 and 2.2.2 were used, and the initial pressures were varied from 1 to 6 bar. The detail of all experimental conditions is shown in Table 1.

2.3. Catalytic performance of ZSM-5 zeolite from fly ash

The catalytic performance of ZSM-5 zeolite synthesized from fly ash was examined in the hydrogenation reaction of carbon dioxide. The experiment was conducted in a catalytic packed bed reactor, made of SUS-316 (id. 7.6 mm). The reactor was 500 mm long, equipped with an infrared furnace. The ZSM-5 zeolite product (powder, 59 wt.% purity)

Table 1
Details of experimental conditions

Series of experiment	SiO ₂ /Al ₂ O ₃ mole ratio ⁶	Holding temperature (°C) ^b	Holding period (h) ^b	Initial pressure (bar)
Effect of SiO ₂ /Al ₂ O ₃ mole ratio (2.2.1)	2.8, 20, 40, 60, 80, 100, 200	210	2	3
Effect of holding temperature (2.2.2)	Α .	150, 180, 210	2	3
Effect of holding period (2.2.2)	Α	В	0, 1, 2, 3, 4	3
Effect of initial pressure (2.2.3)	A	В	С	1, 2, 3, 4, 5, 6

In all experiment; 3 g of fly ash, 50 cm³ of 0.001 M NaOH solution and the heating rate of 1.5 °C/min were used.

was packed in the isothermal zone of the reactor (bed length, 4 cm). The reactor was first flushed with N_2 (purity>99%) and heated to reaction temperatures (200-500 °C). Reactant gases (CO₂ and H₂) were allowed to flow at 50 ml (NTP)/min and the GHSV was approximately 16 h⁻¹. The mole ratio of CO₂ to H₂ was 1:3 and the operating pressure was fixed at 5 bar. The amounts of CO₂, CO and all hydrocarbon products were quantitatively analyzed using gas chromatography (Hewlett Packard 5890 series II) equipped with TCD and FID detectors and Porapack Q columns. The experiment was repeated three to five times in each condition.

3. Results and discussion

3.1. Chemical compositions of fly ash

The chemical compositions of fly ash analyzed by XRF are shown in Table 2, in which SiO₂, Al₂O₃, Fe₂O₃ and CaO are the major components. The X-ray diffraction pattern in

Table 2
The chemical composition of fly ash analyzed by XRF

Composition	Amount (wt.%)
SiO ₂	39.60
Al_2O_3 .	24,25
Fe ₂ O ₃	12.60
CaO	10.66
MgO	2.80
Na ₂ O	1.29
TiO ₂	0.49
P2O5	0.16
Others	8.15

^b A, B, and C were optimum synthesis conditions obtained from experimental Sections 2.2.1 and 2.2.2, respectively.

Fig. 1 revealed the major solid compositions in the fly ash was amorphous in nature. The BET surface area of fly ash was 5 m²/g.

3.2. Synthesis of ZSM-5 zeolite from lignite fly ash

3.2.1. Effect of SiO₂/Al₂O₃ mole ratio and the presence of TPABr

Without addition of sodium silicate solution, the SiO_2/Al_2O_3 mole ratio in fly ash is 2.8. In order to obtain SiO_2/Al_2O_3 mole ratios of 20, 40, 60, 80, 100 and 200, lignite fly ash was mixed with 27.4, 59.1, 90.9, 122.6, 154.4 and 313.2 cm³ of sodium silicate solution, respectively. To dissolve the silica and alumina in fly ash, NaOH solution was added to the mixture while the pH of the mixture was controlled at 11 ± 0.2 . It was found that without TPABr, at the SiO_2/Al_2O_3 mole ratios of 2.8-200, only zeolite P could be synthesized. The XRD pattern of the zeolite P and amorphous solid products are shown in Fig. 2.

The effects of SiO_2/Al_2O_3 mole ratio (in the range of 2.8–200) and the presence of TPABr on the yield of ZSM-5 zeolite were investigated. The yields of ZSM-5 zeolite obtained from XRD patterns are shown in Fig. 3. The results reveal that without sodium silicate solution, the ZSM-5 zeolite could not be synthesized. It is clear that the SiO_2/Al_2O_3 mole ratio of 2.8 is not suitable for ZSM-5 zeolite synthesis. At the SiO_2/Al_2O_3 mole ratio of 20–100, ZSM-5 zeolite can be synthesized. The maximum yield of 43 wt.% was found at the SiO_2/Al_2O_3 mole ratio of 40.

The SEM photographs of the zeolitic products of various SiO_2/Al_2O_3 mole ratios are shown in Fig. 4. The obtained ZSM-5 zeolite is mainly cubic crystals, accompanying with some flake-like structure. As the SiO_2/Al_2O_3 mole ratio increases from 20 to 40, the cubic crystals of ZSM-5 zeolite are increased in size from 5 to 8 μ m. However, the opposite trend was observed when the SiO_2/Al_2O_3 mole ratio is higher than 40. The smallest size of about 1 μ m was found at the SiO_2/Al_2O_3 mole ratio of 100.

From this study, it was noticed that the fast synthesis process without TPABr, even if SiO₂/Al₂O₃ mole ratio was varied, could not produce ZSM-5 zeolite from lignite fly ash.

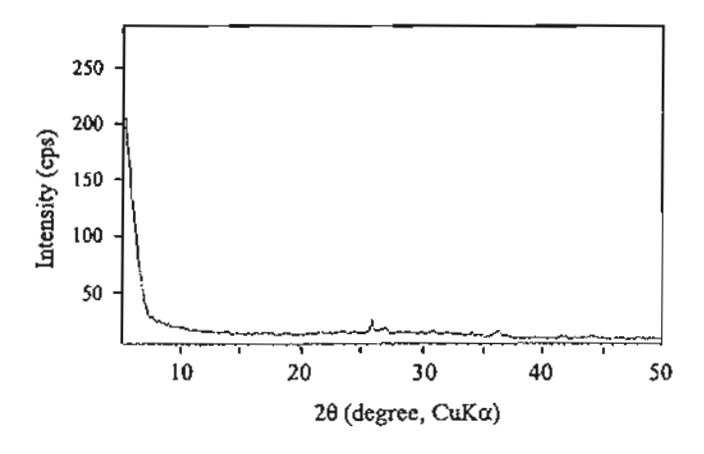


Fig. 1. XRD pattern of Mae-Moh lignite fly ash.

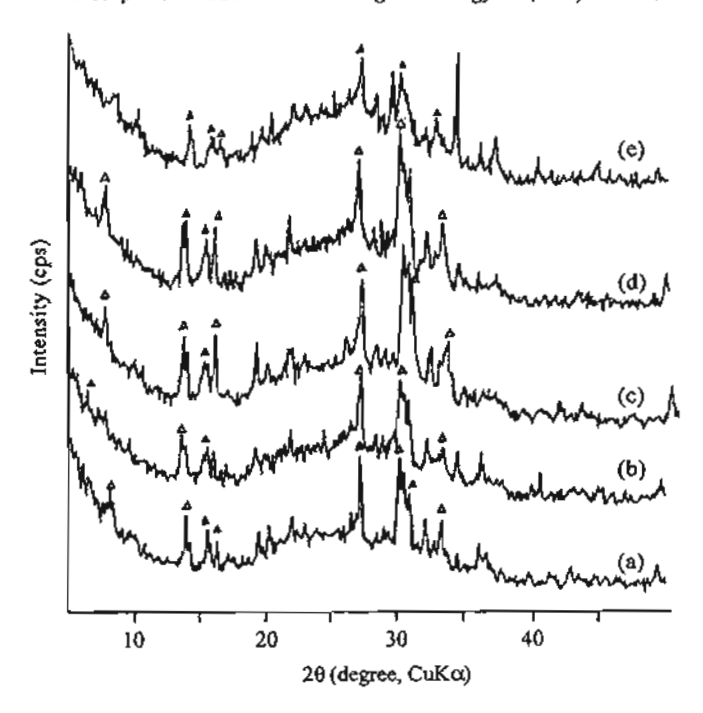


Fig. 2. XRD patterns of zeolitic products obtained from synthesis experiments without the presence of TPABr at SiO_2/Al_2O_3 mole ratios of (a) 20, (b) 40, (c) 60, (d) 80, and (e) 100 (Δ , Zeolite P; Initial pressure: 3 bar, holding temperature: 210 °C, holding period: 2 h).

In addition, irrespective of the SiO₂/Al₂O₃ mole ratio, the addition of TPABr of approximately 20 mol% of alumina in fly ash still could not promote the ZSM-5 zeolite formation.

Since the maximum yield of the ZSM-5 zeolite was obtained at a SiO₂/Al₂O₃ mole ratio of 40, this mole ratio was then used in the following experiments.

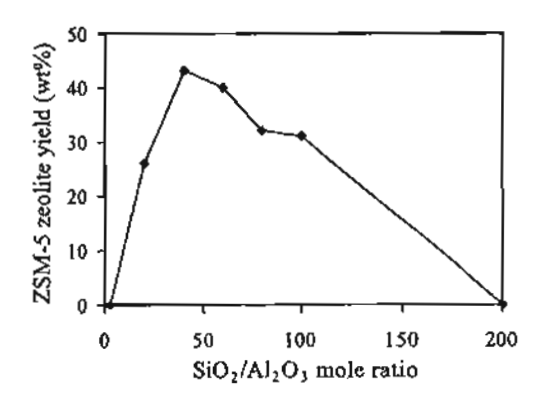


Fig. 3. Yields of ZSM-5 zeolite obtained from various SiO₂/Al₂O₃ mole ratios with TPABr (Initial pressure: 3 bar, holding temperature: 210 °C, holding period: 2 b).

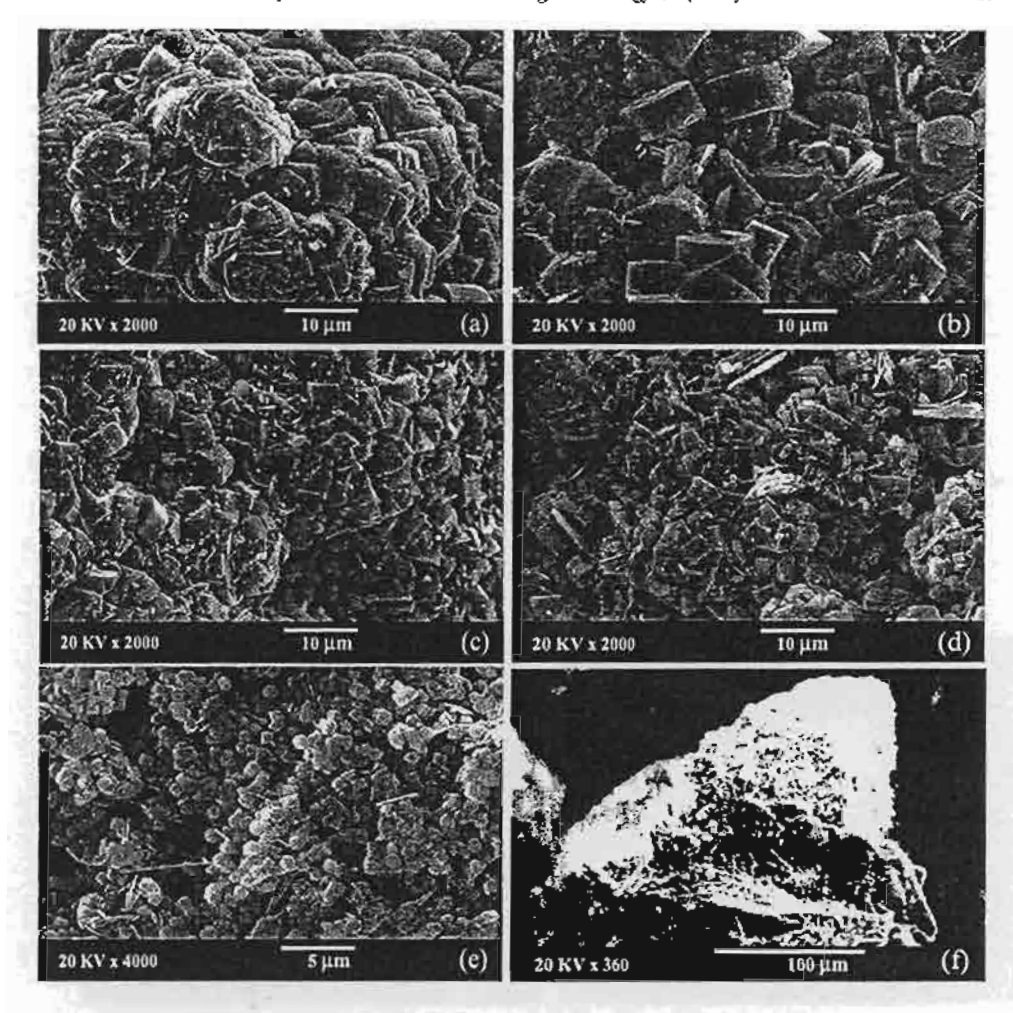


Fig. 4. SEM photographs of treated products obtained from SiO₂/Al₂O₃ mole ratios of (a) 20, (b) 40, (c) 60, (d) 80, (e) 100, and (f) 200 with TPABr (a-e=ZSM-5 zeolite, f-amorphous product; Initial pressure: 3 bar, holding temperature: 210 °C, holding period: 2 h).

3.2.2. Effect of temperature

The yields of the ZSM-5 zeolite obtained at temperatures ranging from 150 to 240 °C are shown in Fig. 5 and the SEM photographs of the products at 150 and 180 °C are shown in Fig. 6. At the temperature of 150 °C, the unknown amorphous solids of irregular shape and crystalline were found. It was noticed that the ZSM-5 zeolite could not be produced under this low temperature. The XRD pattern of the product obtained at 180 °C is shown in Fig. 7, which revealed that ZSM-5 zeolite (16 wt.%) and zeolite P were formed. At 210 °C, only ZSM-5 zeolite was found (43 wt.%). In accordance with the XRD result, the SEM photograph of the product at 180 °C indicates the presence of the cubic crystals of ZSM-5 zeolite and the needle-like crystals of zeolite P, while only the cubic

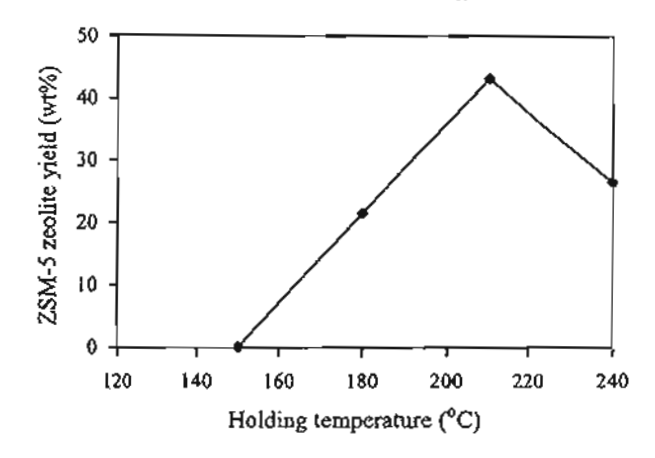


Fig. 5. Yields of ZSM-5 zeolite obtained from various holding temperatures (SiO₂/Al₂O₃ mole ratio: 40, initial pressure: 3 bar, holding period: 2 h).

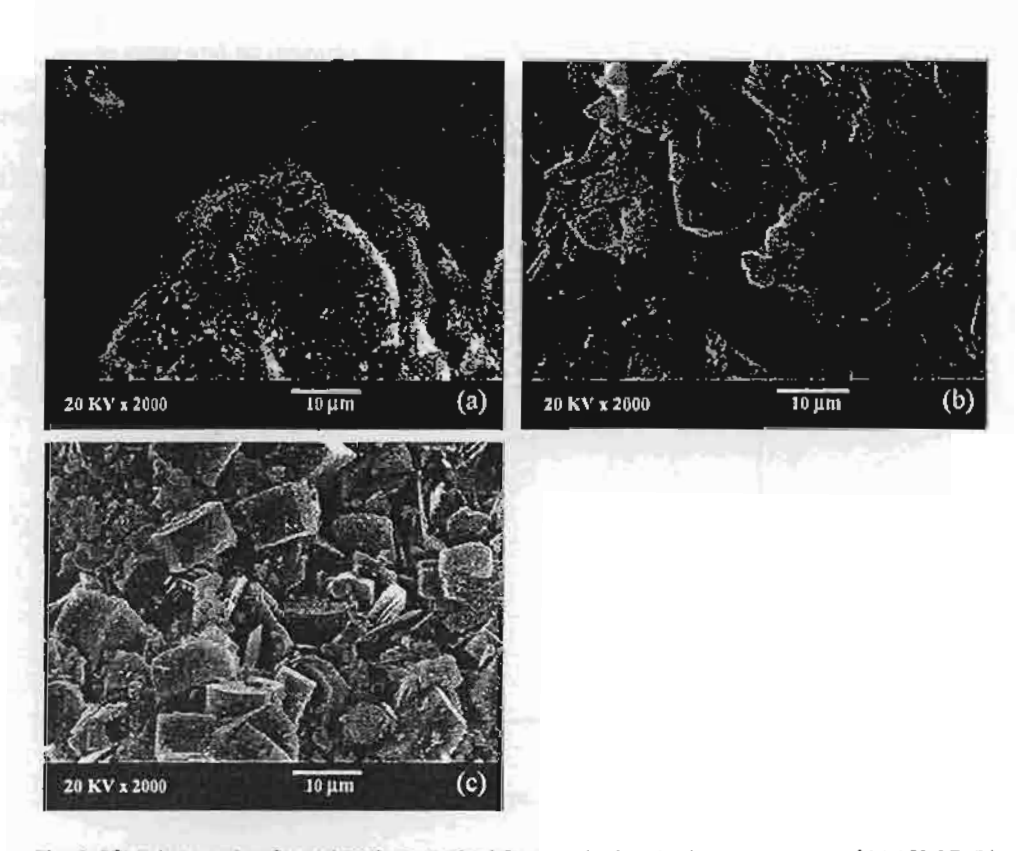


Fig. 6. SEM photographs of treated products obtained from synthesis at holding temperatures of (a) 150 °C, (b) 180 °C, and (c) 210 °C (SiO₂/Al₂O₃ mole ratio: 40, initial pressure: 3 bar, holding period: 2 h).

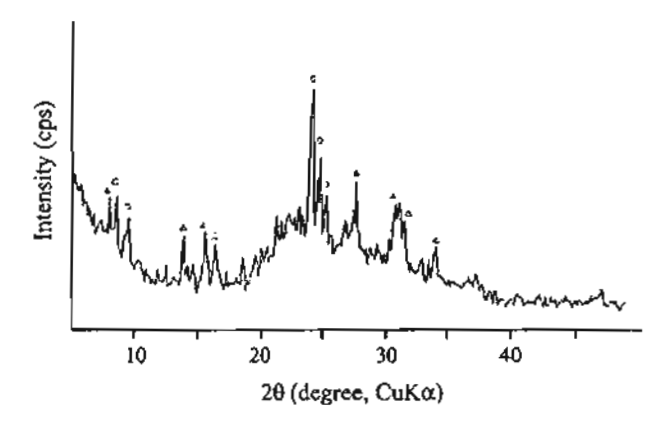


Fig. 7. XRD pattern of zeolitic products obtained from synthesis temperature of 180 °C (O=ZSM-5 zeolite, Δ =Zeolite P) (SiO₂/Al₂O₃ mole ratio: 40, initial pressure: 3 bar, holding period: 2 h).

crystals of the ZSM-5 zeolite were found at 210 °C. The reason is that the formation of metastable phases of zeolites depend on temperature, and then the most stable phase will continue to grow and be detected finally [16]. Not only the temperature, but the holding time and the initial pressure also play an important role on the formation of the specific metastable phase of zeolite.

For the study on the effect of the holding time, the synthesis temperature was fixed at 210°C and the holding time was varied at 0, 1, 2, 3 and 4 h. The yields of the product crystals shown in Fig. 8 notify that the longer the holding time, the greater the yield of ZSM-5 crystalline zeolite. As the holding time increased, the alkaline solution could more thoroughly dissolve silica and alumina from the fly ash. These silica and alumina in the alkaline solution are the sources of precursors for ZSM-5 zeolite formation and growth.

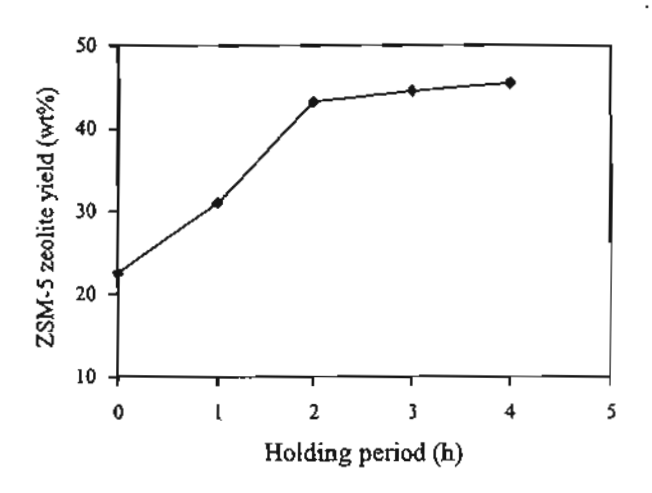


Fig. 8. Yields of ZSM-5 zeolite obtained from various holding periods (SiO₂/Al₂O₃ mole ratio: 40, initial pressure: 3 bar, holding temperature: 210 °C).

Therefore, the longer holding time used (in this study, 4 h) the higher yield of ZSM-5 zeolite could be obtained.

3.2.3. Effect of initial pressure

The effect of the initial pressure of inert gas on the yield of ZSM-5 zeolite was determined in the range of 1-6 bar. The yields of the ZSM-5 zeolite obtained at various initial pressures are shown in Fig. 9. It should be noted that all the XRD patterns of the products confirm the existence of only ZSM-5 zeolite. The ZSM-5 zeolite yields are gradually increased with the increase of initial pressure up to 4 bar (13 wt.% at 1 bar and 43 wt.% at 4 bar) and then decreased (31 wt.% at 5 bar and 26 wt.% at 6 bar). The initial pressure has a significant effect on the ZSM-5 zeolite synthesis. This is because the synthesis process takes place at high temperature under steam saturation condition. The increase of the initial pressure thermodynamically enhances the solubility of silica and alumina in fly ash in the alkaline solution and consequently the rate of formation of the ZSM-5 zeolite. However, at the initial pressure above 4 bar, the yield of ZSM-5 zeolite tends to decrease. This may be due to the competitive formation of different metastable phases of zeolite during the crystalline formation stage, which resulted in the formation of different phases of zeolite [16].

3.3. Hydrogenation of carbon dioxide over ZSM-5 zeolite from fly ash

The catalytic performance of ZSM-5 zeolite synthesized here was preliminary tested and compared with a commercial ZSM-5 zeolite (SiO₂/Al₂O₃ ratio, 40; surface area, 670 m²/g). The average results are shown in Table 3. With both catalysts, CO₂ conversions are gradually increased with the increase of reaction temperature (from 2-3 mol% at 200 °C to 28-30 mol% at 500 °C). In order to investigate the effect of thermal reaction, the reaction was tested under the same operating condition with an inert sand bed. It was

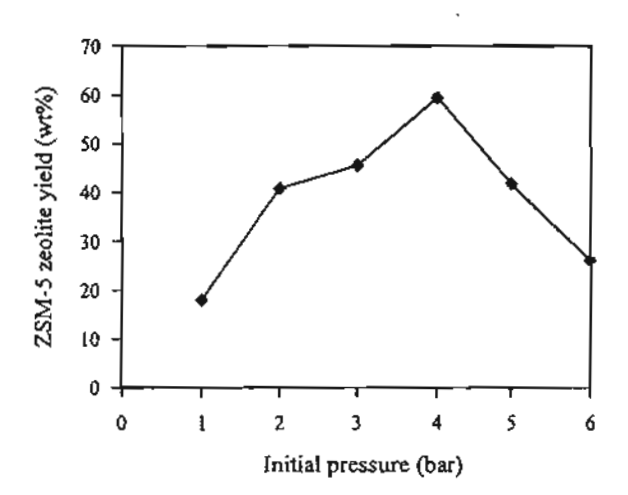


Fig. 9. Yields of ZSM-5 zeolite obtained from various initial pressures (SiO₂/Al₂O₃ mole ratio: 40, holding temperature: 210 °C, holding period: 4 h).

Table 3
Product distribution obtained from the reaction of CO₂ and H₂ over commercial ZSM-5 zeolite and ZSM-5 zeolite synthesized from fly ash and rice husk ash (in mol%)

Temperature (°C)	Commercial	ZSM-5 z	colite		Synthesized ZSM-5 zeolite			
	CO2	Product distribution			CO ₂	Product distribution		
	conversion	co	CH₄	C2-C3	conversion	со	CH₄	C2-C3
200	2	6	87	7	3	7	83	10
300	16	5	83	12	15	17	73	11
400	18	5	84	11	24	10	71	19
500	28	10	78	12	30	17	64	19

found that the conversion of CO₂ over the sand bed at 500 °C was lower than 5 % and methane was the major product.

The CO₂ conversion of the synthesized ZSM-5 zeolite and the commercial one were comparable. The products were mainly CO, methane and ethane. However, higher yields of C2-C3 were obtained with the synthesized ZSM-5 zeolite. At 500 °C, the C2-C3/CH₄ ratios were 0.3 with the synthesized ZSM-5 zeolite and 0.15 with the commercial one. It was suggested that metal oxide impurities remained in the synthesized ZSM-5 zeolite seem to have a little effect on the catalytic hydrogenation reaction.

4. Conclusions

The alternative utilization of Mae-Moh lignite fly ash and rice husk ash as raw materials for ZSM-5 zeolite synthesis is feasible. The effects of SiO₂/Al₂O₃ mole ratio, the presence of TPABr, temperature and initial pressure on the yield of ZSM-5 zeolite have been investigated using the fast synthesis process (about 2-6 h). Without the addition of sodium silicate solution, ZSM-5 zeolite could not be synthesized. With the presence of TPABr, ZSM-5 zeolite could be synthesized in a range of the SiO₂/Al₂O₃ mole ratio of 20-100. At a holding temperature of lower than 210 °C, several types of zeolites were produced. The maximum yield of ZSM-5 zeolite, 59 wt.%, was obtained at a SiO₂/Al₂O₃ mole ratio of 40, synthesis temperature of 210 °C, holding time of 4 h and initial pressure of 4 bar.

The catalytic performance of ZSM-5 zeolite synthesized from fly ash in the hydrogenation of CO₂ is remarkable. The conversion of CO₂ was 30 mol% at 500 °C and the products were carbon monoxide, methane, ethane and propane. With ZSM-5 zeolite synthesized from fly ash, higher yield of C2-C3 was produced when compared with the commercial one.

Acknowledgements

The Kasetsart University Research and Development Institute (KURDI) and the Senior Research Scholar Fund from Thailand Research Fund (TRF) have financially supported this research. Lignite fly ash sample was supplied by the Electricity Generating Authority of Thailand (EGAT).

References

- [1] V.I. Kouprianov, Fuel Process. Technol. 76 (2002) 187.
- [2] J. Majling, D.M. Roy, Am. Ceram. Soc. Bull. 72 (1993) 77.
- [3] B.E. Scheetz, R. Earle, Solid State Mater. Sci. 3 (1998) 510.
- [4] L.D. Chen, Y. Shen, J. Su, X. Wu, Cem. Concr. Res. 30 (2000) 881.
- [5] C.F. Lin, H.C. Hsi, Environ. Sci. Technol. 29 (1995) 1109.
- [6] C. Amrhein, G.H. Haghnia, T.S. Kim, P.A. Mosher, R.C. Gagajena, T. Amanios, L. Torre, Environ. Sci. Technol. 30 (1996) 735.
- [7] V. Berkgaut, A. Singer, Appl. Clay Sci. 10 (1996) 369.
- [8] E.L. Salinas, P. Salas, I. Schifter, M. Moran, S. Castillo, E. Mogica, Progress in zeolite and microporous materials, Stud. Surf. Sci. Catal. 105 (1997) 1565.
- [9] X. Querol, A. Alastuey, A. López-Soler, F. Plana, Environ. Sci. Technol. 31 (1997) 2527.
- [10] G. Steenbruggen, G.G. Hollman, J. Geochem. Explor. 62 (1998) 305.
- [11] A. Srinivasan, M.W. Grutzeck, Environ. Sci. Technol. 33 (1999) 1464.
- [12] X. Querol, J.C. Umana, F. Plana, A. Alastuey, A. Lopez-Soler, A. Medinaceli, A. Valero, M.J. Domingo, E. Garcia-Rojo, Fuel 80 (2001) 857.
- [13] X.S. Zhao, G.Q. Lu, H.Y. Zhu, J. Porous Mater, 4 (1997) 245.
- [14] H.L. Chang, W.H. Shih, Ind. Eng. Chem. Res. 37 (1998) 71.
- [15] G.G. Hollman, G. Steenbruggen, M.J. Janssen, Fuel 78 (1999) 1225.
- [16] D.W. Break, Zeolite Molecular Sieves: Structure, Chemistry and Use, Wiley, 1974.

Partial cross sections for positive and negative ion formation following electron impact on uracil

S Feil¹, K Gluch^{1,3}, S Matt-Leubner¹, P Scheier¹, J Limtrakul^{1,4}, M Probst¹, H Deutsch^{1,5}, K Becker^{1,6}, A Stamatovic^{1,7} and T D Märk^{1,2}

E-mail: kbecker@stevens.edu

Received 4 May 2004 Published 20 July 2004 Online at stacks.iop.org/JPhysB/37/3013 doi:10.1088/0953-4075/37/15/001

Abstract

We report absolute partial cross sections for the formation of selected positive and negative ions resulting from electron interactions with uracil. Absolute calibration of the measured partial cross sections for the formation of the three most intense positive ions, the parent C₄H₄N₂O₂⁺ ion and the C₃H₃NO⁺ and OCN+ fragment ions, was achieved by normalization of the total single uracil ionization cross section (obtained as the sum of all measured partial single ionization cross sections) to a calculated cross section based on the semi-classical Deutsch-Märk formalism at 100 eV. Subsequently, we used the OCN* cross section in conjunction with the known sensitivity ratio for positive and negative ion detection in our apparatus (obtained from the well-known cross sections for SF₄ and SF₄ formation from SF₆) to determine the dissociative attachment cross section for OCN- formation from uracil. This cross section was found to be roughly an order of magnitude smaller, about 5×10^{-22} m² at 6.5 eV, compared to our previously reported preliminary value. We attribute this discrepancy to the difficult determination of the uracil target density in the earlier work. Using a reliably calculated cross section for normalization purposes avoids this complication.

¹ Institut für Ionenphysik, Leopold-Franzens Universität, A-6020 Innsbruck, Austria

Department of Plasma Physics, Comenius University, SK-84248 Bratislava, Slovakia

³ Permanent address: Institute of Mathematics, Physics and Informatics, Maria Curie-Sklodowska University, Lublin 20-031, Poland.

Permanent address: Department of Chemistry, Kasetsart University, Bangkok 10900, Thailand.

Permanent address: Institut f
ür Physik, Universit
ät Greifswald, D-17487 Greifswald, Germany.

⁶ Permanent address: Department of Physics and Center for Environmental Systems, Stevens Institute of Technology, Hoboken, NJ 07030, USA.

Permanent address: Faculty of Physics, University Beograd, PO Box 638, Yu-11001 Beograd, Serbia.

3014 S Feil et al

1. Introduction

Recently, electron interactions with biologically important molecules such as amino acids and nucleotides, in particular (dissociative) electron attachment studies, have gained prominence following the pioneering work of Sanche and co-workers [1]. Electron scattering experiments with complex biomolecules in the gas phase are challenging because of the difficulties in the preparation of well-characterized pure gas targets of these molecules and the difficulties in the subsequent quantitative determination of the target densities. The RNA base uracil (see figure 1 for a schematic molecular structure diagram) and various halo-uracil compounds as well as DNA bases such as thymine, cytosine, adenine, various halo-uracil compounds and simple organic acids such as formic and acetic acid and several amino acids (glycine, deoxyribose) have been studied successfully in gas-phase electron scattering experiments [2-17]. Very recently [2], our group measured the first absolute electron attachment cross sections for the RNA base uracil ($C_4H_4N_2O_2$) and reported peak values ranging from 1 to 30×10^{-21} m² for four fragment anions, CN⁻, OCN⁻, C₃H₂NO⁻ and C₄H₃N₂O₂⁻, at electron energies below 10 eV. The importance of anion formation via dissociative electron attachment in these molecules stems from the fact that it is the only mechanism that can cause bond cleavage at very low electron energies, which are typical for (nearly) thermalized secondary electrons produced by the interaction of high-energy radiation with the complex environments surrounding and constituting living cells. However, it has also been pointed out [10, 15, 18] that positive ion formation induced by electron impact on uracil and halo-uracil compounds is an important fragmentation mechanism for these molecules, particularly for low electron energies just above the ionization threshold.

In this paper, we report the first absolute partial and total cross sections for the electronimpact ionization of uracil. Absolute cross sections were obtained by normalizing the total
single ionization cross section of uracil (at an electron energy of 100 eV) to a calculated
total single ionization cross section using the semi-classical Deutsch-Märk (DM) formalism
[19, 20]. The DM formalism has been shown to yield reliable total single ionization cross
sections (with an accuracy ranging between 5% and 20%) for a large number of molecules,
including complex molecules [19, 21-23]. On the basis of the absolute calibration process for
positive ions in conjunction with a sensitivity ratio measurement for positive-to-negative ion
formation in our apparatus, we also revise our earlier absolute cross section for dissociative
attachment to uracil [2] downward by about an order of magnitude. We attribute this
discrepancy to difficulties in the accurate target number density determination in the earlier
experiment.

2. Experimental procedure and cross section normalization

The current experiments were carried out in our well-characterized double-focusing two-sector field mass spectrometer of reversed geometry described in numerous earlier publications (see, e.g., [24–26]), to which we refer the reader for further experimental details. Figure 2 shows a mass spectrum of positive ions produced by 120 eV electrons on uracil. The most intense peak at a mass-to-charge (m/z) ratio of 112 corresponds to the parent uracil $C_4H_4N_2O_2^*$ ion (m/z=112 Thomson). Two other groups of peaks are seen around the two most abundant fragment ions, $C_3H_3NO^+$ (m/z=69 Thomson), with adjacent weaker peaks corresponding to the loss of additional H atoms, and OCN^+ (m/z=42 Thomson). The additional weaker peaks around m/z=40 correspond to ions with two carbon atoms, one nitrogen or oxygen atom and from 0-3 hydrogen atoms. We recorded relative partial ionization cross sections for the three most intense mass-selected ions in the mass spectrum

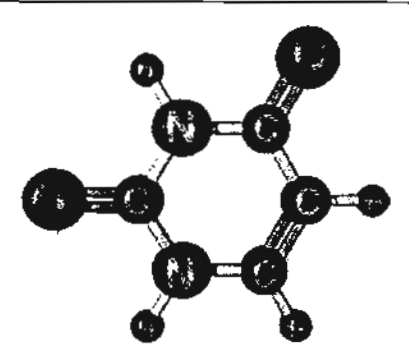


Figure 1. Schematic structure diagram of the tracil C4H4N2O2 molecule,

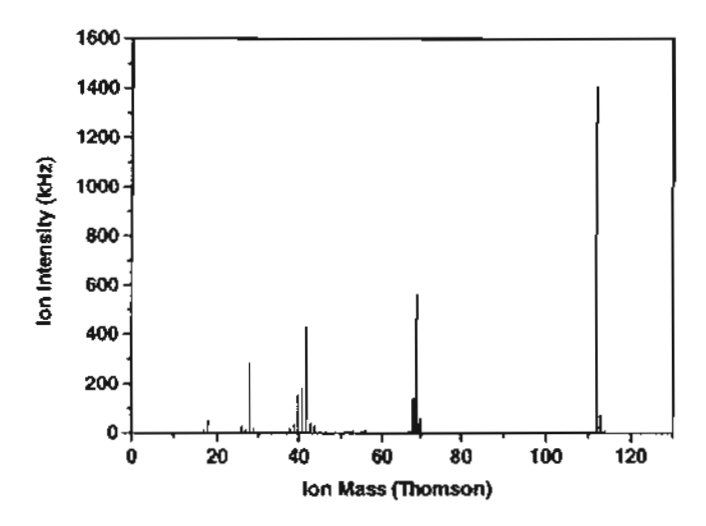


Figure 2. Mass spectrum of positive ions formed by 120 eV electron impact on uracil. The most intense peaks correspond to the parent C₄H₄N₂O₂^{*} ion and two fragment ions C₃H₃NO^{*} and OCN^{*}.

shown in figure 2 for electron energies from threshold to 1000 eV. The sum of all partial ionization cross sections for the formation of singly charged product ions yields the relative total single uracil ionization cross section. We note that we did not find ion signals of appreciable intensity that correspond to the formation of doubly (or more highly) charged ions, so that the total single uracil ionization cross section is essentially identical to the total ionization cross section of this molecule. The relative total single uracil ionization cross section was put on an absolute scale by normalizing the experimentally determined cross section to a calculated total single uracil ionization cross section using the DM formalism at 100 eV, $15.7 \times 10^{-20} \text{ m}^2$. The DM formalism applied to molecules has been shown to yield reliable absolute total ionization cross sections with an accuracy between 5% and 20% for a large number of molecules, including complex molecules such as the silicon-organic compounds tetramethylsilane (TMS), hexamethyldisiloxane (HMDSO) and tetraethoxysilane (TEOS) [19, 21-23]. The only category of molecular targets for which the DM formula shows poor agreement with the experimental data is for fluorine-containing radicals such as CF_x and NF_x (x = 1-3) [27]. A detailed comparison between calculated DM cross sections and

3016 S Feil et al

measured data for more than 40 species has shown that the reliability of the DM calculation depends critically on the accuracy of the quantum chemical representation of the molecular orbitals in terms of the atomic orbitals of the constituent atoms [19]. The accuracy of the DM method is difficult to assess in general as its errors have different sources. For the ionization energies, accurate quantum chemical values can be derived. Concerning the atomic orbital populations, however, this is not possible in the same way. There is no unique definition of dividing up the molecular orbitals into atomic contributions, since in the limit of an infinite basis set even the basis set of a single atom can describe the wavefunction of the whole molecule. While smaller basis sets might even provide more reasonable relative atomic orbital charge contributions than bigger ones, they suffer from the poor quality of the overall wavefunction. This dilemma, which is sometimes found in the quantum chemical calculation of other properties as well, can be partially overcome by using more sophisticated schemes of charge partitioning etc, but the coefficients g and r in the DM formula are still derived from isolated atoms and cannot easily be improved upon without abandoning the general scheme. In light of these arguments, an empirical statement concerning the accuracy of the DM method seems to be most appropriate. The large number of molecules, where comparisons between experimental and cross sections calculated with the DM formula have been made, shows that the errors for molecules of not more than about 20 atoms are not larger than 20% (often significantly smaller) and comparable to the errors reported for the experimental cross sections.

The cross-calibration between the formation of positive and negative ions from the same parent molecule was first described in our earlier paper on the electron impact ionization of C_{60} [28, 29]. Briefly, the method uses the well-known absolute cross sections for formation of SF_4^+ and SF_4^+ ions from SF_6 by electron impact and determines, under exactly identical experimental conditions, the ratio of SF_4^+ ions to SF_4^+ ions detected in our apparatus in an effort to determine the ratio of detection efficiencies for, respectively, negative and positive ions. This ratio in conjunction with the absolute value of the partial ionization cross section for formation of a particular positive ion then determines the absolute dissociative attachment cross section for formation of the corresponding negative ion for a gas under study. In the present case of uracil, we found that electrons incident on this molecule produce both positive OCN⁺ and negative OCN⁻ fragment ions and we used these ions for the cross-calibration.

The uncertainties of the absolute ionization cross sections reported here are in the range of 21–22% for positive ions and about 26% in the case of the attachment cross sections. In the case of the positive ions, we combine the uncertainty in the measurement of the relative cross section curves of 5% (which takes into account the statistical uncertainty and systematic uncertainties due to all fluctuations of the experimental parameters such as gas density, electron beam current, etc) in quadrature with a conservative estimate of a 20% uncertainty in the calculated DM cross section. For the negative ions, we add to this uncertainty in quadrature the 15% uncertainty in the SF₄ to SF₄ cross section ratio [29].

3. Results and discussion

Figure 3 shows the experimentally determined total single uracil ionization cross section from threshold to 1000 eV in comparison with the calculated DM cross section. The experimental data were normalized to the calculation at 100 eV. Both cross sections exhibit the typical shape with a maximum (of about 16×10^{-20} m²) at an energy slightly below 100 eV and a gradual decline towards higher impact energies. The agreement is very good over the entire range of impact energies. The two curves are essentially identical in the low-energy regime from threshold up to about 150 eV. At higher impact energies above about 200 eV, the

S Feil et al

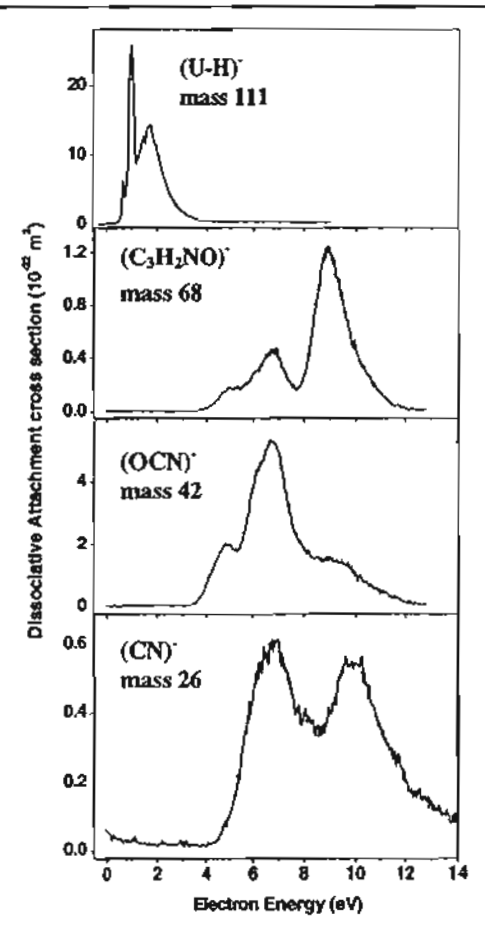


Figure 5. Absolute partial cross sections for dissociative electron attachment to uracil as a function of electron energy. (U-H)⁻ refers to the C₄H₃N₂O₂⁻ ion.

largest peak value of about 4.4×10^{-20} m² (at about 100 eV) whereas the two fragment ions have cross sections that peak around 2.2×10^{-20} m² at a slightly higher impact energy. It is quite noteworthy for a complex molecule such as uracil that the largest partial ionization cross section is the one for parent ion formation. Many complex molecules do not have stable parent ions and their ionization is dominated by dissociative ionization channels [19, 21-23].

Lastly, figure 5 shows four absolute partial cross sections for dissociative electron attachment to uracil leading to, respectively, $C_4H_3N_2O_2^-$, $C_3H_2NO^-$, OCN^- and CN^- ions as a function of electron energy after cross-calibration to the absolute OCN^+ ionization cross section using the relative cross sections given in [2]. (We note that the labels of the two curves corresponding to the $C_3H_2NO^-$ and OCN^- negative ions were interchanged; figure 4 in this paper shows the correct labelling.) In all four cases, the absolute cross sections are about an order of magnitude lower compared to those reported earlier [2]. We attribute the discrepancy between the present absolute calibration of the dissociative attachment cross sections and our earlier measurement to difficulties in the determination of the target number density in the earlier experiments. In the present work, the normalization to a reliable calculated

ionization cross section in conjunction with the positive—negative ion cross-calibration avoids the potential error associated with the target number density determination.

4. Conclusions

We report absolute partial cross sections for the formation of selected positive and negative ions resulting from electron interactions with uracil. Because of the difficulties associated with the preparation of well-characterized gas targets of essentially all biologically important molecules and the absolute determination of the gas target density, we obtained the absolute cross sections in our study by normalizing the total single ionization cross section of uracil (at an electron energy of 100 eV) to a calculated total single ionization cross section using the semi-classical Deutsch-Märk formalism [19, 20]. The DM formalism has been shown to yield reliable total single ionization cross sections (with an accuracy ranging between 5% and 20%) for a large number of molecules, including complex molecules [19, 21-23]. On the basis of the absolute calibration process for positive ions in conjunction with a sensitivity ratio measurement for positive-to-negative ion formation in our apparatus, we subsequently revised our earlier absolute cross section for dissociative attachment to uracil [2] downward by about an order of magnitude.

Acknowledgments

This work was partially supported by the FWF, ÖNB and ÖAW, Vienna, Austria and the EU Commission, Brussels. We would like to acknowledge financial support from the US Department of Energy, Office of Basic Energy Sciences, Chemical Sciences, Geosciences, and Biosciences Division to KB as well as support from the Thailand Research Fund (TRF), Kasetsart University (KURDI) and the Ministry of University Affairs (MUA-ADB) to IL.

References

- [1] Boddaiffa B, Cloutier P, Hunting D, Huels M A and Sanche L 2000 Science 287 1658
- [2] Hanel G, Gstir B, Deniff S, Scheier P, Probst M, Farizon B, Farizon M, Illenberger E and Märk T D 2003 Phys. Rev. Lett. 90 188104
- [3] Desfrançois C, Abdoul-Carime H and Schermann J P 1994 Phys. Rev. Lett. 73 2436
- [4] Desfrançois C, Abdoul-Carime H and Schermann J P 1996 J. Chem. Phys. 104 7792
- [5] Desfrançois C, Periquet V, Boutellier Y and Schermann J P 1998 J. Phys. Chem. 102 1274
- [6] Aflatoori K, Gallup G A and Burrow P D 1998 J. Phys. Chem. 102 6205
- [7] Huels M A, Hahndorf I, Illenberger E and Sanche L 1998 J. Chem. Phys. 108 1309
- [8] Abdoul-Carime H, Huels M A, Brüning F, Illenberger E and Sanche L 2000 J. Chem. Phys. 113 2517
- [9] Abdoul-Carirne H, Huels M A, Sanche L and Illenberger E 2001 J. Am. Chem. Soc. 123 5354
- [10] Coupier B et al 2002 Eur. Phys. J. D 20 459
- [11] Abdoul-Carine H., Huels M. A., Illenberger E and Sanche L. 2003 Int. J. Mass Spectr. 228 687
- [12] Deniff S, Prasinska S, Cingel M, Matejcik S, Scheier P and Märk T D 2003 Chem. Phys. Lett. 377 27
- [13] Abouaf R, Pommier J and Dunet H 2003 Int. J. Mass Spectrom. 226 397
- [14] Deniff S, Matejik S, Gstir B, Hanel G, Probst M, Scheier P and Märk T D 2003 J. Chem. Phys. 118 4107
- [15] Denift S, Ptasinska S, Scheier P and Mäck T D 2004 Int. J. Mass Spectrom. 232 99
- [16] Gianturco F et al 2004 Phys. Rev. Lett. at press
- [17] Deniff S, Ptasinska S, Hanel G, Gstir B, Scheier P and Märk T D 2004 J. Chem. Phys. 120 6557
- [18] Wetmore S D, Boyd R J and Eriksson L A 2000 Chem. Phys. Lett. 322 129
- [19] Deutsch H, Becker K, Man S and Märk T D 2000 Int. J. Mass Spectrom. 197 37
- [20] Deutsch H, Scheier P, Becker K and Märk T D 2004 Int. J. Mass Spectrom. 233 13
- [21] Deutsch H, Hilpert K, Becker K, Probst M and Märk T D 2001 J. Appl. Phys. 89 1915
- [22] Probst M, Deutsch H, Becker K and Märk T D 2001 Int. J. Mass Spectrom. 206 13

3020

- [23] Bernhardt P and Pareizke G H 2003 Int. J. Mass Spectrom. 223/224 599
- [24] Grill V, Walder G, Margreiter D, Rauth T, Poll H U, Scheier P and Märk T D 1993 Z. Phys. D 25 217
- [25] Poll H U, Grill V, Matt S, Abramzon N, Becker K, Scheier P and Märk T D 1998 Int. J. Mass Spectrom. Ion Proc. 177 143
- [26] Gluch K, Scheier P, Schustereder W, Tepnual T, Feketeova L, Mair C, Matt-Leubner S, Stamatovic A and Märk T D 2003 Int. J. Mass Spectrom. 228 307
- [27] Huo W M, Tarnovsky V and Becker K 2001 Chem. Phys. Lett. 358 328
- [28] Dünser B, Lezius M, Scheier P, Deutsch H and Märk T D 1995 Phys. Rev. Lett. 74 3364
- [29] Matt S, Dünser B, Lezius M, Deutsch H, Becker K, Stamatovic A, Scheier P and Märk T D 1996 J. Chem. Phys. 105 1880

Theoretical Study of the Adsorption of Ethylene on Alkali-Exchanged Zeolites

SOMBAT KETRAT, JUMRAS LIMTRAKUL

Laboratory for Computational & Applied Chemistry, Physical Chemistry Division, Kasetsart University, Bangkok 10900, Thailand

Received 30 August 2002; accepted 8 May 2003

DOI 10.1002/qua.10706

ABSTRACT: The structures of alkali-exchanged faujasite (X-FAU, X = Li* or Na* ion) and ZSM-5 (Li-ZSM-5) zeolites and their interactions with ethylene have been investigated by means of quantum cluster and embedded cluster approaches at the B3LYP/6-31G (d, p) level of theory. Inclusion of the Madelung potential from the zeolite framework has a significant effect on the structure and interaction energies of the adsorption complexes and leads to differentiation of different types of zeolites (ZSM-5 and FAU) that cannot be drawn from a typical quantum cluster model, H₃SiO(X)Al(OH)₂OSiH₃. The Li-ZSM-5 zeolite is predicted to have a higher Lewis acidity and thus higher ethylene adsorption energy than the Li-FAU zeolites (16.4 vs. 14.4 kcal/mol), in good agreement with the known acidity trend of these two zeolites. On the other hand, the cluster models give virtually the same adsorption energies for both zeolite complexes (8.9 vs. 9.1 kcal/mol). For the larger cation-exchanged Na-FAU complex, the adsorption energy (11.6 kcal/mol) is predicted to be lower than that of Li-FAU zeolites, which compares well with the experimental estimate of about 9.6 kcal/ mol for ethylene adsorption on a less acidic Na-X zeolite. © 2003 Wiley Periodicals, Inc. Int J Quantum Chem 94: 333-340, 2003

Key words: ZSM-5 zeolite; faujasite zeolite; DFT study; ethylene adsorption; embedded cluster

Introduction

地名加加加加西西部

eolites are of prime importance as catalysts for many industrial processes, due mainly to their shape selectivity and acid sites [1–9]. Cation-exchanged zeolites have been found to be potential catalysts for hydrocarbon reactions [10–19]. Of par-

Correspondence to: J. Limtrakul; e-mail: fscijrl@ku.ac.th

ticular interest in this area of active research is the alkene adsorption on alkali-exchanged zeolite, which is the foundation of several industrially important reactions, namely, aromatization of olefins [18], formation of ethylbenzene and styrene [19], and the production of xylene [20].

7.00

٠:.

The importance of metal-exchanged zeolites suggests that a better understanding of the structure and mechanistic properties at the molecular level of the catalyst is certainly required [21]. A review of quantum chemical calculations applied to zeolites and their interaction with unsaturated hydrocarbon has been recently reported [22]. All early works of adsorption of C₂H₄ on bare zeolite clusters were limited to small model fragments that are not specific to a particular zeolite but represent a generic tetrahedral subunit in an unconstrained environment [22–26]. It is known that small zeolitic clusters may inadequately reflect adsorption complexes at the active site and the cluster environment may enhance binding energy and, hence, more accurately predict the structures of reaction intermediates, transition states, and products [5, 27].

To include the effects of the zeolite framework on adsorption of C₂H₄ in zeolites, a periodic electrostatic structure method can be utilized [28-31]. This corresponds to the high loading case and is often computationally expensive for most zeolites due to their relatively large unit cells.

Alternatively, the embedded cluster approach [5, 9] provides a more practical methodology with little additional computational cost when compared to the bare cluster calculation. To the best of our knowledge, no theoretical work regarding the metal-exchanged zeolite-ethylene complex has been carried out so far.

In this study, we examine the effects of cations and the zeolitic framework on the adsorption properties of ethylene in alkali-exchanged faujasite and ZSM-5 using the embedded cluster methodology.

"Methods

"Y Zeolites have elementary building units of tetrahedral SiO₄ and AlO₄ commonly called T atoms. A 3-D framework of faujasite-type zeolite is built on 24-T cubo-octahedral sodalite cages linked via their six-membered rings forming large cavities called supercages [Fig. 1(a)]. On the other hand, the ZSM-5 zeolite framework is built on connected penfasil units forming straight and sinusoidal pore systems [Fig. 1(b)].

We employed the clusters illustrated in Figures 2–4 as the models of interaction of unsaturated hydrocarbon on alkali-metal-exchanged zeolites. The models H₃SiO(X)Al(OH)₂OSiH₃, where X = Li and Na, will hereafter be referred to as [Li-FAU], [Na-FAU], and [Li-ZSM-5], and their complexes, H₃SiO(X)Al(OH)₂OSiH₃/[C₂H₄], will be referred to as [Li-FAU]/[C₂H₄], [Na-FAU]/[C₂H₄], and [Li-ZSM-5]/[C₂H₄]. The bare quantum clusters are specifically modeled according to crystallographic

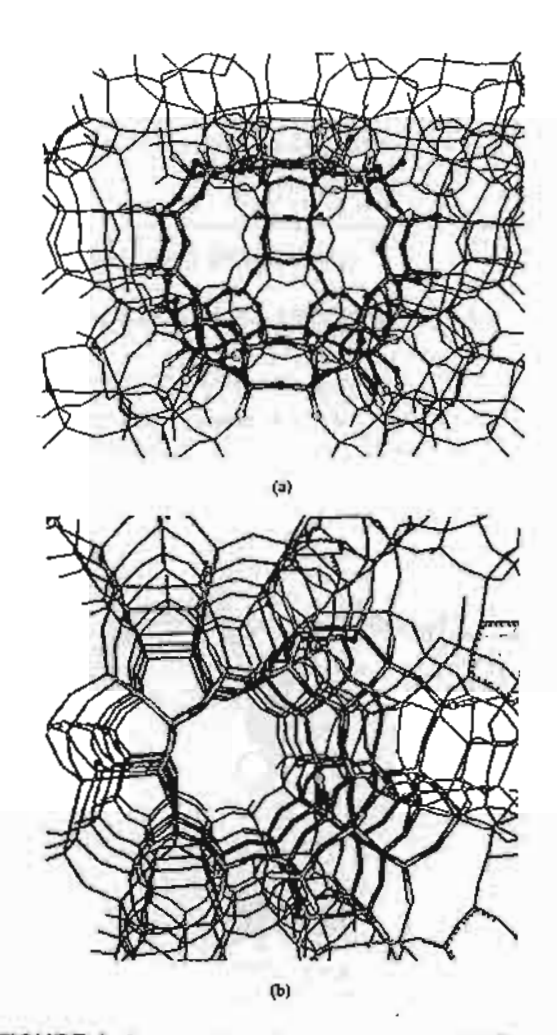


FIGURE 1. Presentation of zeolite structure. (a) Structure of faujasite showing the supercage. (b) Structure of ZSM-5 viewed from the straight direction. [Color figure can be viewed in the online issue, which is available at www.interscience.wiley.com.]

structures of active sites in faujasite [31] and ZSM-5 [32] zeolites. In these models, the dangling bonds of the Si atoms are terminated by H atoms and the Si—H bonds are aligned with the corresponding S—O bonds of the structures of zeolites, respectively. The naked alkali–cation/ C_2H_4 adducts, Li⁺/ $[C_2H_4]$ and Na⁺/ $[C_2H_4]$, are also included for comparison with the effect of the negative zeolite oxygen framework surrounding the alkali cations.

In the embedded cluster model (cf. Fig. 5), the static Madelung potential due to atoms outside of the quantum cluster is represented by charges located at the zeolite lattice sites. Charges close to the

tal.

(a)

134.1

[133.8]

(a)

134.1

[133.8]

(b)

194.6

[187.3]

194.6

[187.3]

194.6

(b)

他以前がおけいた

3.

41

ch that that that that

FIGURE 2. Li-FAU zeolite structures and their interaction with ethylene optimized at 83LYP/6-31G(d, p) using embedding and cluster calculations (values in parentheses); bond distances in pm. (a) Li-FAU. (b) Li-FAU/C₂H₄. [Color figure can be viewed in the online issue, which is available at www.interscience.wiley.com.]

quantum cluster are treated explicitly, while the Madelung potential from the remaining charges from an infinite lattice is represented by a set of surface charges that were derived from the surface charge representation of external embedded potential (SCREEP) method. More details on our method can be found elsewhere [5, 9]. For faujasite, the total Madelung potential is represented by 288 explicit charges and 960 surface charges, whereas for ZSM-5 the potential is represented by 360 explicit charges and 240 surface charges. With this small number of point charges, the additional computational cost is often less than 5% when compared to bare cluster calculations.

Geometry optimizations were carried out at the B3LYP level using the 6-31G (d, p) basis with the Gaussian 98 program [33]. The computations were carried out on PC clusters at the KU Computing Center and a DEC alpha station 250 workstation at

the Laboratory for Computational and Applied Chemistry at Kaselsart University and a cluster of IBM RISC/6000 workstations at the Henry Eyring Center for Theoretical Chemistry, University of Utah.

Results and Discussion

METAL-EXCHANGED FAUJASITE (X-FAU)

Li-Zeolite (Li-FAU)

Cluster and embedded cluster models for alkalimetal-exchanged zeolites are shown in Figures

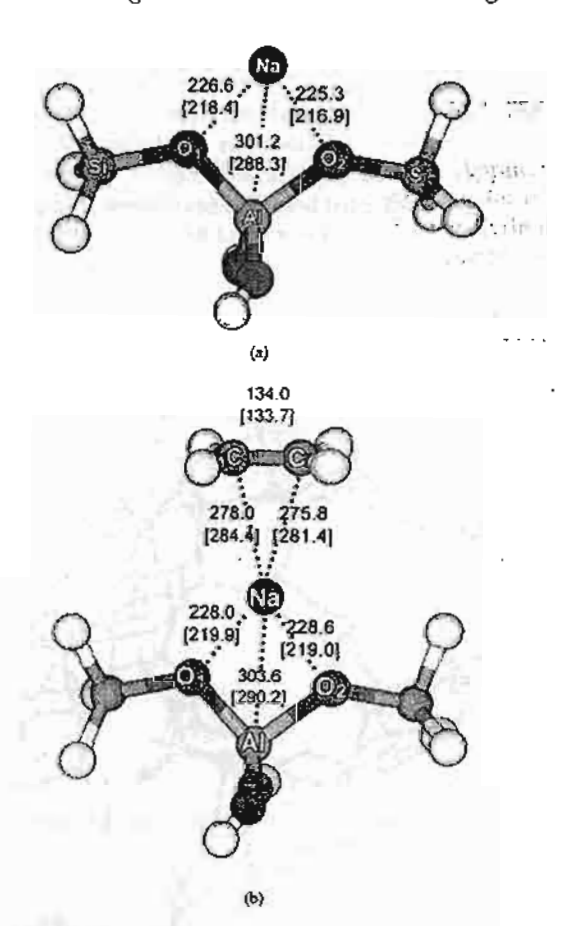


FIGURE 3. Na–FAU zeolite structures and their interaction with ethylene optimized at B3LYP/6-31G(d, ρ) using embedding and cluster calculations (values in parentheses); bond distances in pm. (a) Na–FAU. (b) Na–FAU/C₂H_a. [Color figure can be viewed in the online issue, which is available at www.interscience.wiley. com.]

KETRAT AND LIMTRAKUL

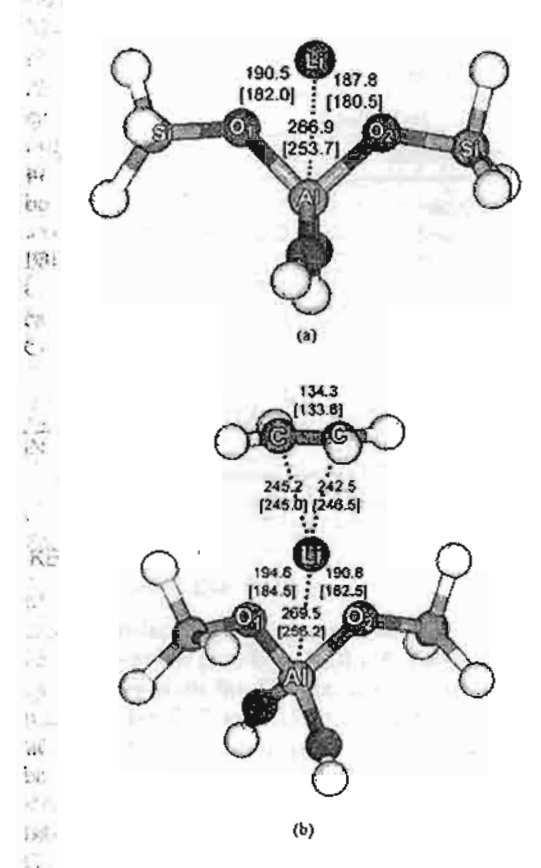


FIGURE 4. Li–ZSM-5 zeolite structures and their interaction with ethylene optimized at the B3LYP/6-31G(a, p) level using embedding and cluster calculations (values in parentheses); bond distances in pm. (a) Li–ZSM-5. (b) Li–ZSM-5/C₂H₄. (Color figure can be viewed in the online issue, which is available at www.interscience.wiley.com.)

2(a)-4(a). Selected optimized geometric parameters and atomic charges for bare quantum cluster and embedded cluster models are documented in Tables I and II. For the Li-FAU zeolite [see Fig. 2(a)], the alkali-metal cation does not bind with a particular bridging oxygen atom in the [AlO₄] but is symmetrically bidentated to O1 and O2 of [AlO₄] tetrahedron, in agreement with the previously reported ESR experiment [34]. The interaction of the cationic metal with the zeolite framework leads to substantial perturbation of the active acidic site. In particular, we found that the Al-O distances were élongated by 2.3 pm, but by only 0.9 pm for the Al-O2 and Al-O1 distances, respectively, while the Si—O bonds were shortened by 3.6 and 4.0 pm for the Si-O1 and Si-O2 bonds, respectively, but

100

10 .

bl. th da

there was no significant change for the O1—Al—O2 angle. A reciprocal effect is that the zeolite framework reduces the Li charge. The charge on Li* cation was reduced to 0.53, and 0.63 a.u. for the bare cluster and the embedded models, respectively. The increase of charges on Li cation is clearly observed by the changes of charges on Al and Si atoms of the Li-FAU complexes as compared to the corresponding charges of their anionic framework (cf. Table II). The Madelung potential was found to have a significant effect on the structure of Li-exchanged FAU. In particular, it elongates the Li-Al by 10.7 pm. The extent of Li-O distances increased with the embedded model (Li. O1 = 185.1 pm vs. 191.4 pm and Li···O2 = 183.9 pm vs. 190.4 pm). This indicates that the Madelung field weakens the attachment of the Li cation to the zeolite framework, and thus reduces the strength of the complexes, which is reflected by lower complexation energy (-135.92 kcal/mol) of Li(1) and zeolitic anion than those obtained from the bare quantum cluster (-160.78 kcal/mol).

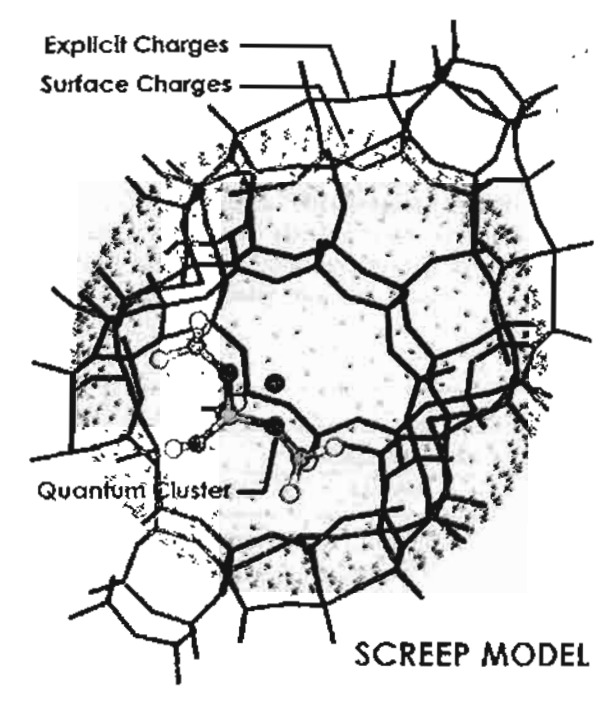


FIGURE 5. SCREEP embedded cluster model. {Color figure can be viewed in the online issue, which is available at www.interscience.wiley.com.}

VOL. 94, NO. 6

	(Li	-ZSM-5]	וַן	Ji-FAU]	[Na-FAU]		
Parameters	Bare	Embedded	Bare	Embedded	Bare	Embedded	
У Х*—АІ	253.7	266.9	249.8	260.5	288.3	301.2	
X ⁺ 01	182.0	190.5	185.1	191.4	218.4	226.6	
X+02	180.5	187.8	183.9	190.4	216.9	225.3	
O1-X+-O2	88.4	83.5	92.2	88.6	76.8	73.6	
AIO1	176.8	178.5	180.2	181.1	179.3	180.4	
AI—02	177.1	178.3	180.8	183.1	180.0	182.3	
O1-AI-O2	91.1	89.9	94.9	94.2	97.6	96.5	
SI02	164.3	160.7	166.7	162.7	165.1	161.3	
SI01	164.1	160.0	166.6	163.0	164.8	161.5	
qX*	0.52	0.63	0.53	0.63	0.67	0.73	

Bond lengths are in pm and bond angles in degrees.

Na-Zeolite (Na-FAU)

A similar trend has been observed for the Na-EAU complex [see Fig. 3(a)] (cf. Tables I and II). The charges on the Na+ cation within the zeolite models are 0.67 and 0.73 for cluster and embedded cluster models, respectively. The Na · · · O distances are elongated with the embedded model $(Na \cdot \cdot \cdot O1 = 218.4 \text{ pm vs. } 226.6 \text{ pm and}$ $Na \cdot O2 = 216.9 \text{ pm vs. } 225.3 \text{ pm}$). The calcufated Na. Al distance of the embedded model is 12.9 pm larger than that of the bare cluster, indicating that the embedding environment weakens the attachment of the metal cation to the zeolite framework. Regarding the energetics of the Na-FAU complexes, the complexation energy of the Na cation to the zeolitic framework leads to change in the geometric structures (the O1-Al-O2 bond angles and X+-Al distances, the distance between the cation and the A1 atom of zeolite framework, are increased with the increasing cationic size). These are, as expected, smaller than those for the Li-FAU complex (cf. Table II). The complexation energies of the monovalent ions Li+ and Na+ that are bound to a zeolitic framework are -135.92 (Li-FAU) and -118.19 (Na-FAU) kcal/mol at the embedded cluster models, following the conventional electrostatic trend. We found that the extended structure decreases the complexation energy by 24.86 kcal/mol in the Li-FAU and by 17.43 kcal/mol in the Na-FAU zeolites. This implies that the complexation energy of alkali cation bound to FAU zeolites cannot be obtained accurately by small bare quantum cluster models.

TABLE II ______Atomic charges of LI-FAU and Na-FAU complexes.

É.		Bare cluster		Embedded cluster				
Åtoms	Isolated	Ŀi~FAU	Na-FAU	Isolated	Li-FAU	Na-FAU		
Şi1	0.67	0.74	0.74	1.34	1.23	1.23		
Si2	0.69	0.73	0.73	1.27	1.25	1.23		
Q 1	-0.66	-0.79	-0.76	-0.61	-0.75	-0.72		
Ò2	-0.67	-0.79	-0.77	-0.61	-0.75	-0.73		
O1 O2 A)	0.80	0.99	0.89	0.76	0.90	0.83		
Cation	1.00	0.53	0.67	1.00	0.63	0.73		
©òmplexation energy								
(kcal/mol)	_	-160.78	-135.62	_	135.42	-118,19		

ú

:00

B3LYP/6-31G(d, p)-optimized geometric parameters of the complex of ethylene with naked Li*, Li-ZSM-5, Li-FAU, naked Na+ and Na-FAU zeolites.

	Li ⁺ /C₂H₄	Ú-ZS	6M-5/C₂H₄	Li⊷F	AU/C ₂ H ₄	Na ⁺ /C ₂ H ₄	Na-FAU/C ₂ H ₄	
Parameters	Naked	Bare	Embedded	Bare	Embedded	Naked	Bare	Embedded
C-Ca	134.5	133.8	134.3	133.8	134.1	134.3	133.7	134.0
X*-C1	238.3	245.0	245.2	248.9	242.9	272.2	284.4	278.0
X⁺—C2	238.5	246.5	242.5	244.7	242.5	272.2	281.4	275.8
X+—(C—C) ^b	228.7	236.5	233.1	237.6	233.3	263.8	274.9	268.6
AlX ⁺		256.2	269.5	252.9	263.6		290.2	303.6
X*—01	_	184.5	194.6	187.3	194.6		219.9	228.0
X+—02	_	182.5	190.8	187.2	193.8		219.0	228.6
01-X*-02		87.0	82.2	90.5	86.9	_	76.0	72.7
AI01	-	176.3	177.8	179.7	180.5	_	179.0	180.0
AI02	_	176.7	177.7	180.2	182.5	_	179.6	181.9
Q1-Al-O2	_	91.4	90.4	95.3	94.8	_	97.8	96.7
Si—O1	_	163.5	159.3	166.1	162.5	_	164.5	161.2
\$FO2	_	163.9	160.3	166.1	161.8	_	164.8	160.8
qX⁺	0.69	0.30	0.36	0.32	0.36	0.77	0.52	0.54

Bond lengths are in pm and bond angles in degrees.

2. A The calculated B3LYP/6-31G(d, p) of C=C bond distance in the gas phase is 133.0 pm.

The distances between Li cation to the midpoint of the C—C bond.

FAUJASITE (X-FAU) WITH ETHYLENE INTERACTION OF METAL-EXCHANGED

Interaction of Li-Zeolite (Li-FAU) with Ethylene

7. Cluster and embedded cluster models for the adsorption of ethylene on alkali metal-exchanged zeolites are illustrated in Figures 2(b)-4(b). Selected geometric parameters of the adduct complexes are listed in Table III. Adsorption energies have been évaluated by employing different models and are

given in Table IV. For the Li-FAU/ C_2H_4 zeolite [see Fig. 2(b)], the Optimized Li. . . C2H4 distances between Li cation to the midpoint of the C=C bond are found to be 233.3 and 237.6 pm, and the corresponding energies are 14.35 and 9.08 kcal/mol with basis set superpo-

sition error (BSSE) correction for the embedded cluster and quantum cluster, respectively. It is interesting to compare the adsorption of C2H4 on Li-FAU zeolite with the case where the zeolite framework is absent, i.e., in the naked Li-C₂H₄ system. As expected, C2H4 binds more strongly by a factor of 2 to the Li+ cation (23.15 kcal/mol) than in the Li-PAU zeolite in the binding energy. The simple naked Li-C2H4 model obviously overestimates the interaction of C2H4 in a real Li-exchanged-FAU system due to the large electrostatic field generated by the naked Li cation. The bare cluster model causes a large reduction of the positive charge of the Li cation and, thus, possibly underestimates the interaction of C2H4 with the Li-exchanged-FAU system. The embedding environment improves the results of the bare cluster

TABLE IV Calculated adsorption energies (kcal/mol) of C2H4 on naked Li+, Na+, bare quantum cluster, and embedded cluster model of Li-ZSM-5, Li-FAU, and Na-FAU zeolites.

	ધા*/ C₂H₄	Li-ZS	M-5/C ₂ H ₄	Li–F	AU/C₂H₄	Na ⁺ / C₂H₄	Na-l	FAU/C₂H₄
	Naked	Bare	Embedded	Bare	Embedded	Naked	Bare	Embedded
<u>.</u> ΔΕ	-24.83	11.55	-18.98	~11.58	-16.87	-17.76	-9.42	-13.76
ΔE _{ess∈}	~23.15	-8.94	-16.41	9.08	-14.35	15.97	-7.35	-11.63

VOL. 94, NO: 6

338

Ί, ÷.

٠;

model. One can see that the adsorption energy of the embedded cluster model lies between those of the bare quantum cluster model and the simple naked $\text{Li}/\text{C}_2\text{H}_4$ system.

interaction of Na-Zeolite (Na-FAU) with Ethylene

For the cluster model [see Fig. 3(b)], the adsorption energy of Na-FAU/C2H4 complexes is calculated to be 7.35 kcal/mol lower than that of the Li-FAU/C2H4 complex (9.08 kcal/mol); this may be attributed to its large cationic size (relative to Li+), which causes its interactions to be weaker than that of the Li complex. We found that the Madelung potential increases the adsorption energy by 5.27 kcal/mol in the Li-FAU and by 4.28 kcal/mol in the Na-FAU zeolites. With the inclusion of BSSE correction and the effects of the Madelung potential, we predict that the Li-FAU/C2H4 complex is more stable by about 2.72 kcal/mol compared to the Na-FAU/C2H4 complex. The adsorption energy is predicted to be 11.63 kcal/mol for the embedded cluster model of the Na-FAU/ C2H4, which compares well with the experimental value of 9.6 kcal/mol for the less acidic Na-X zeolite complex [35]. The lower adsorption energy in Na-X zeolite, which is an aluminum-rich faujasite zeolite with an Si/Al ratio in a range of 1-1.5, corresponds to the lower acid strength of the Na-X zeolite because the acid strength of zeolite decreases as the aluminum content increases.

at Effect of the Zeolite Framework on the Adsorption Properties of Ethylene

Another point of interest is the comparison of the results obtained using both cluster and embedded cluster models for exploring the different types of zeolites (faujasite and ZSM-5). Faujasite is considered a large-pore-size zeolite with a pore diameter of 74 pm and spacious supercages with a diameter of 130 pm, while ZSM-5 is a middle-pore-size zeolite with a pore diameter of about 50 pm. Although the two types of zeolites have different crystal structures (see Fig. 1), the cluster models give virtually the same adsorption energies (9.08 vs. 8.94 kcal/mol) for both Li-FAU/C₂H₄ [cf. Fig. 2(b)] and Li-ZSM-5/C₂H₄ [cf. Fig. 4(b)] complexes as listed in Table IV.

We found that inclusion of the Madelung potential increases the adsorption energy by 7.47 and 5.27 kcal/mol for the Li-ZSM-5 and Li-FAU zeolites,

₹.

ķ.,

respectively. With the inclusion of BSSE correction and the effects of the Madelung potential, the Li-ZSM-5/C₂H₄ complex is more stable by about 2.06 kcal/mol as compared to the Li-FAU/C₂H₄ complex. Thus, the Madelung potential was found to reveal that adsorption properties of zeolite do not depend only on the acidic site center but also on the framework structure where the acidic site is located.

Conclusion

The structures of alkali-exchanged faujasite (X-FAU, $X = Li^+$, or Na^+ ion) and ZSM-5 (Li-ZSM-5) zeolites and their interaction with ethylene have been investigated by means of both the quantum duster and embedded cluster approaches at the B3LYP/6-31G (d, p) level of theory. The effects of the Madelung potential were found to be important. The bare quantum cluster is too small to account for the extended structure and, therefore, yields almost the same binding energies (8.94 vs. 9.08 kcal/mol) for both Li-ZSM-5/C2H4 and Li-FAU/C2H4 complexes. On the other hand, the binding energy derived from the embedded model of Li-ZSM-5/C2H4 is calculated to be 16.41 kcal/ mol, which is larger than that obtained from the Li-FAU complex (14.35 kcal/mol), indicating that the metal-exchanged ZSM-5 is more acidic than the metal-exchanged FAU zeolites and leads to a better agreement with the experimental observation. The ion (X)...Al distance increases with the increase in ionic radii. The predicted adsorption energy for Na-FAU/C₂H₄ (11.63 kcal/mol) is comparable with the experimental estimate of about 9.6 kcal/ mol for ethylene adsorbed on Na-X zeolite. The results obtained in the present study suggest that the embedded cluster approach yields a more accurate and practical model than the bare quantum cluster for exploring the zeolite framework and catalytic properties.

ACKNOWLEDGMENTS

This work was supported by the Thailand Research Fund (TRF) in supporting the TRF Senior Research Scholar to J.L., by ADB-MUA, and by the Kasetsart University Research and Development Institute (KURDI). Sincere thanks are extended to Professor R. Ahlrichs (Karlsruhe, Germany) and Professor T. N. Truong (University of Utah, Salt